Driving Performance of Liquid Crystalline Actuators

by

Zhou Yuan

A dissertation submitted to
Kochi University of Technology
in partial fulfillment of the requirements
for the degree of
Doctor of Philosophy

Special Course for International Students
Department of Engineering
Graduate School of Engineering
Kochi University of Technology
Kochi, Japan

February 2012

Abstract

Liquid crystalline materials are able to be regarded as one of functional fluids, and they can convert input factors, such as electric or magnetic energies, a thermal energy, and an optical energy, into output factors by utilizing the easy change in orientation state. By choosing proper couplings of the factors, the liquid crystals can work as converter devices. The most common and successful application of liquid crystal technology is liquid crystal display. The liquid crystalline materials convert the input of electric energy and change the output of light transmission. This application has rapidly grown into a multi-billion-dollar industry, and many significant engineering discoveries have been manufacture.

Recently, Chono and Tsuji proposed actuator devices driven by liquid crystalline flows, which converted electric energy into kinetic energy. In comparison with the other micro-actuators, the liquid crystalline actuator has the advantages, such as low driving voltage (～V), high shape adaptability, and the structure of the liquid crystalline actuators is simple enough to easily downsize. These advantages make the liquid crystalline actuator particularly suitable for bio-medical applications.

In our experiment, the liquid crystalline material (5CB) is placed between two glass plates with surface orientation treatment. When a pulsed electric field is applied between the plates, the liquid crystalline molecules alternately exhibit clockwise and counterclockwise rotation, inducing the flow of the material. This flow is the source of the actuator drive.

To utilize the liquid crystalline actuators for driving or controlling micro-devices, such as micro-robots and micro-sensors, we have experimentally investigated the driving performance of liquid crystalline actuators which are

recently proposed for micro-actuators. The driving performances of actuators include the motion trajectory driving speed, driving speed and energy efficiency. These performances of liquid crystalline actuator strongly depend on voltage, frequency, duty ratio of the pulsed electric field and the loads of the liquid crystalline actuator.

Firstly, we investigated the motion trajectory and the maximum driving force of liquid crystalline actuators. The driving force of liquid crystalline actuator, which is one of the most important performances of actuators, has not been measured, since the force is too small to be measured directly using force sensors. In this research, we have tried to establish a way to estimate the force by analyzing the images of the driving actuators. From the estimated force, the applicability of the liquid crystalline actuators to the micro-devices is discussed.

The second step is to measure the output power, input power and energy efficiency of liquid crystalline actuators. As a capacitor, the input energy of liquid crystalline actuator is very difficult to be measured, because the time for charging is very short and the current is too small to be buried in the noise from the experimental environment. In this research, we used the power meter of PPA5500 (N4L) which can measure the precision power. From the energy efficiency, we will evaluate the capability of liquid crystalline actuators.

Thirdly, from the results we measured, we proposed the way to improve the performance and affordability of liquid crystalline actuators by optimizing the mechanical properties of liquid crystalline materials, the input parameters and the actuator geometry.

Key words:

Liquid crystalline actuator, Backflow, Driving performance, Motion trajectory, Driving force, Energy efficiency

Content

Figure List

Table List

Chapter 1

Introduction

1.1 Background

There is a growing worldwide interest in the possible applications of micro scale devices, such as micro electromechanical systems (MEMS) (Bustillo, Howe and Muller, 1998), micro-robots (Gray and Caldwell, 1996), μ–TAS (micro total analysis system) (Edwin and Van A, 2003; Cenk and Andrei, 2008) and so on. They have the potential to dramatically revolutionize human life. More and more research groups around the world are concentrating their efforts to develop new functional materials and operate new device systems to satisfy different requirement of the industry, science and technology field. The demands which people request from the micro scale device are: micro size, high efficiency, better adaptability to the work surrounding, short response time, easy to realize accurate control, and so on.

A micro scale device is a motion control system, which responds to variations of a given process or environmental mechanical properties such as position, velocity, acceleration, force, pressure, and work by using a small control energy to generate an controllable perturbation. From a functional standpoint, a motion control system is composed of a sensor and an actuator. While sensors serve to collect information from the environment, the actuators are required to perform corresponding mechanical motions. The development of micro-sensors has already reached a high level of maturity. Thus, this is forced

that the development of micro-actuators must speed up to match the development of micro-sensors.

Micro-actuators can broadly be defined as devices or mechanisms typically in the (tens of) micron size range which convert one type of energy into kinetic energy for moving or controlling a mechanism or system. There are several difficulties for designing and operating a micro-actuator. The down scaling of actuators is more difficult due to the limitation of forces and displacements that can be generated in a micro device. Surface related effects such as friction and adhesion are becoming more dominant due to an increased surface-to-volume-ratio. So the implications of the scaling of actuators have to be taken into consideration in the design and development of micro-actuators for wide ranging applications. On the other hand, the driving source of actuators also limit the range of applications.

Some micro-actuators have been proposed, which are electrostatic, electromagnetic, piezoelectric, and electro-conjugate fluid micro-actuator. Micro-actuation mechanism based on different principles and materials have to be chosen carefully for a given application, as shown in Table 1.1. Piezoelectric micro-actuators can generate large forces over small displacements when a voltage is applied across the piezoelectric material. They are presently being used in many well known applications, such as inkjet print-heads, micro-valves, micro-motors, and micro-grippers. The main advantages of this actuation principle are in its high precision, high speed and mechanical force. The most widely used piezoelectric ceramic material are PZT (lead circonium titanate) (Zurn and Hsieh, 2001) or zinc oxide (Jerkins and Cunnungham, 1997) due to their large mechanical force. However, there are some greatest difficulties associated with their use. The stroke length of all piezoelectric actuators is too small (~μm) because of the solid state driving source, which restricts the usage and the design for the micro-machine and the micro-structuring systems. For example, piezoelectric ceramic materials are usually brittle, and have a

relatively large Young's modulus, thus limiting the achievable strain. Moreover, the deposition technologies required for preparing thin/thick films of these ceramic materials need extensive optimization. Patterning these films into the required structures is also a big challenge. Further, the piezoelectric actuators need high voltage about several kilo volts to drive.

In a similar way, magnetic and electrostatic actuators also provide relative advantages on the some applications. For example, bearings are conventionally designed using electromagnetic whereas micro-motors are more popularly fabricated using electrostatic principles. The magnetic micro-actuators can achieve larger forces over larger air gaps than their electrostatic counter parts. However, an electromagnetic actuator requires a long cable to make the electric coil that generates the magnetic field, and has large resistance with large Joule loss, so it is not suitable for miniaturization. On the other hand, using electrostatic force as the driving force is that high voltage is needed to generate it. The high electric field gradients attract appreciable quantities of dust particles easily. Because of that, isolation and an energy source are important problems in developing the electrostatic actuators.

At the same time, the fluid powered actuator has also been proposed, such as electro-conjugate fluid actuator (Yoshida and Yokota, 1993). The output power density increases as the actuator becomes compact. Thus, the electro-conjugate fluid effect can construct an effective micro pressure muscle that used on development micro artificial muscle actuator (Takemura, Yokota and Edamura, 2005). Since the electro-conjugate fluid micro-actuators require high voltage (～ kV) for driving, it is hard to apply them to micro-medical robots which work inside human bodies. Overall, these actuators cannot completely meet the current application requirements, such as simple structure, low driving voltage and precise manipulation.

Table 1.1 Micro actuators and their characteristics

Kind of micro actuator	Size	Driving voltage	Stroke
Liquid crystalline actuator	~μm	~V	Infinite
Piezoelectric actuator (PZT)	~μm	~kV	Short
Electromagnetic actuator	~mm	~	Infinite
Electrostatic actuator	~μm	~kV	Infinite
Electro-conjugate fluid actuator	~mm	~kV	Infinite

Recently, Chono and Tsuji (Chono and Tsuji, 2006; Liu, Chono, and Tsuji, 2006; Takanori, Tsuji and Chono, 2009) have been developing a new type of micro-actuator using the flow of liquid crystalline material, which converted electric energy into kinetic energy. In comparison with the other micro-actuators, the liquid crystalline actuator has the advantages, such as low driving voltage (～V), high shape adaptability, and the structure of the liquid crystalline actuators is simple enough to easily downsize.

1.2 Research Objectives

In general, actuators are used under dynamic operation conditions. Dynamic operation entails continuous changes in the reference trajectory and in the loading conditions imposed by the mechanical interaction with the environment at the output port. Dynamic operation usually produces changing conditions in the amount of power requirements of the actuator, in the relative value of the velocity and force at the mechanical port and in the efficiency of

transduction between input and output energy. The relationship of driving performance of actuators is shown in Fig. 1.1. The driving performance must be measured before we used it.

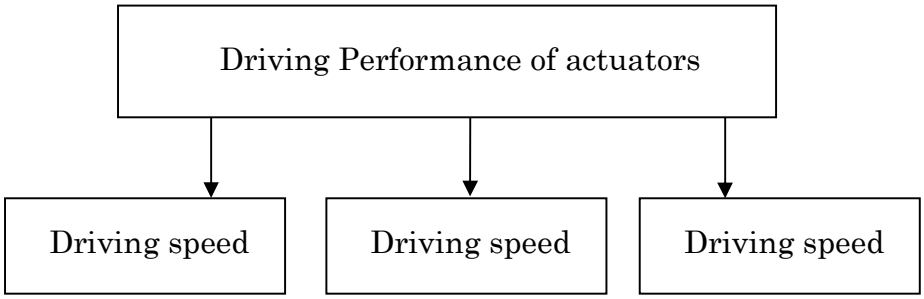

Fig. 1.1 Driving performance of actuators

In previous works on the liquid crystalline actuators, the effects of the voltage, duty ratio, and frequency of the imposed pulsed electric field, and also the thickness of the liquid crystal layer on the driving speed are studied. These previous works are only concerned with the driving speed of the liquid crystalline actuators. However, the important driving performances of actuators are not only the driving speeds, but also driving forces and energy efficiencies, which haven't been measured yet, as shown in Table 1.2. To utilize the liquid crystalline actuators for driving or controlling micro-devices, such as micro-robots and micro-sensors, all of the information on these performances must be collected.

In this thesis, we have systematically investigated the driving performance of the liquid crystalline actuators. Based on the experimental observations，we have elucidated the relations between actuator driving speed and voltage, frequency, and duty ratio of the input electric field. It is found that the liquid crystalline actuator can generate the sufficiently driving force with relatively low input voltage. Moreover, we also measured the input power and elaborated

the method to calculate the energy efficiency of liquid crystalline actuators. In terms of these results, the practical application of the liquid crystalline micro-actuator can be expected.

Table 1.2 Driving performance of micro actuators

Kind of micro actuator	Driving performance of actuators		
	Driving speed	Driving force	Energy efficiency
Liquid crystalline actuator	~μm/s	?	?
Piezoelectric actuator (PZT)	~μm/s	~kN/m^2	high
Electromagnetic actuator	~mm/s	~N/m^2	low
Electrostatic actuator	~mm/s	~mN/m^2	low
Electro-conjugate fluid actuator	~m/s	~N/m^2	high

We developed an experimental prototype of liquid crystalline actuator by means of the method proposed by Chono and Tsuji. Using the knowledge obtained from the simulation results, a prototype liquid crystalline actuator is designed and built as follows.

The liquid crystalline material was placed between two plates with surface orientation treatment to obtain homogeneous molecular orientation field at equilibrium state. When an electric field higher than a certain threshold is imposed between the plates, the liquid crystalline molecules will be forced to rotate parallel to the direction of the electric field. These rotating molecules

generate a flow called backflow and shear force. Then, the upper plate of liquid crystalline actuator is driven. When the molecular direction becomes parallel to the field direction, the molecules stop rotating, and then the flow will disappear and cannot drive the actuator any more. To drive the actuator again, a pulsed electric field is employed for the continuous drive of the actuator.

Based on the experimental prototype described above, the three research objectives are achieved in the thesis. Firstly, we plan to investigate the motion trajectory and driving force of liquid crystalline actuators. These two related properties are important for the practical use of the actuators. Secondly, we investigated the input power and energy efficiency of liquid crystalline actuators. In terms of the results, we will evaluate the driving capability of liquid crystalline actuators. Finally, from results, we proposed the way to improve the performance and affordability of liquid crystalline actuators by optimizing the mechanical properties of liquid crystalline materials, the input parameters and the actuator geometry.

1.2.1 Measurement of Driving Force

In order to put the liquid crystalline actuator into practical application, it is necessary to know the driving performance of micro actuators. These include the motion trajectory, driving speed, driving forces, displacements, power efficiency, linearity, repeatability, and bandwidth which are related to the response time. Among these properties, the driving force is particularly important, which determines the capacity to drive the objects.

The difficulty here is that the driving force is too small to be directly measured by force sensors. We employed the image processing to evaluate the driving force from the motion trajectory, which is obtained by monitoring the movement of upper plate by the high speed camera. The below three steps are taken to measure the driving force.

Firstly, the movement of the upper glass plate of the liquid crystalline cell was monitored at room temperature via a polarizing microscope equipped with a high speed camera. Because the movement of the liquid crystalline actuator is affected by changing the parameters including voltage, frequency, and duty ratio of the input electric field, the rotation of liquid crystalline molecules can be strongly influenced by these parameters. We recorded the motion trajectories for the conditions with different combination of voltage, frequency, and duty ratio of the input electric field.

Secondly, we employed the image processing technique to obtain the motion trajectory from the continuous images. The moving object in image sequences is detected by aligning pairs of images and creating the difference image using active contour algorithms. By analyzing the small changes in brightness that accompanies even sub pixel displacements between every two images, it is possible to compute the motion trajectory of the liquid crystalline actuator.

Finally, we computed the driving speed and driving force of the liquid crystalline actuator. The influence on the driving force from the weight of upper glass plate and the strength, the duty ratio, and the frequency of the applied voltage is also evaluated.

1.2.2 Measurement of Energy Efficiency

Actuators can be treated as active transformers that transform one type of energy into another form with a transfer function. Design of the actuator is decided by how to obtain the physical energy required. Thus, the input power and the energy efficiency must be measured precisely.

The difficulty here is that the input energy of liquid crystalline actuator is very difficult to be measured as a capacitor. Because the time for charging is very short and the current is too small to be buried in the noise from the

experimental environment, the measure setup should be careful chosen, and the experimental method should be considered with the property of liquid crystalline actuator. The below three steps are taken to measure the driving force.

Firstly, we should choose a setup which can measure the low current precisely with high sample rate. In this experiment, the precision power analyzer (PPA 5500 *N4L*) is used for measuring the input power of liquid crystalline actuator. The PPA5500 builds in high precision current shunt about 10Arms and fast sample rate about 2.2M samples/s. high accuracy is maintained even with noisy or distorted power applications.

Secondly, we recorded the input power for the conditions with different combination of the weight of the upper glass plate of liquid crystalline actuator and the voltage and frequency of the input electric field. Because the impedance and capacitance of the liquid crystalline actuator is affected by changing the parameters including voltage and frequency of the input electric field, the dielectric permittivity ($\varepsilon_{\parallel}$ and $\varepsilon_{\perp}$ are dielectric permittivity components along and perpendicular to the director) of liquid crystalline molecules can be strongly influenced by these parameters.

Finally, we analyzes the movement of liquid crystalline actuator to calculate the output power of liquid crystalline actuator. Then, the input power and output power are combined to calculate the energy efficiency of liquid crystalline actuator. The influence on the energy efficiency from the weight of upper glass plate and the strength and the frequency of the applied voltage is also evaluated.

1.2.3 Optimization of liquid crystalline actuator

Based on the measurement of driving force and energy efficiency, it is expected to optimize the design of actuator to achieve the best performance in

the application. In the thesis, we discussed the effect of liquid material, temperature, and the surface aligning method on the actuator performance.

It is also important that a micro actuator can be fabricated economically using available batch processing technologies for fabrication. The mechanical micro actuation is used to the generation of forces, usually leading to mechanical motion. Therefore, different principles of actuation have to be judged according to their desired design priorities for the parameters mentioned above.

1.3 Thesis Organization

The thesis is organized as follows. In the Chapter 2, the properties of liquid crystals and actuators are introduced. We firstly described the dynamic properties of liquid crystalline, especially the mechanism of backflow generation. Then, we introduced the general concept of micro actuator, and also illustrated the design and performance for different types of current existed micro actuator including electrostatic, electromagnetic, piezoelectric, and shape memory alloy actuators. We finally describe the working principle of liquid crystalline actuator. And the advantage of the liquid crystalline actuators compared to that of other actuators will be summarized.

The Chapter 3 focused on describing how to measure the driving force of liquid crystalline actuator. As the driving force is too small to be directly measured, we calculate it in terms of the motion trajectory at different conditions. The details of experimental design. According to the working principle of backflow, we designed and developed the experimental prototype of liquid crystalline actuator. This chapter provides the technical details about the liquid crystalline cell and experimental setup, such as the Surface Treatment of ITO Layer, Alignment Layer and the selection of Liquid Crystalline. We also discussed the method of motion track based on the computer vision, which is the

key technology to measure the driving force of actuator.

In Chapter 4，we measured the input power and energy efficiency based on the experimental prototype described in the chapter 4. We chose the experimental setup and designed the experimental method to measure the low current of the electric circuit. We also discussed the relationship between the energy efficiency and the conditions with different combination of the weight of the upper glass plate of liquid crystalline actuator and the voltage and frequency of the input electric field.

In Chapter 5, we discussed the performance enhancement of liquid crystalline actuators in terms of the measurements of the driving force and energy efficiency. We presented the possible methods to improve the performance, including the appropriate selections for material and temperature and mechanical design of the actuator. Then, we will give the general conclusion and future inquires.

Chapter 2

Liquid Crystals and Actuators

2.1 Introduction

Now the development of liquid crystal science and technology underpins a wide variety of products, from large industrial displays to a wide array of consumer electronics in homes and offices. Non-display applications of liquid crystals in optical communication, nonlinear optics, data/signal/image processing and optical sensing are also receiving increased attention. Due to their constituent molecules along with physical fluidity, liquid crystals can be easily incorporated into desired configurations for a variety of device applications. The large anisotropy of liquid crystals, allows for realization of external control of the optical properties of liquid crystal based devices, which makes liquid crystal materials suited for implementing tunable photonic devices for both optical communications and optical sensing systems.

Since the discovery of the applicability of liquid crystals to display devices in the 1960s, many studies on liquid crystals have been carried out both fundamentally and practically. As a result, liquid crystal displays have established a strong position as a substitute for cathode ray tube displays. The manufacturing of such displays has grown into a large industry with a global scale and further development has reached a plateau except for a few trivial

improvements.

In the recent research field, several studies have explored the mechanical applications of liquid crystals. The Fig. 2.1 depicts the conceptual mechanism of these possible applications. When the input factor (e.g., electromagnetic field, flow, heat, and light) are imposed into liquid crystals, the orientation states of liquid crystals will be changed. Consequently, this orientation change will generate the output energy such as heat, light, mechanical flow [43-46]. In the process described above, the liquid crystal can be regarded as a medium of converting energy by combining input and output factors appropriately. By optimizing the combination of input and output factors, it is possible to design the practical applications of liquid crystals in the various environments.

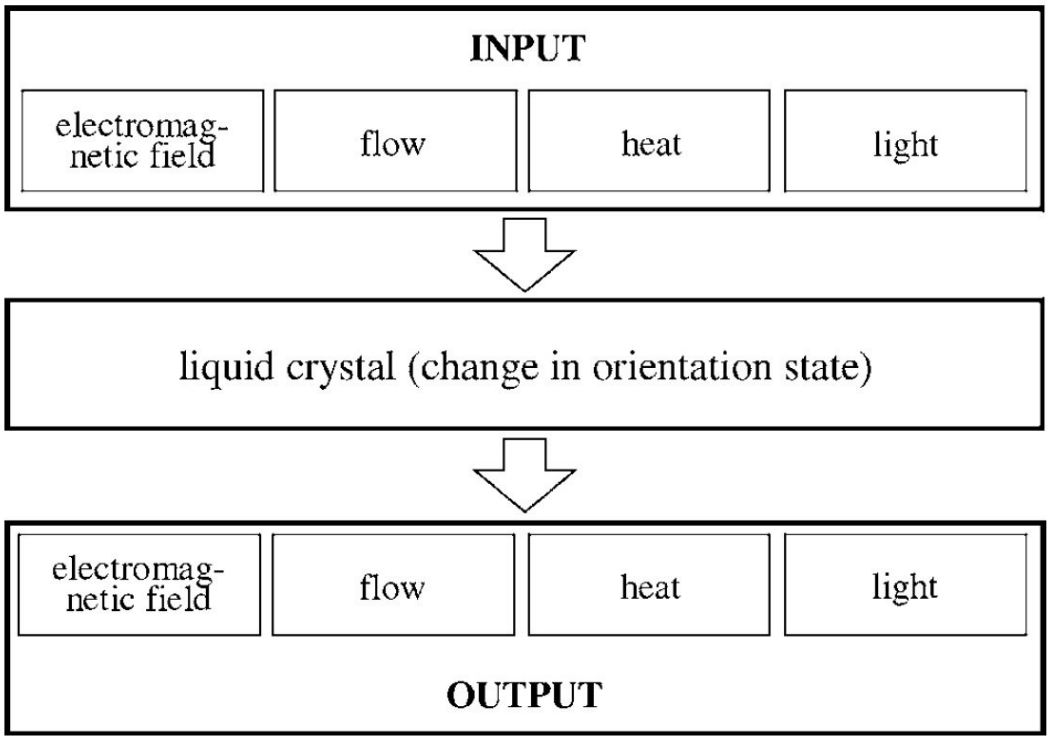

Fig. 2.1 Applications of liquid crystal

For example, by applying the electric field onto the liquid crystal, the rod-like liquid crystalline molecules change their orientation direction parallel to the field direction and the path of a light passing through the liquid crystal becomes different from the path without electric field. This mechanism is used in liquid crystal displays. Recently, Chono and Tsuji proposed actuator devices driven by liquid crystalline flows.

In this introductory chapter, Section 2.2 provides a concise description of liquid crystal phases and a short review of physics characteristics of liquid crystal. Section 2.3 introduces what is micro actuator, compares several kind of micro actuator and discusses the advantages of liquid crystalline micro actuator.

2.2 Liquid Crystals

Solid, liquid and gaseous states were the only known states of matter before the discovery of liquid crystals. A solid can be either crystalline or amorphous, being the former characterized by a three-dimensional lattice with both long-range positional and orientational atomic order and the latter having only short-range order. When a solid is heated above its melting point, it turns into an isotropic liquid having neither positional nor orientational order. In addition, a liquid state can turn back into a solid after cooling. The term liquid crystal describes a state of matter that is intermediate between an isotropic liquid and a crystalline solid. Since their discovery in the late 19th century by Reinitzer (1888) and Lehmann (1889), there have been thousands of compounds identified to exhibit this unusual phase of matter – the liquid crystalline. The underpinning prerequisite for the liquid crystalline is that the molecule of liquid crystal must exhibit a high degree of shape anisotropy (e.g., rod-like or disk-like). This shape anisotropy causes the liquid crystalline state having some other properties at same time, such as dielectric anisotropy and optical anisotropy. These properties are the principle characteristics leveraged in the

well-known display technologies. Depending on the nature of the molecular structure, a compound may pass through one or many different liquid crystal phases, characterized by the order and symmetry, before transforming into the isotropic liquid phase. The state of liquid crystalline has no positional order but has orientational order.

2.2.1 Liquid Crystal Phases

According to the mechanism that initiates the transition to the liquid crystal phase, there are two generic classes of liquid crystal, those whose transitions are thermotropic, and those strongly influenced by solvents, known as lyotropics. Most known liquid crystals are produced by varying the temperature of various substances (in particular, by raising the temperature of certain solids or lowering the temperature of certain liquids) and are commonly termed thermotropic. Below the melting point temperature, T_{mp} , thermotropic liquid crystals are solid, crystalline and anisotropic; as the temperature is raised above the clearing point and $T_{cp} > T_{mp}$, they are a clear isotropic liquid. Between T_{mp} and T_{cp} they are in the liquid crystal mesophase, as illustrated in Fig. 2.2. The process is usually reversible by lowering the temperature, though there may be a small temperature hysteresis (for example, T_{mp} when reducing temperature may be slightly less than T_{mp} when increasing temperature). The liquid crystals Reinitzer and the early researchers discovered were all thermotropic. Among the thermotropic liquid crystals there are two fundamental classes of substances, those that are enantiotropic, which are able to enter the liquid crystalline state both by cooling a liquid and heating a solid, and those that are monotropic, which can enter the liquid crystalline state via one or the other of those methods, but not both.

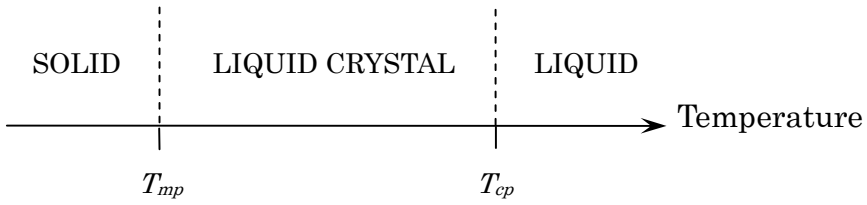

Fig. 2.2 The temperature range of a thermotropic liquid crystal is comprised between the melting and clearing points

The other fundamental way to make a substance enter a liquid crystalline phase in by the action of a solvent, and the concentration of the solution is primarily responsible for the occurring phase. More specifically, concentration (and secondarily temperature) is the most important controllable parameter for the lyotropic phase, which temperature (and secondarily pressure) is the most important controllable parameter for the thermotropic phase. Lyotropic liquid crystals are broadly present in nature. For instance, by adding water to soap (which is not a liquid crystal) above a minimum concentration, we cause the soap molecules to form lyotropic liquid crystals.

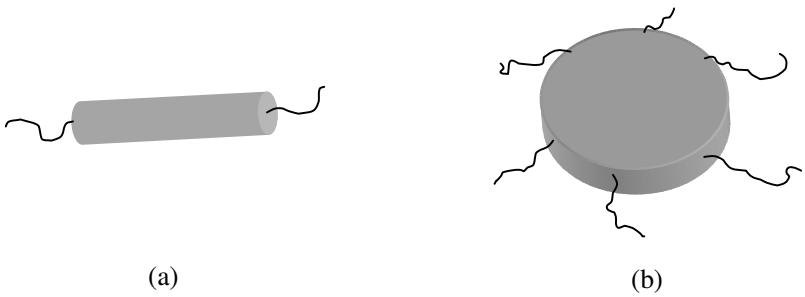

Fig. 2.3 Shape of liquid crystal molecules: (a) calamitic and (b) discotic

As far as the shape of liquid crystalline is concerned, we distinguish two main types (though there are less usual but more complex shapes); in the first the molecules appear like a rod (rod-like or cigar-like liquid crystals) as

sketched in Fig. 2.3(a), in the second the molecules are shaped like a disc (disc-like or discotic liquid crystals), as sketched in Fig. 2.3(b).

We represented the molecules in Fig. 2.3 as made up of a rigid central part (core) plus some flexible ramifications (lateral, or side chains) whose chemical structures are generally different each other.

Unlike liquids, whose molecules posses no type of order and are free to move in all the three dimensions, liquid crystals possess a certain degree of orientational order and positional relationships between the molecules. The majority of thermotropic liquid crystals are comprised of rod-like molecules, which can be broadly classified as nematic, cholesteric, and smectic. Fig. 2.4 illustrates a particular phase sequence with increasing temperature: crystal, nematic, and isotropic liquid.

A unit vector $\mathbf{n}$, known as the director, can be defined, parallel to the average direction of the long axis of the molecules in the immediate neighborhood. This vector is not constant throughout the whole medium, but is a function of space. To put in evidence this last aspect, $\mathbf{n}(r)$ is often used to designate the director.

Next to the clearing point, increasing the temperature to T_{mp}, the nematic phase appears. Nematic liquid crystals are the most widely used liquid crystals in display applications. In the nematic phase all molecules are aligned approximately parallel to each other, with only a one-dimensional (orientational) order and without a positional order. Molecules can translate in all the three directions and can rotate freely along the long molecular axes. The illustration of nematic phase is given in Fig. 2.4.

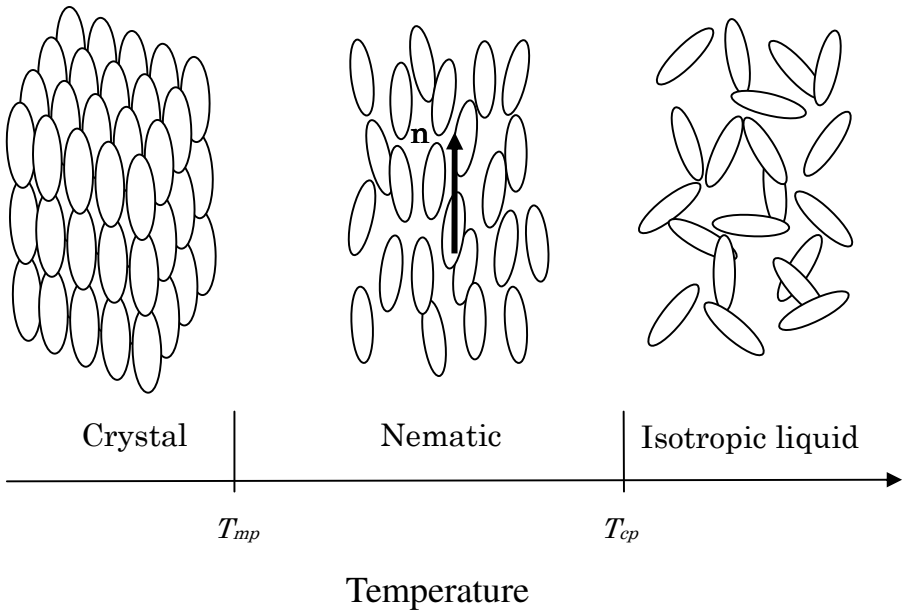

Fig. 2.4 Schematization of phase transitions as a function of temperature for rod-like molecules. T_{mp} and T_{cp} are respectively the temperatures at the melting point and clearing point

2.2.2 Anisotropic Properties of Liquid Crystals

In this section, the nematic liquid crystal phase will be discussed. The molecules of the nematic have no positional order, but they have long-range orientational order. The nematic liquid crystals are not as rigid as solids, easily reoriented, realigned, or deformed by applying mechanical stresses, electric and magnetic fields, and by the proximity actions with surfaces that have been properly prepared.

Because of their specific molecular shape and alignment, nematic liquid crystals exhibit anisotropic physical characteristics. Their dielectric susceptibility, electrical conductivity, magnetic permeability, refractive index, and viscosity measured in the direction of the long axis are different from those measured in the plane normal to the long axis.

Liquid crystal is the state between solid and liquid, it has properties of a

both a fluid and a crystalline material, that is fluidity like general liquid and directivity like solid (crystal). This is because the special structure of the liquid crystal molecules, the most common liquid crystal molecules are long-rod shaped, consisting of atoms with different values of the electro negativity. The molecule has polarity and the dipole moment of a chemical bonding is a vector and therefore, a compensation or increase of the bond moments in a molecule can be observed. As a result of the polar of the liquid crystal molecules, the anisotropy of optical, dielectric and diamagnetic are shown. Utilizing the fluidity of the liquid crystal, we can feed it into vessels of any shape, in addition to this, the anisotropy including mainly the optical and electrical anisotropy. These are the most important factors that the liquid crystal has been successfully applied on the display field.

The lowest energy state for bulk nematic liquid crystals corresponds to a single director orientation throughout the material. Bounding surfaces, mechanical stress and external fields deform director alignment; this induces elastic torque. As a consequence of the deformation of director field, there exists always a elastic torque on the director which opposites to deformation of director field.

The deformation of director field of nematic liquid crystals can be considered for three elementary cases, illustrated in Fig. 2.5.

The first is a “splay” deformation, where molecules are spread (Fig. 2.5(a)), the second is a “twist” deformation where molecules are twisted (Fig. 2.5(b)), and the third is a “bend” where molecules are bent (Fig. 2.5(c)). General deformations are a combination of these three types.

The relationship between the deformation and the restoring torques opposing to the director deformation is expressed by the splay, twist and bend elastic moduli (also known as Frank elastic constants), k_{11}, k_{22}, k_{33}, whose dimension is energy/length and hence N in SI units.

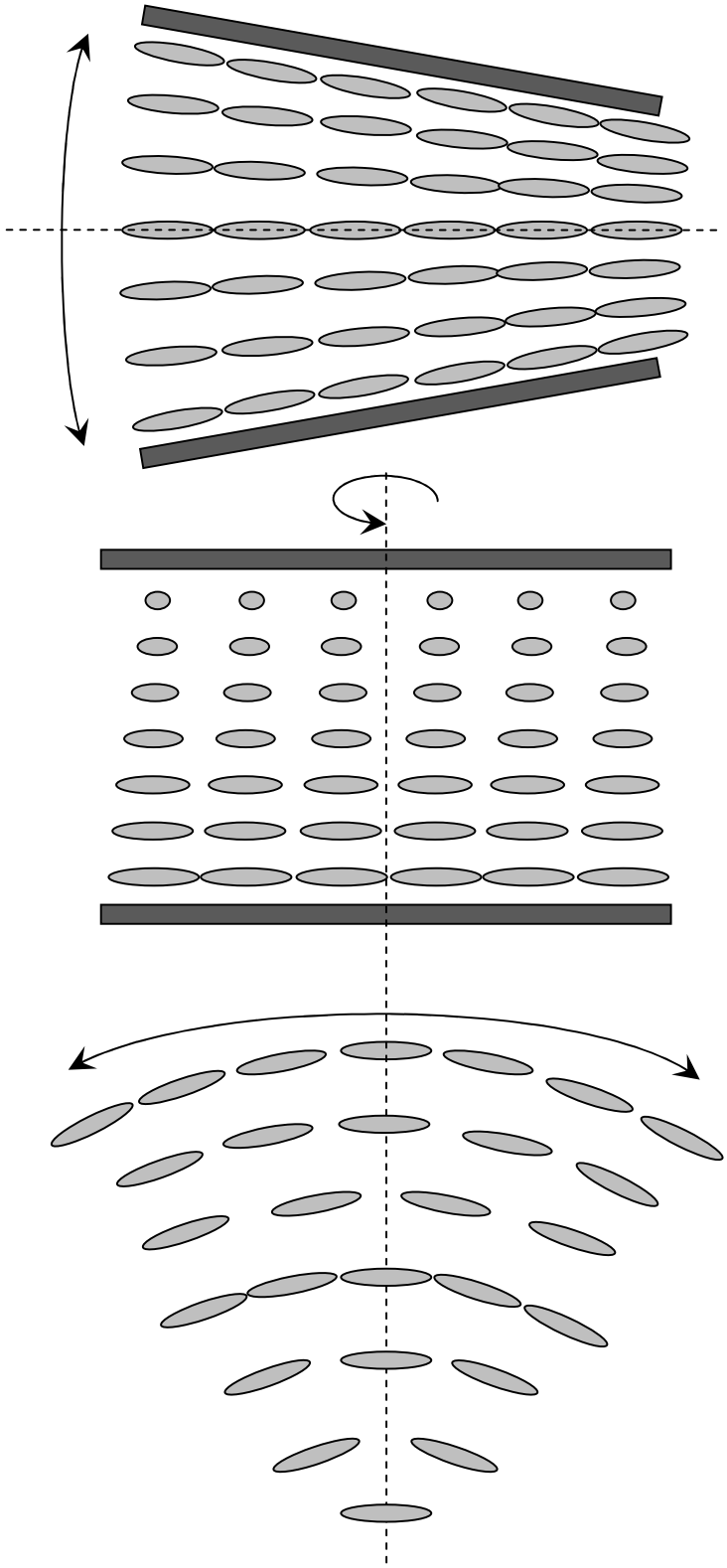

Fig. 2.5 Molecular alignments of nematic liquid crystals under external mechanical stress: (a) splay, (b) twist, (c) bend

The elastic increment of the volume free energy density (per m^3), f_k, due to splay, twist and bend is, according to the elastic theory for (non compressible) liquid crystals, quadratic in the director gradients

$$f_k = \frac{1}{2}\left[k_{11}(\nabla \cdot \mathrm{n})^2 + k_{22}(\mathrm{n} \cdot \nabla \times \mathrm{n})^2 + k_{33}|\mathrm{n} \times \nabla \times \mathrm{n}|^2\right]$$

This is the well-known Frank-Oseen elastic free energy density for nematic liquid crystals [Frank, 1958]. The elastic constants are temperature dependent and are proportional to the square of the orientation order parameter.

It is usually sufficient to consider the splay, twist, and bend deformations go the liquid crystal director in determining the configuration of the director.

Because of the ordering of rod-like molecules, liquid crystals are commonly uniaxially symmetric (i.e., the axis of symmetry is parallel to the axis of the molecules, the director **n**). As a consequence of this uniaxial symmetry, the dielectric constants differ in magnitude along the long axis ($\varepsilon_{\parallel}$) and perpendicular to it ($\varepsilon_{\perp}$). This dielectric anisotropy ($\Delta\varepsilon$) is defined as:

$$\Delta\varepsilon = \varepsilon_{\parallel} - \varepsilon_{\perp}$$

Because of the anisotropy in the dielectric constant, the molecules can align parallel or perpendicular to the applied fields, as illustrated in Fig. 2.6. Most commonly, compounds exhibit a positive dielectric anisotropy ($\Delta\varepsilon > 0$) that aligns them parallel to applied electric fields, but the converse is also possible ($\Delta\varepsilon < 0$). In classical dielectric theory, the macroscopic dielectric constant is proportional to the molecular polarizability. In rod-like liquid crystals, the polarizability along the long axis is often greater than that perpendicular to it. For non-polar rod-like liquid crystals, the dielectric anisotropy tends to be positive ($\Delta\varepsilon > 0$). In Fig. 2.6, the dielectric anisotropy is demonstrated as an induced dipole moment. For the $\Delta\varepsilon > 0$ case, an induced dipole is formed in the presence of the electric field and results in the reorientation of the long

molecular axis parallel to the electric field direction **E**. For polar rod-like liquid crystals, the permanent dipole moment can result in an increase or decrease in $\Delta\varepsilon$ which is also shown in Fig. 2.6. The dielectric constant is a function of temperature and goes to zero ($\Delta\varepsilon \rightarrow 0$) in the isotropic phase.

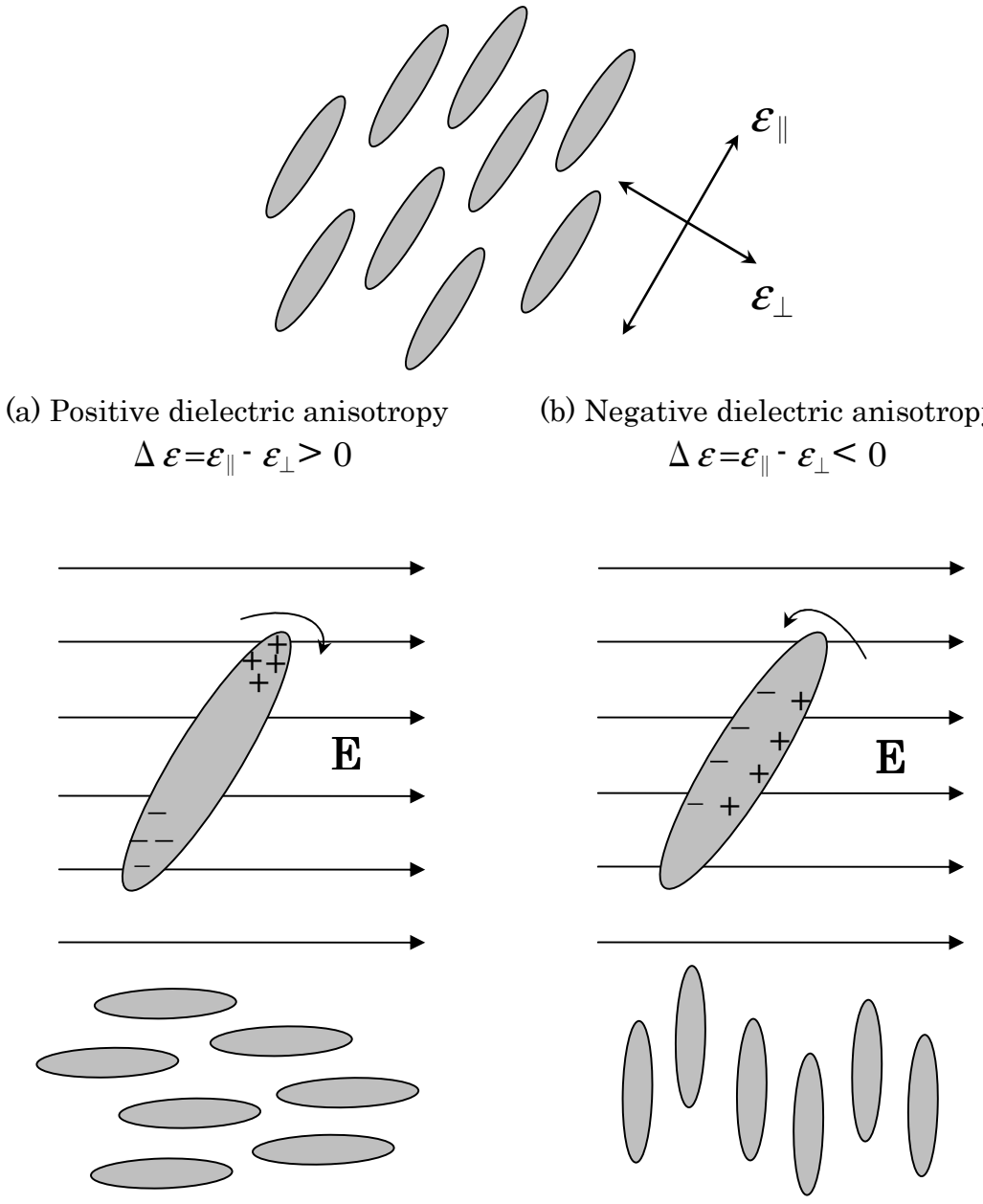

(a) Positive dielectric anisotropy
$\Delta\varepsilon=\varepsilon_{\parallel}-\varepsilon_{\perp}>0$

(b) Negative dielectric anisotropy
$\Delta\varepsilon=\varepsilon_{\parallel}-\varepsilon_{\perp}<0$

Fig. 2.6 A graphical illustration of (a) positive and (b) negative dielectric anisotropy

2.2.3 Backflow of Liquid Crystals

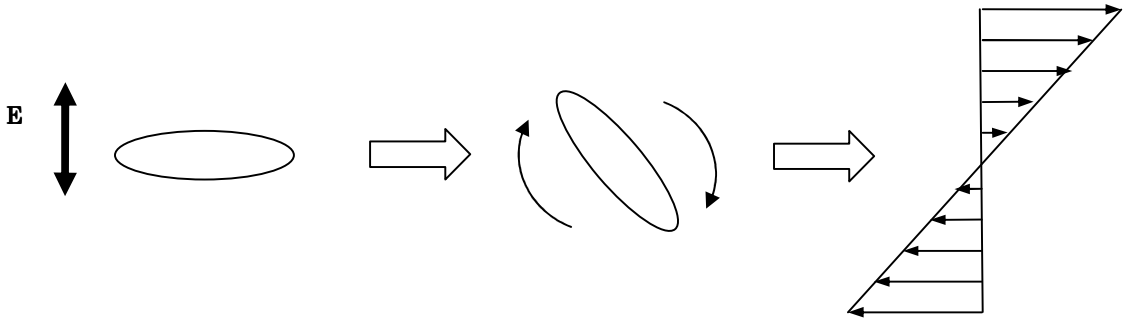

(a) Velocity gradient generate

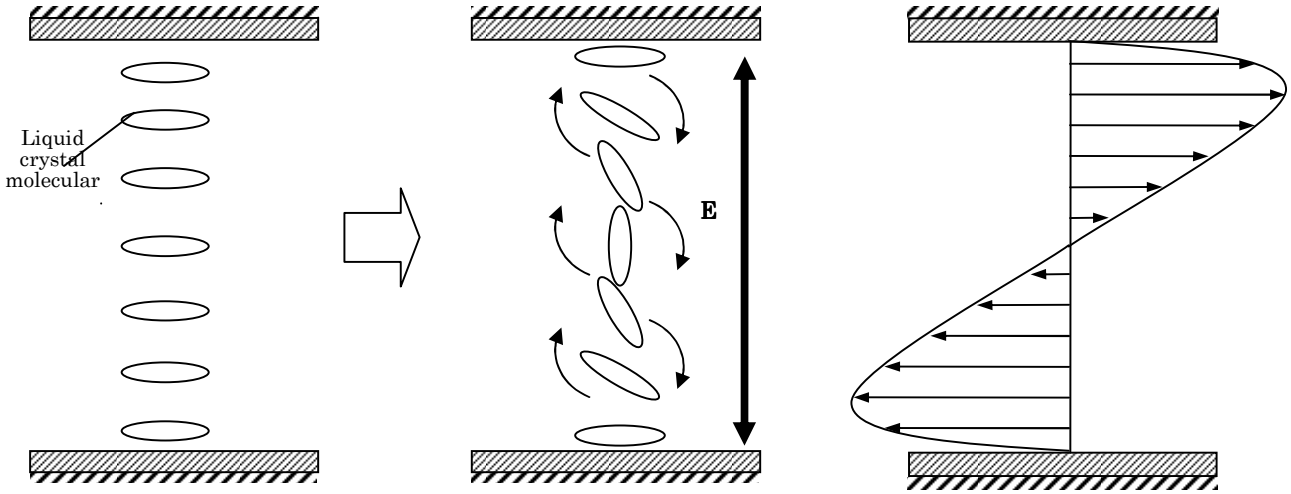

(b) Backflow generate

Fig. 2.7 Velocity gradient and backflow generating of liquid crystal molecule

When an external applied field is imposed on the liquid crystal, the molecule of liquid crystal is forced to rotate to parallel to the applied field. At the same time, the velocity gradient is generated, as shown in Fig. 2.7(a). An external torque applies on the director of liquid crystal which is placed in a

sample container, as shown in Fig. 2.7(b), and there is usually a fixed director orientation at the surfaces of the sample container. Because of the affect of the long-range orientation and the surface alignment, the director rotation of liquid crystal is inhomogeneous and is coupled with generating a velocity gradient. The flow called backflow is induced and the shear force generated by this liquid crystal backflow acts on the surfaces of the sample container, as shown in Fig. 2.7(c).

2.3 Micro Actuators

An actuator can be defined as an energy converter which transforms energy from one form into another in a controllable way, for example, from electric, magnetic or hydraulic into kinetic energy (Judy, 2001; Madou, 2001). The input quantities of an actuator depend on the type of energy used and can be chosen among all the quantities involved in the energy conversion from the energy source to the output mechanical quantities.

Actuators play a very important role in industrial mechatronic systems. Research and development efforts have been directed towards using different actuation principles (Dufour and Sarraute, 1999; Fujita, 1998) and designing various structures for specific applications. Fatherly, there is a growing worldwide interest in the possible applications of micro scale devices, such as MEMS, micro-robots, μ–TAS (micro total analysis system) and so on. For driving or controlling these devices, there must be a micro-scale actuator. For these purpose, some micro-actuators have been proposed, which are electrostatic, electromagnetic, piezoelectric, and shape memory alloy actuators.

2.3.1 Electrostatic micro actuator

Electrostatic micro actuators have been constructed out of metal or heavily doped semi-conductors and designed with flexures, rotary or linear bearing

surfaces. They have been used extensively in MEMS devices since it is relatively easy to fabricate closely spaced conductive plates with narrow gapes in between. The fundamental principle behind electrostatic actuators is the attraction of two oppositely charged plates. Electrostatic forces are inversely proportional to the distance between the plates, usually preventing large displacements unless high voltages are used (tens to hundreds of volts). Well-known designs are the lateral comb drive developed at Berkeley by R.S. Muller's group (Tang, Nguyen and Howe, 1992), and the rotary electrostatic micro motor (Fan, Tai and Muller, 1989; Hirano and Fan, 1998). More recently, electrostatic comb-drive actuators have been designed for large deflections up to 150μm with a response time of less than 1ms (Grade, Jerman and Kenny, 2003), operating at less than 150V.

However, due to the inverse square relationship of Coulomb forces with the distance (between the two arms of an actuator), they usually work in small gaps and require high voltage. The large voltage requirements often prevent electrostatic micro actuators from being conveniently driven with typical on-chip circuits and voltages. In addition, high voltages on small features may create high electric field gradients that attract dust particles. Also, electrostatic actuators will not function in conductive fluids and are not safe in humid environments.

2.3.2 Electromagnetic micro actuator

Electromagnetic micro actuators often follow the conventional macroscopic design, despite the significant challenge involved in integrating ferromagnetic cores, rotors and copper coils (Ahn, Ki and Allen, 1993; Guckel, 1998; Guckel and Christenson, 1993). Even though electromagnetic actuation employed in conventional motors or solenoids is the most successful principle used on a macro scale, MEMS magnetic devices are still relatively unestablished. This is due to the fact that 3D coils are difficult to fabricate by typical MEMS

technologies. Successful commercial devices are magnetic read/write heads for computer disk drives (Hirano and Fan, 1998).

Electromagnetic micro actuators can achieve large forces over wider air gaps than their electrostatic counter parts. They can operate at low voltages but use comparatively large currents. As a result, the power dissipation is high. Electromagnetic micro actuation is a more robust mechanism than electrostatics. These advantages make it attractive to do research in this field. Extensive work has been done by several groups (Cho and Ahn, 2002; Ghantasala et al., 2000; Guckel, 1998; Judy and Myung, 2002; Lagorce et al., 1999; Liu et al., 1995; Wangner and Benecke, 1990). Even though different structures are used in these example, the force is always generated between the electric coil and the magnet.

Electromagnetic force has been used as the driving force of conventional actuators produced by popular machining, since the electromagnetic force is able to be controlled by the electric signals such as an electric current. However, an electromagnetic actuator requires a long cable to make the electric coil that generates the magnetic field, and has large resistance with large resistance with large Joule loss, so it is not suitable for miniaturization.

2.3.3 Piezoelectric micro actuator

Piezoelectric micro actuators generate large forces but only small displacements by applying a voltage to the piezoelectric materials. Typically used constructions are the bimorph (Robertson, 1979; Todals et al., 1979) and multi-layer structures. In addition, more and more unimorph composite beams (DeVoe, 2001; Elvin et al., 2001; Kueppers and Leuerer, 2002; Zurn and Hsish, 2001) are employed to meet to increasing requirements of special applications.

The piezoelectric principle can be used in many applications, such as electric fans (Todals et al., 1979) hydrophones (Lau et al., 2001), microphones

(Lee et al., 1996; Schellin and Hess, 1992), inkjet printers, control valves (Roberts and Li, 2003), micro pumps (Yoseph and Chang, 2000), tactile sensor (Dargahi et al., 2000), acoustic control (Li et al., 2001) and micro motors (Ruprecht et al., 1996), etc.

In addition, the piezoelectric actuator has high resolution (order of nm) and good response (order of kHz), and generates a large force. Therefore, the piezoelectric actuator is often applied in sevo-positioning mechanisms such as the precision positioning of X-Y automatic table. Since the PZT has the problems of hysteresis and creep phenomena, the designer should consider properly to control the PZTs.

On the other hand, the piezoelectric actuator has the characteristic that a high voltage is needed to drive it, and that its strain is small (about 0.1%). The stroke length of these actuators is too small because of the solid driving source.

2.3.4 Electro-conjugate fluid micro actuator

An “electro-conjugate fluid” or “ECF” is the generic name for a class of low conductivity dielectric functional fluids that can be propelled when subjected to a non-uniform electric field. A micro motor using Electro-conjugate Fluid is also proposed and developed. The ECF allows direct converting electrical energy to mechanical energy, the proposed micro motor has simple structure and is driven by a direct-current electric power supply. ECF motors have simple structure and light weight, which are suitable for miniaturization. In addition, ECF motors have no electromagnetic radiation.

However, since the electro-conjugate fluid micro-actuators require high voltage (～kV) for driving, it is hard to apply them to micro-medical robots which work inside human bodies.

2.3.5 Liquid Crystalline Micro-actuator

These actuators we discuss in the above section can't completely meet the current application requirements, such as simple structure, low driving voltage and precise manipulation. Recently, Chono and Tsuji have been developing a new type of micro-actuator using the flow of liquid crystalline material, which converted electric energy into kinetic energy. In comparison with the other micro-actuators, the liquid crystalline actuator has the advantages, such as low driving voltage (~V), high shape adaptability, and the structure of the liquid crystalline actuators is simple enough to easily downsize.

The schematics of the electric field induced flow generation and the actuation of the liquid crystalline actuator are shown in Fig. 2.7. The liquid crystalline material, which has the rod-like molecules, was placed between two plates with surface orientation treatment to obtain homogeneous molecular orientation field at equilibrium state, as shown in Fig. 2.7(a). When an electric field higher than a certain threshold which is several volts for typical liquid crystals is imposed between the plates, the liquid crystalline molecules will be forced to rotate parallel to the direction of the electric field, as shown in Fig. 2.7(b). These rotating molecules generate a flow called backflow and shear force, as shown in Fig. 2.7(c). Then, the upper plate of liquid crystalline actuator is driven. When the molecular direction becomes parallel to the field direction, the molecules stop rotating, and then the flow will disappear and cannot drive the actuator any more. To drive the actuator again, we must need to let the molecular orientation back to the orientation at equilibrium by releasing the electric field. A pulsed electric field is employed for the continuous drive of the actuator.

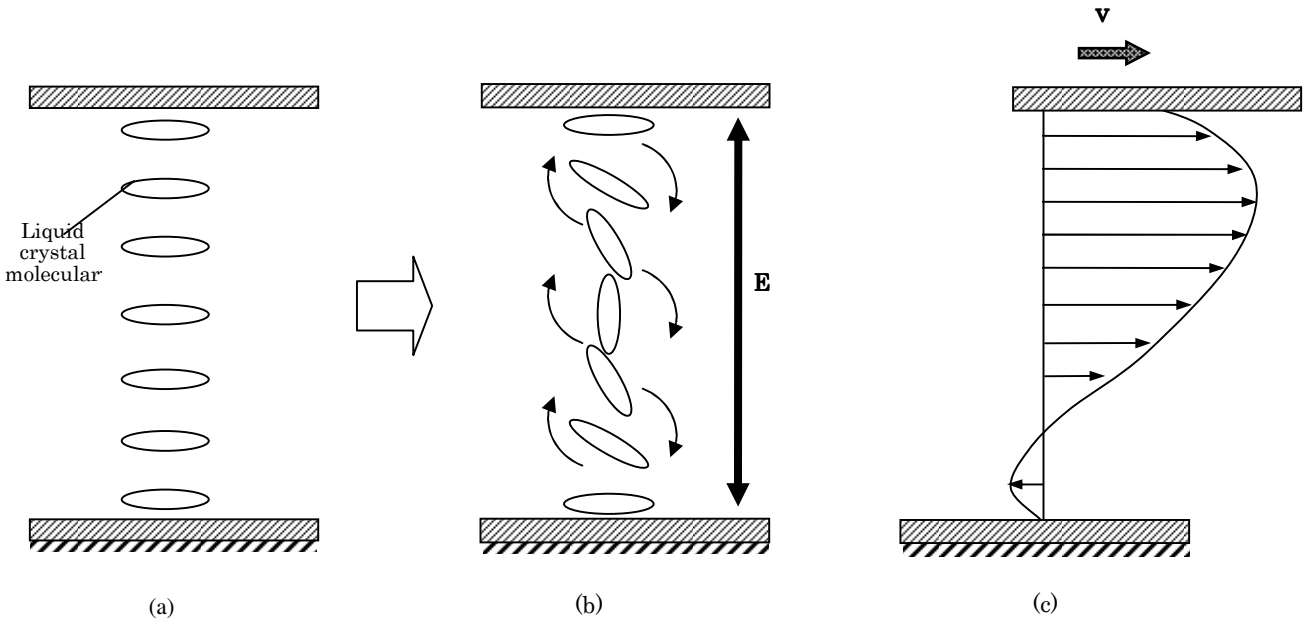

Fig. 2.7 Mechanism of liquid crystalline actuator

Advantages of Liquid Crystalline Actuator are as follows:

Driven by low voltage

To drive the micro actuator, only 3~10 volts is needed, as shown in Fig. 2.8. It is very low compare to electromagnetic actuator and it is safe to human or animals, so this kind of micro actuator can be used in medical mechanism.

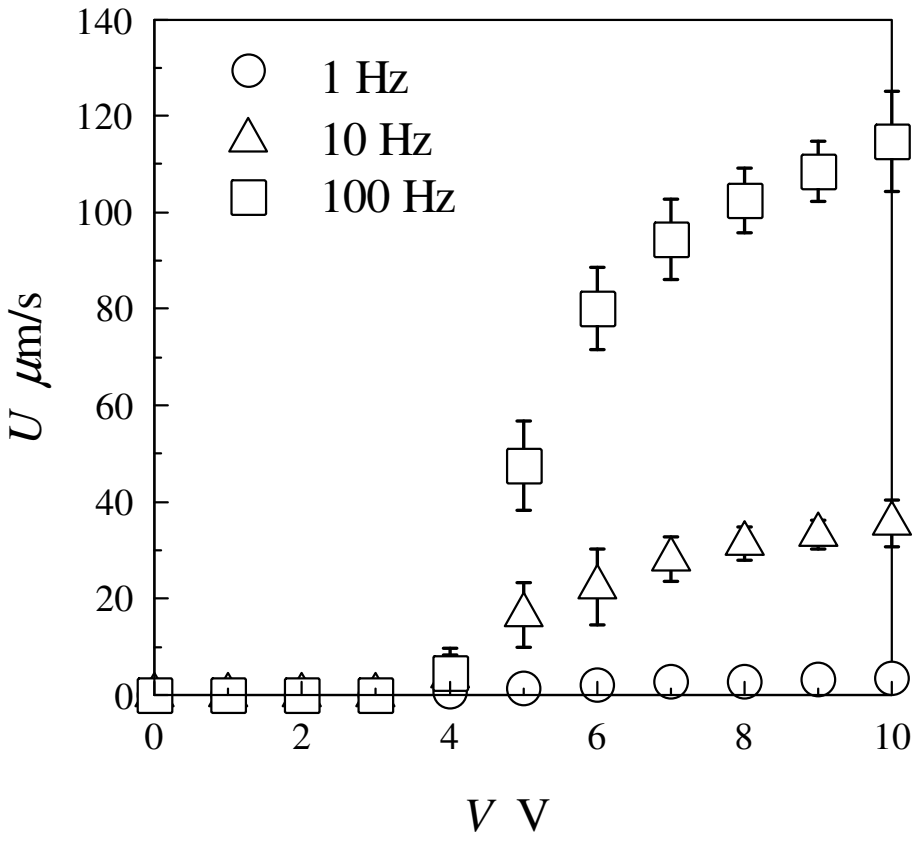

Fig. 2.8 The effect of the voltage of input electric field on the driving speed of liquid crystalline actuator

Simple structure and easy down-sizing

In the liquid crystalline actuator, the energy source can be used to the execution part, that is to say take out the force induced by backflow out of the liquid crystal through the electrode, so the structure of the actuator can be designed to be very simple. At the same time, the aim to reduce exterior size of the actuator can be easily achieved.

Infinite deformation

Liquid crystal has the properties of liquid such as fluidity and no regular

shape, so if it is used to make actuator, there is no limitation for the shape of the actuator. This can offers more flexibility to the designer and bring up the efficiency of the actuator.

Realize of micro manipulation

The average speed of liquid crystalline actuator is about one hundred um/s. the micro manipulation of the actuator can be realized micro meter perfectly.

As the above statement, the liquid crystalline actuator have a expansive application to develop.

Chapter 3

Measurement of Driving Force of Liquid Crystalline Actuator

3.1 Introduction

Liquid crystalline materials are able to be regarded as one of functional fluids,[1-3] and they can convert input factors, such as electric or magnetic energies, a thermal energy, and an optical energy, into output factors. By choosing proper couplings of the factors, the liquid crystals can work as converter devices.[4,5] Recently, Chono and Tsuji proposed actuator devices driven by liquid crystalline flows, which converted electric energy into kinetic energy.[6-8] In comparison with other actuators, liquid crystalline actuators have advantages: (1) low driving voltage, (2) easy downsizing, and (3) high shape adaptability.

In previous works on the liquid crystalline actuators, the effects of the voltage, duty ratio, and frequency of the imposed pulsed electric field, and also the thickness of the liquid crystal layer on the driving speed are studied. However, the driving forces of liquid crystalline actuators are not measured. To utilize the liquid crystalline actuators efficiently, this information on these performances must be collected.

Normally, people measure force by using force sensor directly, which is expensive, has less mechanical robustness, and has limited measuring range. This method is not suitable for measuring the driving force of liquid crystalline actuators because it is too small to be measured.

This chapter presents a driving force estimation method by analyzing the motion trajectories of liquid crystalline actuators. Using the high speed camera, we recorded the motion trajectories for the conditions with different combination of voltage, frequency, and duty ratio of the input electric field. The moving object in image sequences is detected by aligning pairs of images and creating the difference image using active contour algorithms. Then, we computed the driving speed and driving force of the liquid crystalline actuator.

Overall, this chapter describes the proof of concept of a liquid crystalline actuator and the method to estimate the driving force. From the estimated force, we will discuss about the applicability of the liquid crystalline actuators to the micro-devices.

3.2 Experiment

3.2.1 Physical Properties of 5CB

Liquid crystal compounds presently used in these actuators are all derivatives of compounds having this long rod-like structure. The chemical schematics of liquid crystal 4-n-pentyl-4`-n-cyanobiphenyl (5CB) which used in this research, is shown in Fig. 3.1. The chemical formula at top in Fig. 3.1a shows that 5CB has an intrinsic electric dipole polarization triple bond (C=N) moment.

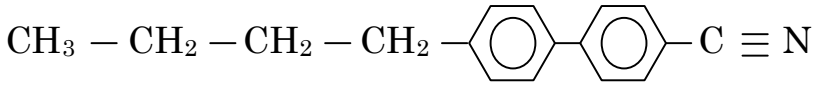

(a) Chemical formula

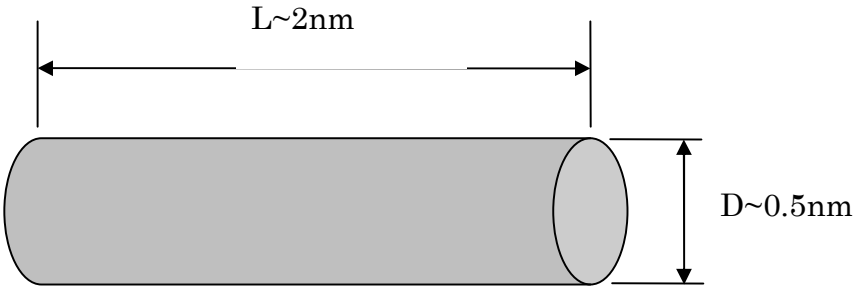

(b) A hard cylindrical long rod

Fig. 3.1 Structure of the liquid crystal 5CB [Yang，2006]

The 5CB molecule obviously is not a perfect cylinder, but owing to random thermal motions and the fact that there are no obstacles to rotation around its cylindrical axis, 5CB molecules can and do rapidly and freely rotate about the long axis, and since standing upright or upside-down is equivalent, 5CB physically can be represented by a hard cylindrical long rod as shown in Fig. 3.1(b). The long rods are used to model uniaxial liquid crystal molecules.

The rod-like shape of liquid crystal molecules means that ht physical properties of the liquid crystal states also possess a degree of anisotropy, i.e., they exhibit different values when measured parallel or perpendicular to the director.

The liquid crystal 5CB has simple phase transitions. It changes from a solid to a nematic liquid crystal at 22.5℃, and melts to an isotropic liquid at 35℃. On

a microscopic level, the rod-like 5CB molecules are locked in place and aligned when the sample is a solid. When the sample becomes a liquid crystal, the molecules are free to translate and can rotate somewhat. Secondly, the physical properties of 5CB are widely measured and tested by many researches. The physical properties of 5CB is shown in Table 3.1.

Table 3.1 Physical properties of 5CB at 26℃

Density	$\rho = 1000\ kg/m^3$
The Frank Elastic Constants	$k_{11} = 6.37\times10^{-12}N$ $k_{22} = 3.81\times10^{-12}N$ $k_{33} = 8.6\times10^{-12}N$
The Viscosity Coefficients	$\alpha_1 = 0$ $\alpha_2 = -0.086\ Pa\ s$ $\alpha_3 = -0.004\ Pa\ s$ $\alpha_4 = 0.089\ Pa\ s$ $\alpha_5 = 0.059\ Pa\ s$ $\alpha_6 = -0.031\ Pa\ s$
The Dielectric Constants	$\varepsilon_{\parallel} = 15.7\times10^{-11}$ F/m $\varepsilon_{\perp} = 5.7\times10^{-11}$ F/m

3.2.2 Liquid Crystalline Actuator Cell Preparation

The first step of the cell preparation deals with the cell substrates with plane electrodes. For this purpose, one may use parallel glass plates covered with a thin metal layer from one side of the plate. In this work, thin layer (~25nm) of Indium Tin Oxide (ITO) is traditionally used as optically

transparent electrode.

The surfaces of ITO substrates were cleaned according to the following procedure:

A thin nematic layer (of 2~10μm) is sandwiched between two substrates, which are glass plates. Near the substrate surface the liquid crystalline molecules can exhibit aligning effects, which can be accentuated by special surface coatings (through certain organic or inorganic films) and/or treatments to allow the director alignment to be controlled. The so called orienting (or alignment) layers force the director to a preferred orientation near their surface. Often, the interaction between the liquid crystal and the surface is strong enough not to allow a change of the direction of n at the boundaries (strong anchoring) even in presence of director gradients within the bulk. The surface treatments combined with the elastic torques ensure the initial homogeneous director alignment of liquid crystal cells (i.e., without spatial variations in the plane of the layer).

Simple and widely used process to achieve homogeneous alignment is rubbing. A coating polymer layer (e.g., polymide, nylon or polyvinylalcohol) is deposited on the glass surface and rubbed repeatedly in the same direction with a soft tissue (cotton cloth). In this manner, the rubbing creates micro-grooves along the rubbing direction in the form of ridges and troughs, as depicted in Fig. 3.2. When the liquid crystal is aligned parallel to the grooves, there is no orientational deformation.

It should be noted that rubbing gives a pretilt to the liquid crystalline molecules that is, one end of the molecule is slightly lifted of some degrees. This speeds up and homogenizes the liquid crystalline realignment under an electric field (avoiding the occurrence of reverse tilt and reverse twist creating different domains).

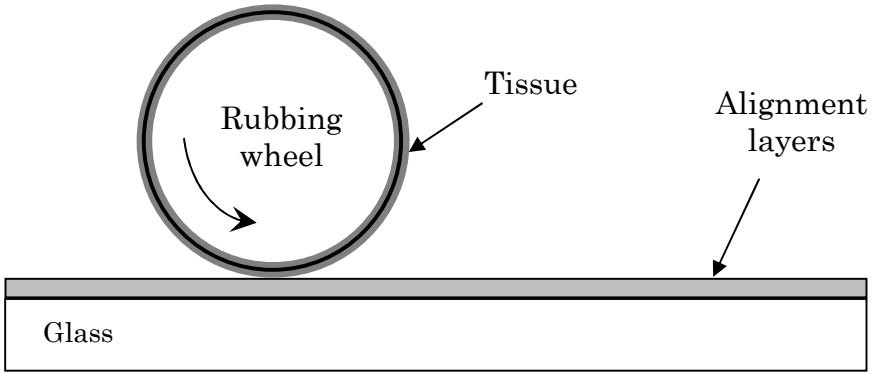

(a)

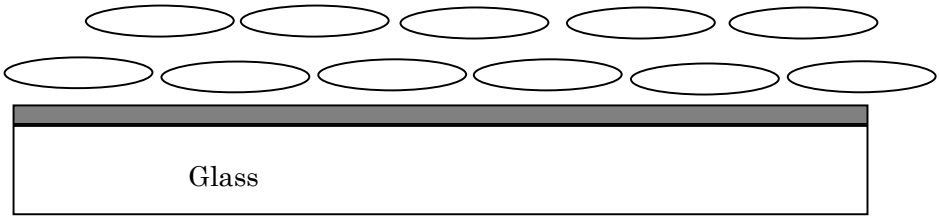

(b)

Fig. 3.2 (a) Roller used for rubbing. (b) In proximity of a surface where grooves are rubbed, liquid crystalline molecules align along the direction of the grooves (In the homogeneous case, the director is parallel to the substrate)

The third step is to prepare the liquid crystalline material. A spacer is used to maintain the cell gap (the distance) between the two glasses.

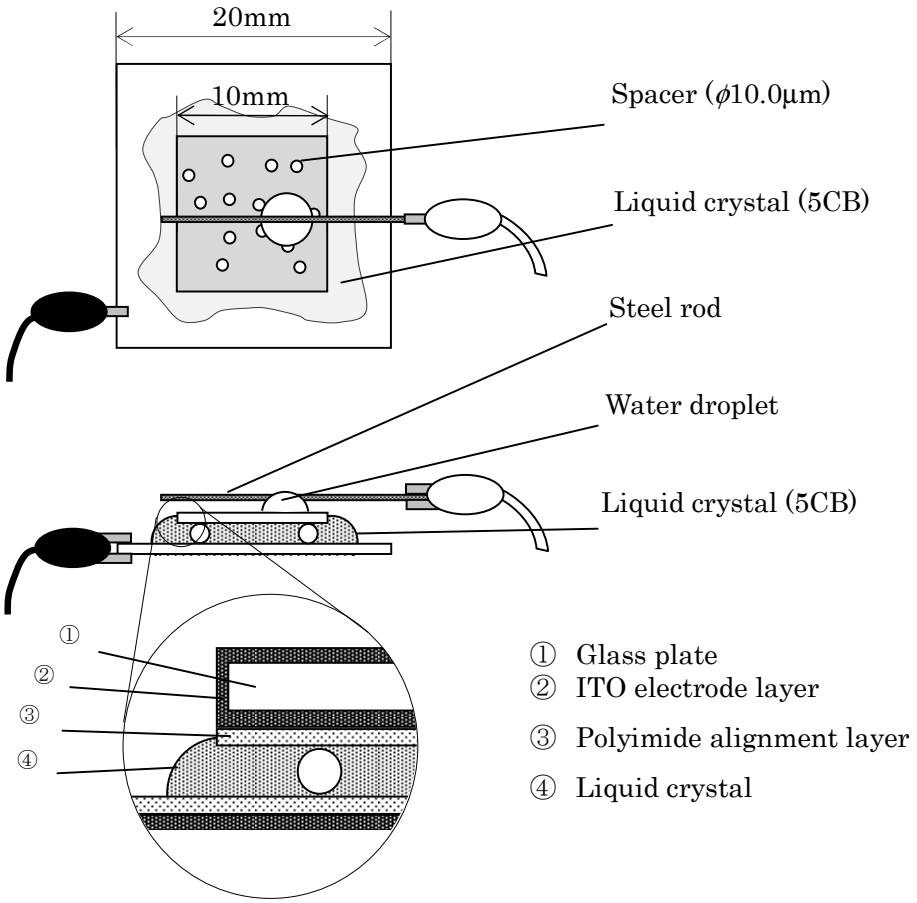

Fig. 3.3 Liquid crystalline actuator cell

Follow the produce as above, the experimental liquid crystalline cell as shown in Fig. 3.3 was prepared. The liquid crystalline material, 4-n-pentyl-4`-n-cyanobiphenyl (5CB), was placed between two parallel glass plates with 10μm gap, which was achieved by mixing small spherical particles of 10μm diameter. The size of the upper glass plate and the lower glass plate are 10×10mm and 20×20mm respectively. The mass of the upper glass plate is about 0.0475g. The bounding glass plates were coated with an optically

transparent ITO layer to apply an electric field onto the liquid crystal, and a thin rubbed polyimide alignment layer to obtain homogeneous molecular orientation field at equilibrium state. An electrode is connected to the upper plate through the steel rod and the water droplet to avoid the contact friction. By applying a pulsed rectangle electric field between the glass plates, liquid crystalline backflow is induced and the upper plate will be driven by the flow.

3.2.3 Experimental Setup

The movement of the upper glass plate of the liquid crystalline cell was monitored at room temperature via a polarizing microscope (Nikon *Optiphot-pol*) equipped with a high speed camera (Photron *FASTCAN-512 PCI*), as shown in Fig. 3.4(a). Images were recorded with a spatial resolution of 512× 256 pixels, corresponding to an image size of 79×39.5μm, and a time resolution of 4000s. Figure 3.4(b) is the photo of the experimental setup.

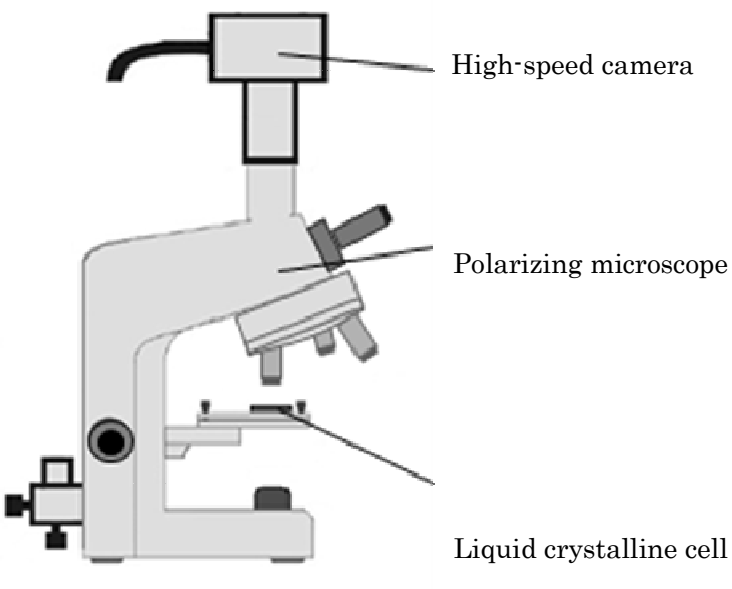

(a)

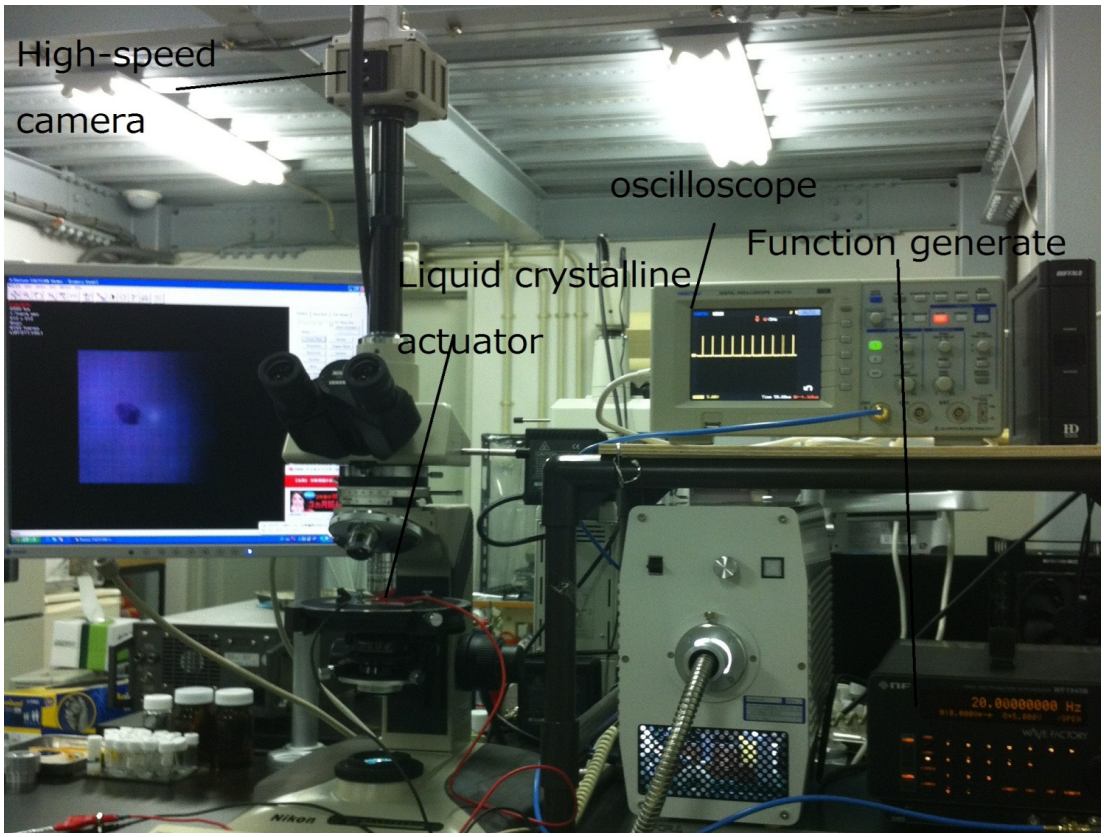

(b)

Fig. 3.4 Experimental setup

The movement of the liquid crystalline actuator is affected by changing the parameters, such as the voltage, frequency, and duty ratio of the input electric field, because the rotation of liquid crystalline molecules can be strongly influenced by these parameters. Electric fields were applied at varying amplitude, frequency and duty radio by a function generator (NF *Wave Factory WF1945B*).

On the other hand, the weight of the upper glass plate of liquid crystalline actuator also affects the movement of the liquid crystalline actuator. In order to meaure the relationship between the movement of the liquid crystalline actuator and the weight of the upper glass plate, every 0.05g as a weight coated with no-charge membrane is placed on the upper glass plate, as shown in Fig.

3.5. Every time we place 0.1g as load on the previous ones symmetrically.

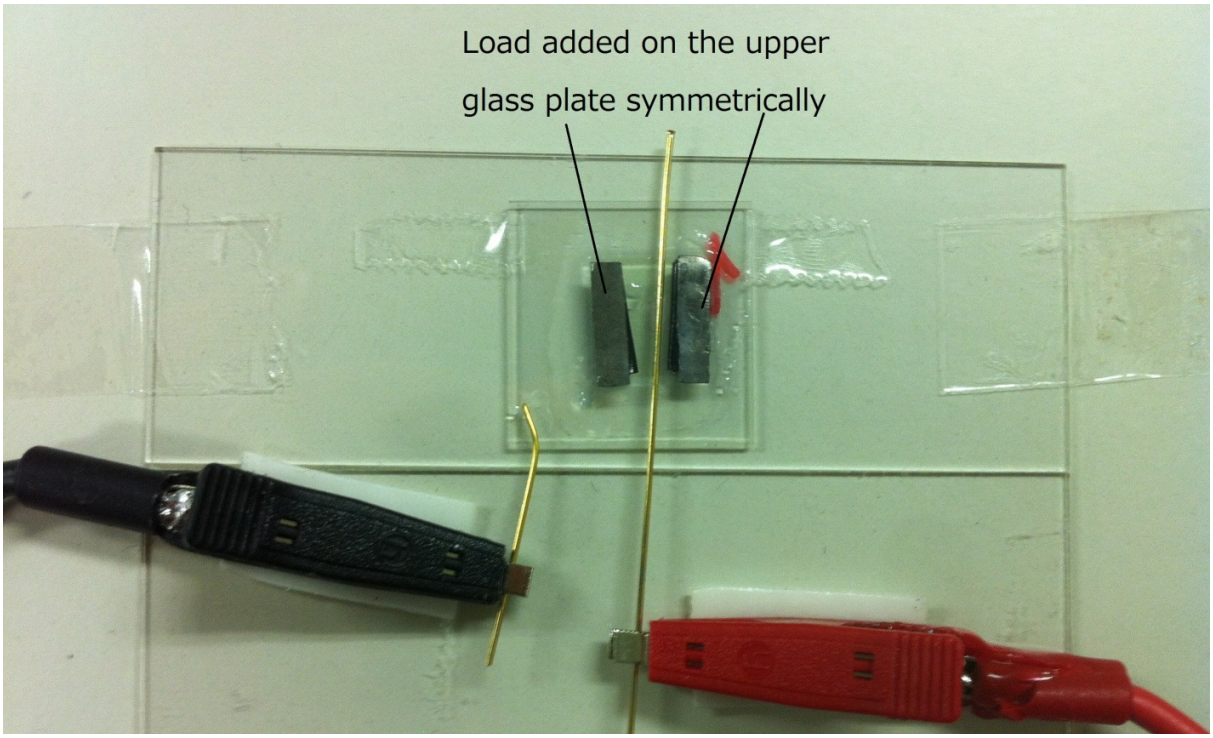

Fig. 3.5 Experimental cell of changing the weight of the upper glass plate of liquid crystalline actuator

3.2.4 Experimental Method

The difficulty here is that the driving force is too small to be directly measured by force sensors. We employed the image processing technique to evaluate the motion trajectory from the subsequent images. Detecting moving object in a video sequence is usually done by aligning pairs of images and creating the difference image. Moving objects can be found in the difference image using algorithms such as clustering, unfortunately image alignment is usually not exact at every image point, and the difference image is noisy, causing false alarms. Another problem with image alignment and subtraction is execution time, as every image point is examined in both the registration, the

alignment, the subtraction, and the clustering.

We employed the image processing to evaluate the driving force from the motion trajectory. According to the distance we evaluated, we can calculate the speed, acceleration and then we can get the force that works on the liquid crystalline actuator. The analyzed method is shown in Fig. 3.6.

We employed the image processing technique to evaluate the motion trajectory from the subsequent images. Subsequent image analysis was carried out with software (DITECT *DIPP-Motion Pro2D*). Motions are determined by analyzing the video images from small changes in brightness that accompanies even sub pixel displacements. As shown in Fig. 3.7, the motion trajectory, the speed and the acceleration can be analyzed by the software.

The driving speed and the driving force at various conditions are calculated from the motion trajectories.

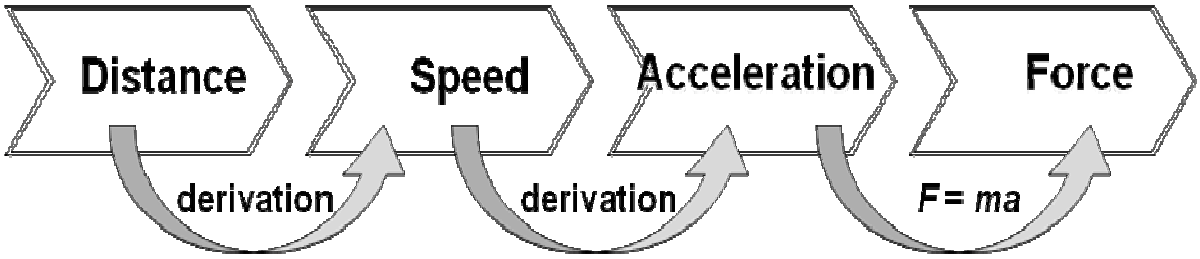

Fig. 3.6 Experimental method

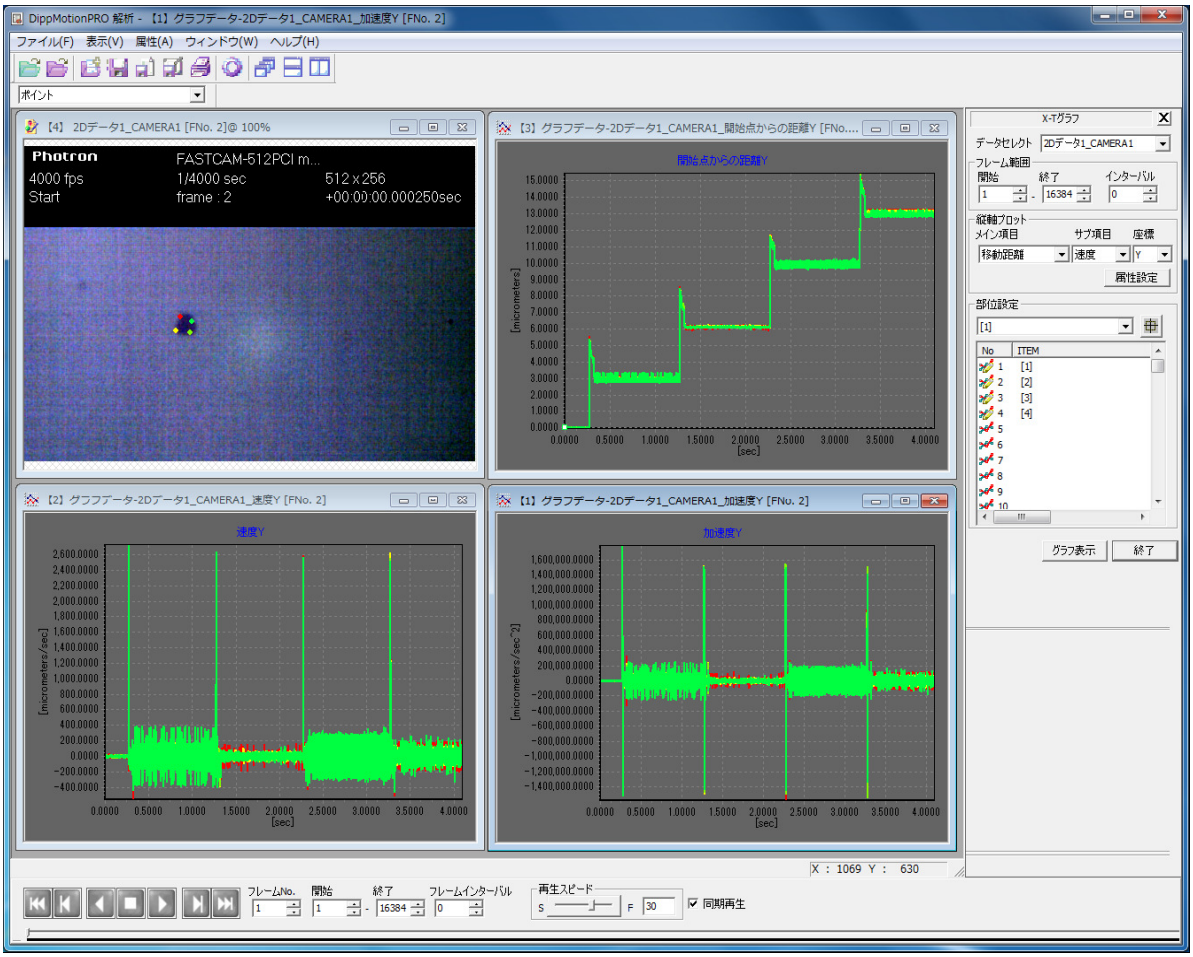

Fig. 3.7 The interface of motion analysis software

3.3 Results and Discussions

3.3.1 Motion Trajectory

In order to examine the influences of the input factors on the motion trajectory of the liquid crystalline actuator, we measured the motion trajectories for the conditions with different combination of voltage, frequency, and duty ratio of the input electric field.

An Example of the Motion Trajectory

Fig. 3.8 shows an example of a time series of the position of the upper plate for the voltage V = 10V, the frequency f = 10Hz, the duty ratio D = 5% of the pulsed voltage, and the mass of the upper glass plate $m \approx 0.0475$g.

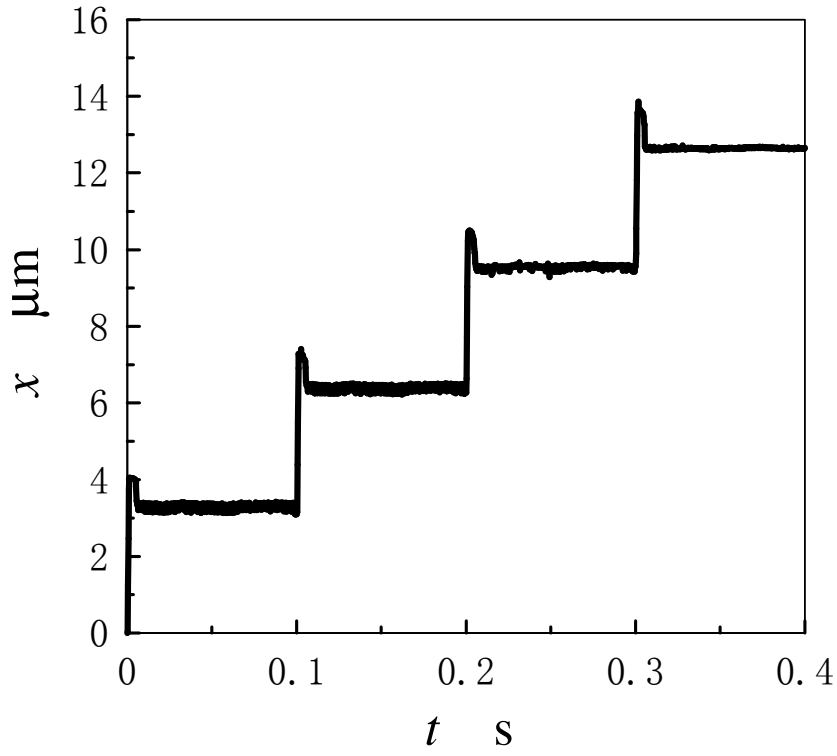

Fig. 3.8 The location of the actuator as the function of the time (V = 10V, f = 1Hz, D = 5%)

The vertical axis of the figure is the position x along the moving direction of the upper plate. The step-like movement of the upper plate is observed. The rapid increase in the position arises every 0.1 second at which the voltage is turned ON. At this time, the electric field forces the molecular orientation to rotate to align parallel to the field inducing the backflow. It also should be noticed that a small backward movement occurs in a short time after the forward movement. To see the detail of the motion of the upper plate, a part of Fig.3.8 (t = 0~0.02s) is zoomed up in Fig.3.9. The movement of the upper plate

after the voltage turned ON finishes at about $t \approx 1$ms and the upper plate keeps its position until the voltage is turned OFF at $t = 5$ms. When the voltage is turned OFF, the backward movement of the plate occurs because of the rotation back of the molecular orientation to the orientation at the equilibrium.

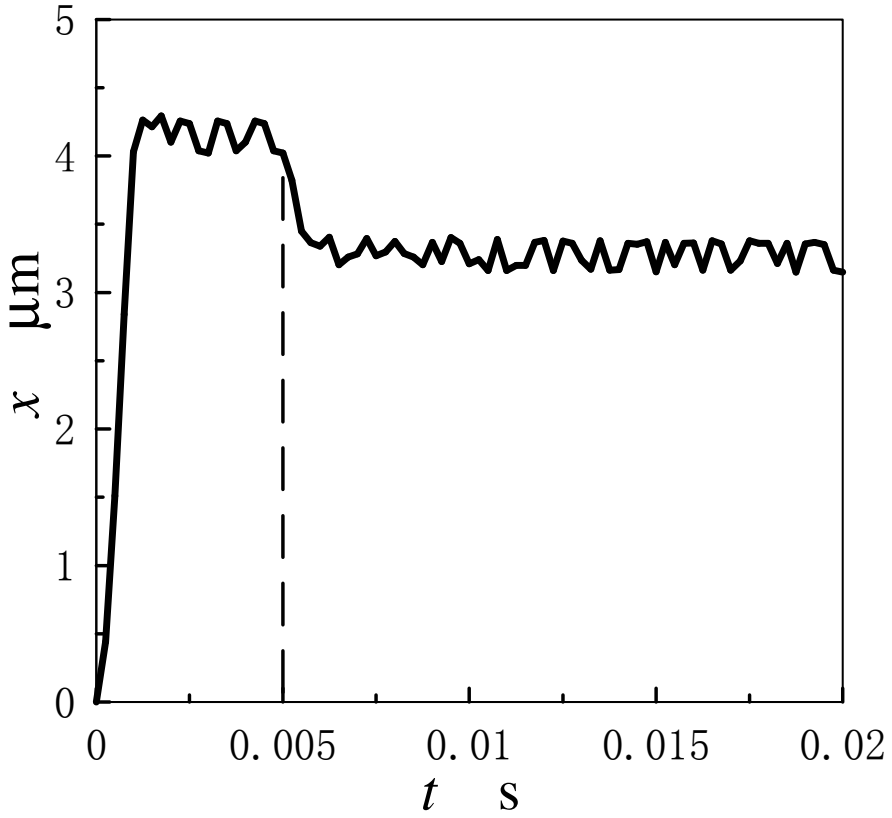

Fig. 3.9 The location of the actuator as the function of the time
$t = 0$~0.02s ($V = 10$V, $f = 1$Hz, $D = 5\%$)

For explaining the motion trajectory of the liquid crystalline actuator, the schematics of the actuation of liquid crystalline cell are shown in Fig. 3.10. When the voltage is turned ON, the molecular directions, which are parallel to the boundary plates at the equilibrium, as shown in Fig. 3.10(a), are forced by the electric field to rotate to align parallel to the field, as shown in Fig. 3.10(b). The molecules near the glass plates rotate at a small angle because of an anchoring effect and the molecules in the center region between the plates can

rotate about 90°. The rotating molecules induce the backflow and the upper glass plate is driven to move, as shown in Fig. 3.10(c). When the voltage is turned OFF, the backward movement of the upper plate occurs because of the relaxation of the molecular orientation field to the equilibrium, as shown in Fig. 3.10(e). The inverse rotation of the molecules at the relaxation stage induces a relatively small backward flow and the upper glass plate has a little backward movement, as shown in Fig. 3.10(f).

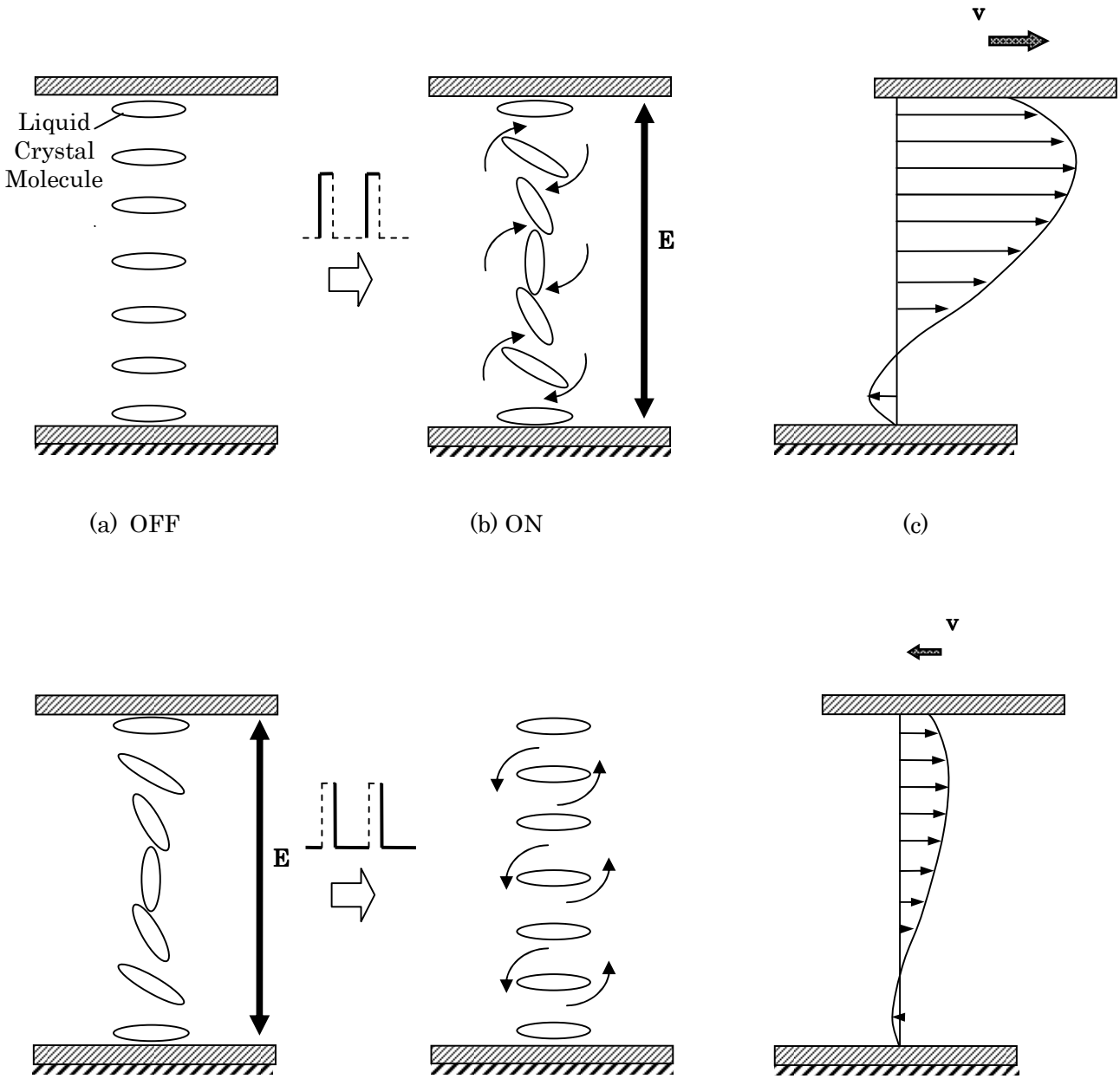

Fig. 3.10 Schematics of the molecular orientation field and the backflow in the liquid crystalline actuator

Noise Source

When a device (such as camera or scanner) captures an image, the devices

sometimes bring extraneous noises to the image. This noise must be removed from the image for other image processing operations to return valuable results.

There is an obvious problem existed in the data shown in Fig. 3.8. Due to the fluctuations in the liquid crystalline molecular configurations, a microscope light source and the image sensor of the high speed camera, the obtained data includes noises.

Because the high frequency noises, shown in Fig. 3.11 which is the amplitude spectrum of $x(t)$ of Fig. 3.8, will be amplified when the data is differentiated, the high frequency noises must be removed.

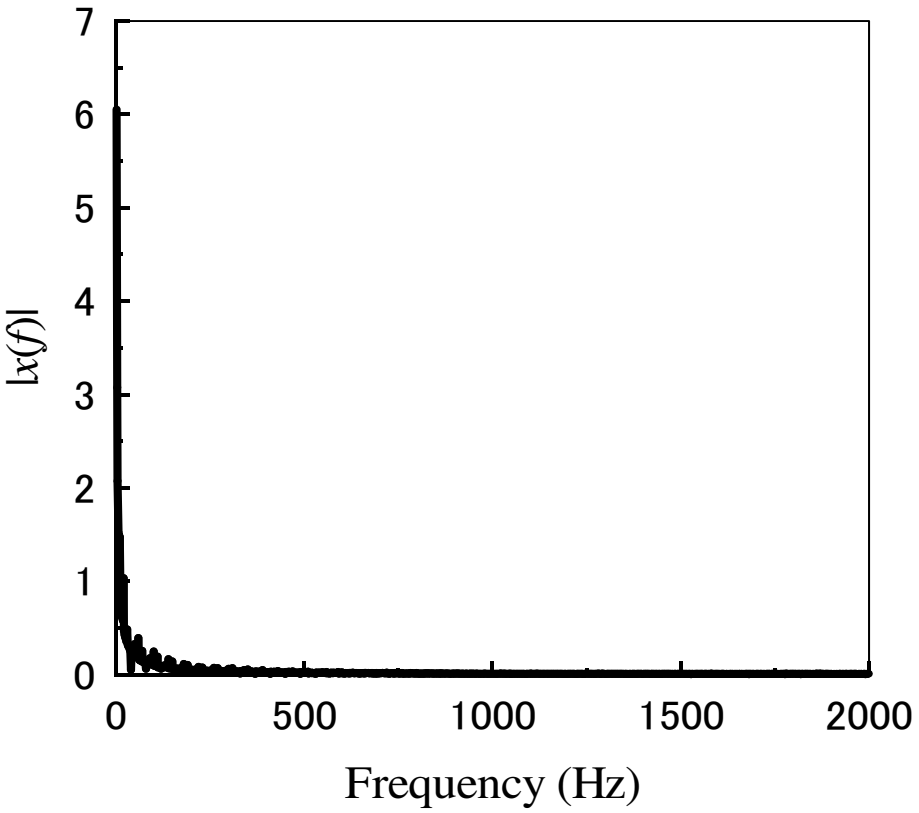

Fig. 3.11 The amplitude spectrum of $x(t)$ of Fig. 3.8

Noise Reduce

We applied the fast Fourier transform (FFT) to the position data to reduce

the high frequency noises. Applying the FFT to the position data of Fig. 3.9 is shown in Fig. 3.12. The red line is the original data and the blue one is the data after reducing noise. It can be seen that the position data maintains the motion trajectory.

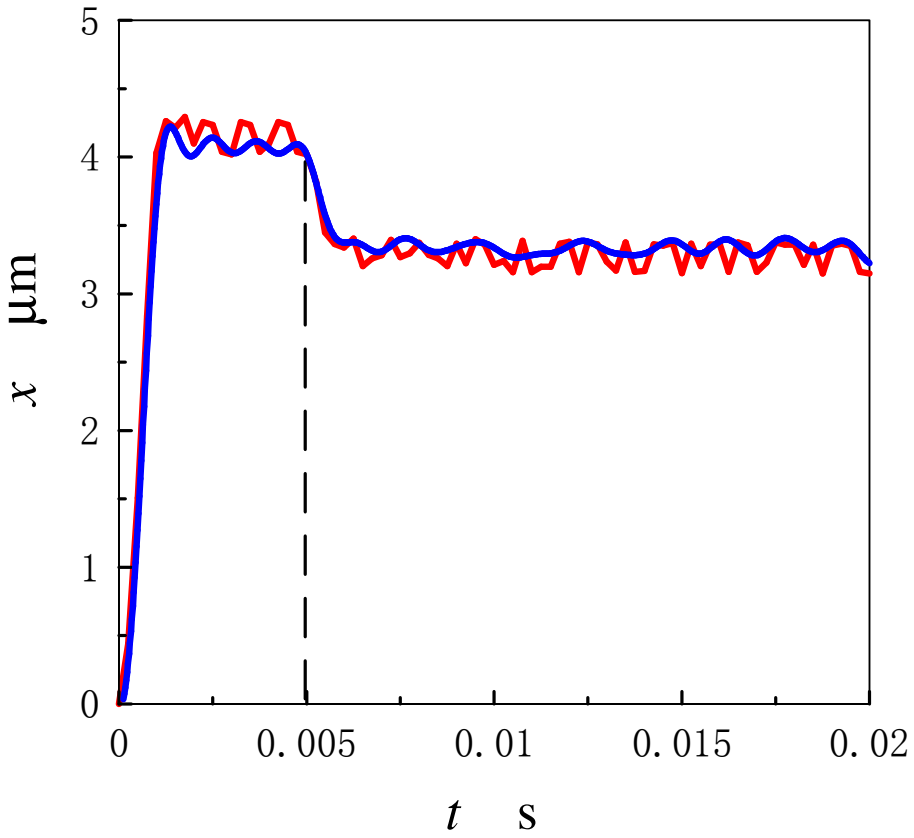

Fig. 3.12 The location of the actuator as the function of the time t = 0~0.02s after reducing noise

Motion Trajectory at Different Conditions

The displacement of the upper plate can be affected by the applied voltage. Fig. 3.13 shows the movements of the upper glass plate for the frequency f = 1Hz and the duty ratio D = 5% of the voltage V = 10V. Fig. 3.13 shows the movements of the upper glass plate for the frequency f = 1Hz and the duty ratio D = 5% of the voltage V = 6V. Compare with these two figures, the displacement

in one cycle (about 1μm) for the voltage V = 6V is much smaller than that for the voltage V = 10V (about 6μm). The rotation speed of the molecules is proportional to the square of the strength of the electric field. Thus, for the lower voltage case, the rotation speed of the molecules is lower and the induced flow also smaller. Then, the moved distance of the upper plate in one cycle is smaller for lower voltage.

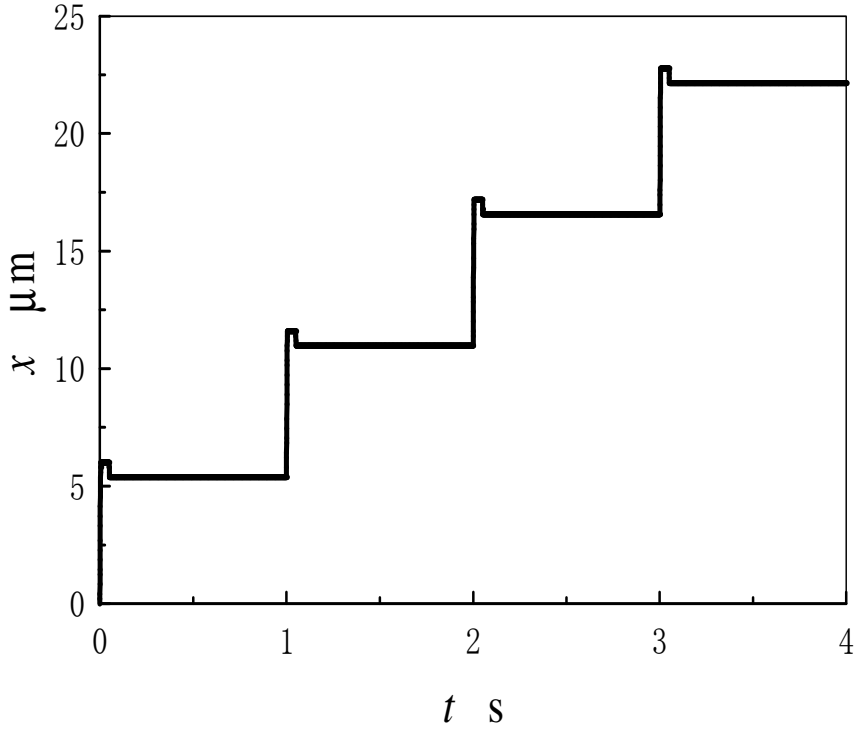

Fig. 3.13 The location of the actuator as the function of the time (V = 10V, f = 1Hz, D = 5%)

The duration of the ON-state of the applied field also influences the movement of actuator. Fig. 3.15 shows the movements of the upper glass plate for duty ratio D = 50%, with the frequency f = 1Hz and the voltage V = 10V. In this case, the duty ratio is 50%, and thus the backward movement occurs at t = 0.5s.

Fig. 3.16 shows the movements of the upper glass plate for the frequency f = 50Hz and the duty ratio D = 5% of the pulsed voltage V = 10V. The moved

distance of the upper plate in one cycle for the frequency f = 50Hz is about 2μm and smaller than that for the frequency f = 1Hz, which is about 6μm. When the frequency is 1Hz, the molecules have enough time to rotate until they are parallel to the applied field direction at ON-state period, as shown in Fig. 3.17(a). However, for the frequency f = 50Hz, the molecules start rotating back before the molecular orientation reaches the direction parallel to the applied field direction, as shown in Fig. 3.17(b), because of short-ON state period. On the other hand, the moved distance per one second is larger for f = 50Hz, since the number of the actuation cycle per unit time is higher than that for f = 1Hz.

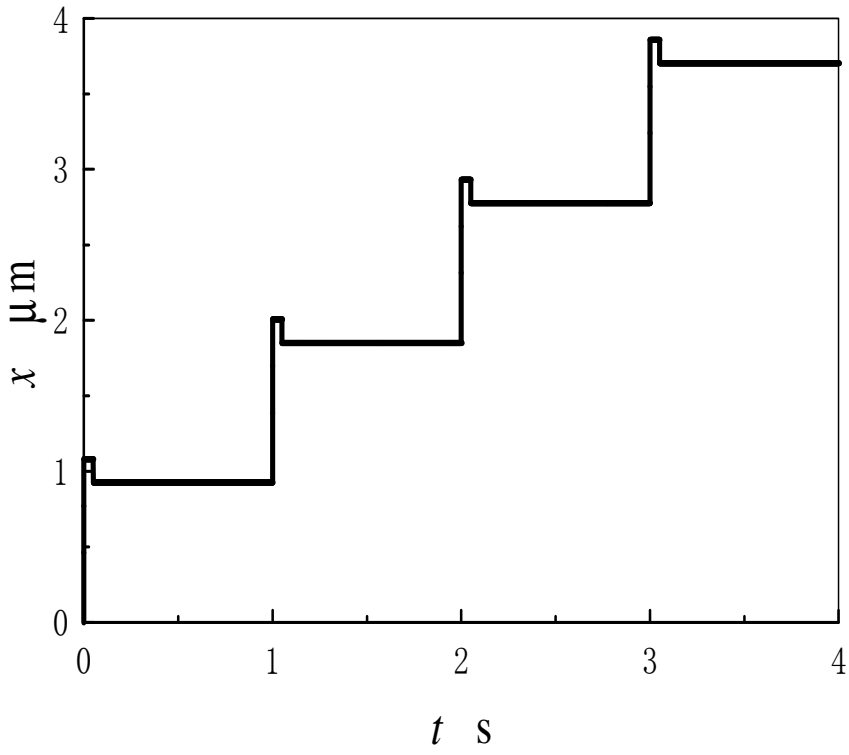

Fig. 3.14 The location of the actuator as the function of the time (V = 6V, f = 1Hz, D = 5%)

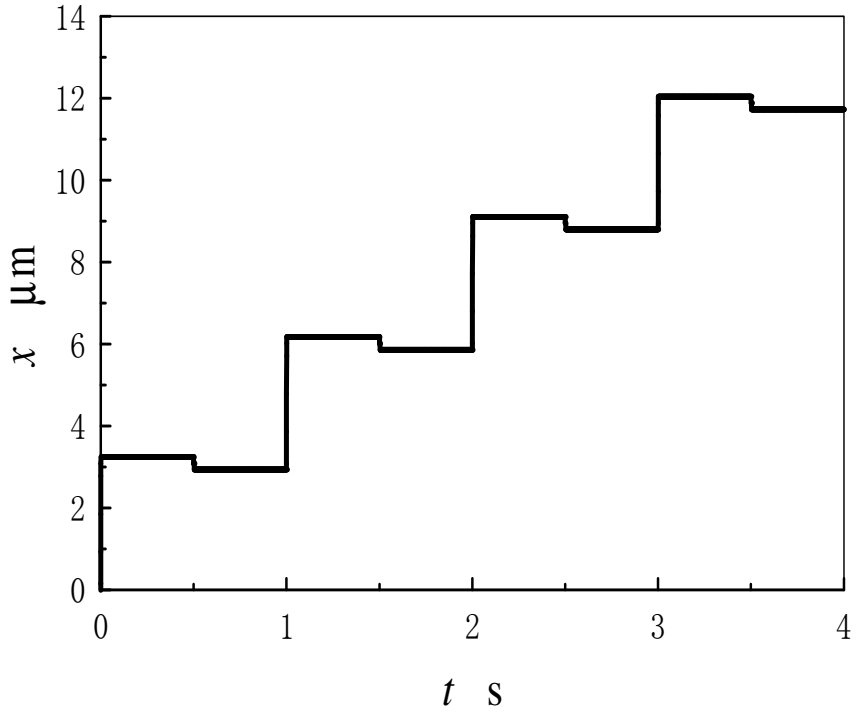

Fig. 3.15 The location of the actuator as the function of the time (V = 10V, f = 1Hz, D = 50%)

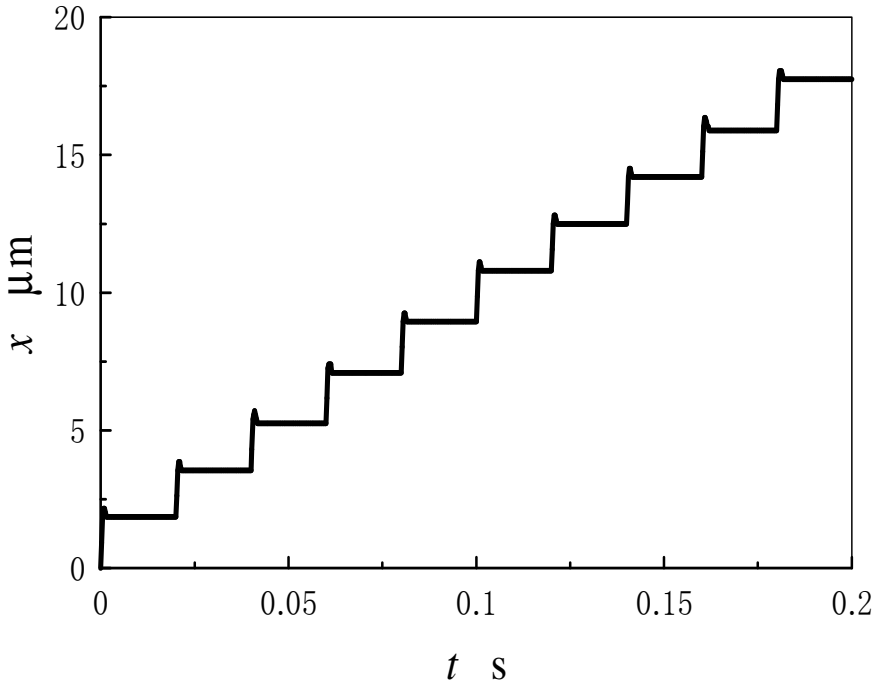

Fig. 3.16 The location of the actuator as the function of the time (V = 10V, f = 50Hz, D = 50%)

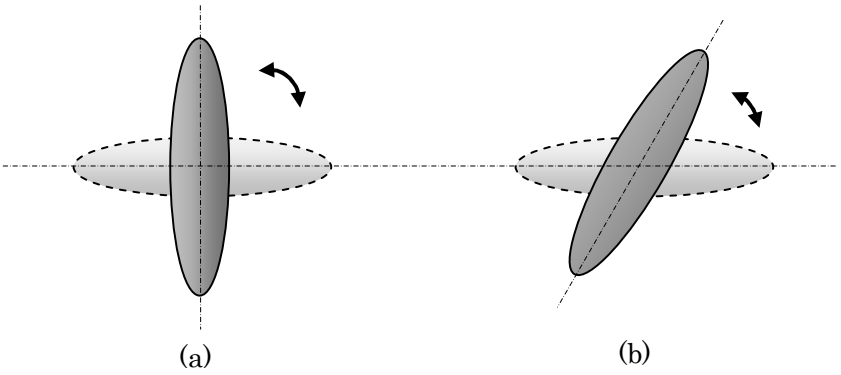

Fig. 3.17 Schematics of the molecular rotation

The upper glass plate of the liquid crystalline cell shows the step-like periodic movements when the pulsed electric field is applied. A large forward movement and a small backward movement of the upper glass plate of the liquid crystal cell are observed corresponding to the turn ON and OFF of the electric field.

3.3.2 Driving Speed

The averaged driving speed of the upper glass plate can be derived from the motion trajectories.

The effect of the applied voltage and the frequency

Figure 3.18 shows the averaged driving speed of the upper glass plate for V= 2, 4, 6, 8, and 10V, and f = 1, 10, and 50Hz. As the applied voltage increase, the averaged driving speed increase because of the higher molecular rotation speed. However, for the voltage higher than a certain critical value, the liquid crystalline material meets the hydroelectric instability and the induced flow field will be disordered. Under the instability, the induced flow can't be a driving source of the liquid crystalline actuator. Thus, one must choose the proper input voltage. The averaged driving speed also increases with increasing of the frequency of the applied pulsed voltage. It is reported that the averaged driving speed of the liquid crystalline actuators becomes the

maximum at $f \approx 120$Hz. As mentioned above, the driving speed becomes higher for the higher frequency. However, for the frequency higher than 120Hz, the molecular rotation behavior can't follow the pulse of the applied electric field and the driving speed decreases.

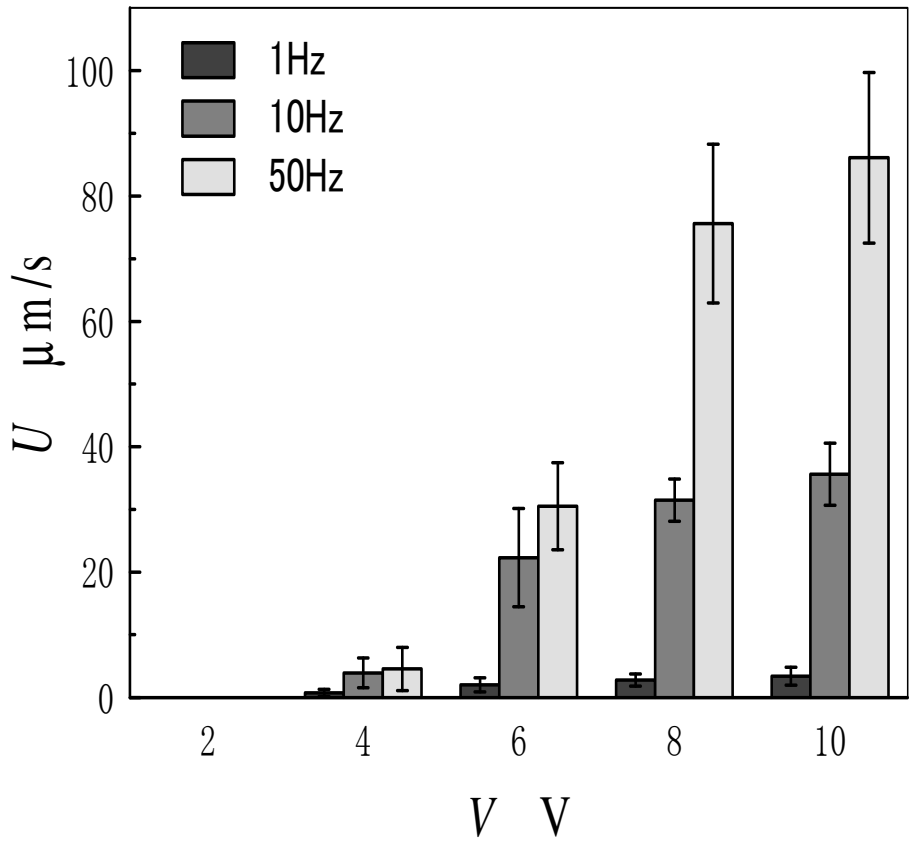

Fig. 3.18 Effect of applied voltage on the average driving speed of the upper plate

The effect of the Duty ratio of the applied voltage

Figure 3.19 shows the effect of the duty ratio on the averaged driving speed of the upper glass plate. The averaged driving speed decreases with increasing duty ratio. Since the OFF-state period of the pulsed electric field decrease with increasing duty ratio and the time for the backward rotation of molecules becomes insufficient, the flow becomes weak for higher duty ratio.

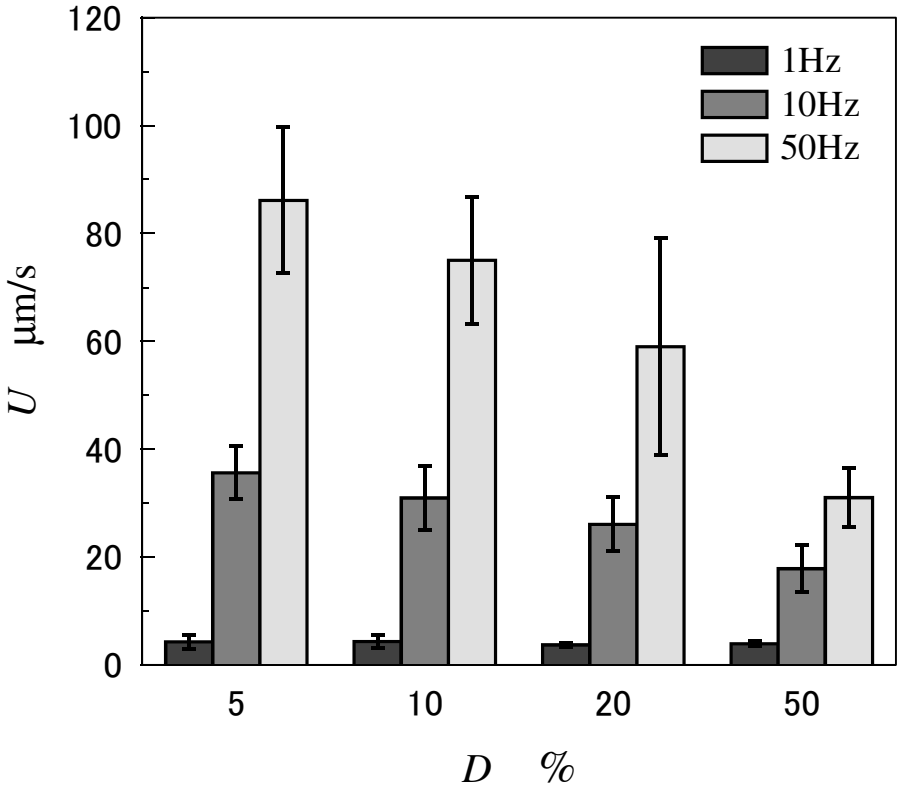

Fig. 3.19 Effect of the Duty ratio of the applied voltage on the average driving speed of the upper plate

The effect of the mass of the upper plate

The effect of the mass of the upper plate on the average speed of the upper plate is shown in Fig. 3.20. Comparing the data for the frequency of 1Hz, 10Hz, and 50Hz, we may conclude that the average driving speed in the higher frequency is faster than that in the lower frequency. Although the maximum instantaneous speeds are equal for different frequency, as shown in Fig. 3.21, the period for positive movement becomes shorter for high frequency. In addition, the upper plate is driven 50 times per second for f = 50Hz by the molecular rotation compared to f = 1Hz, thus the actuator moves fast for the high frequency. On the other hand, the results suggest that as increasing the loads on the actuator, the driving speed almost linearly decreased. In order to explain this observation, we record the effect of the mass of the upper plate on the instantaneous driving speed of the upper plate, as shown in Fig. 3.22. From this

figure, we can find that as increasing the weight of the upper glass plate, the maximum instantaneous speed is decreased linearly. In this research, we just increase the loads to 0.8g. Because when the loads become heavier than about 1g, the driving force is insufficient to overcome the static friction. At this condition, the driving force cannot be measured from the movement of the liquid crystalline actuator.

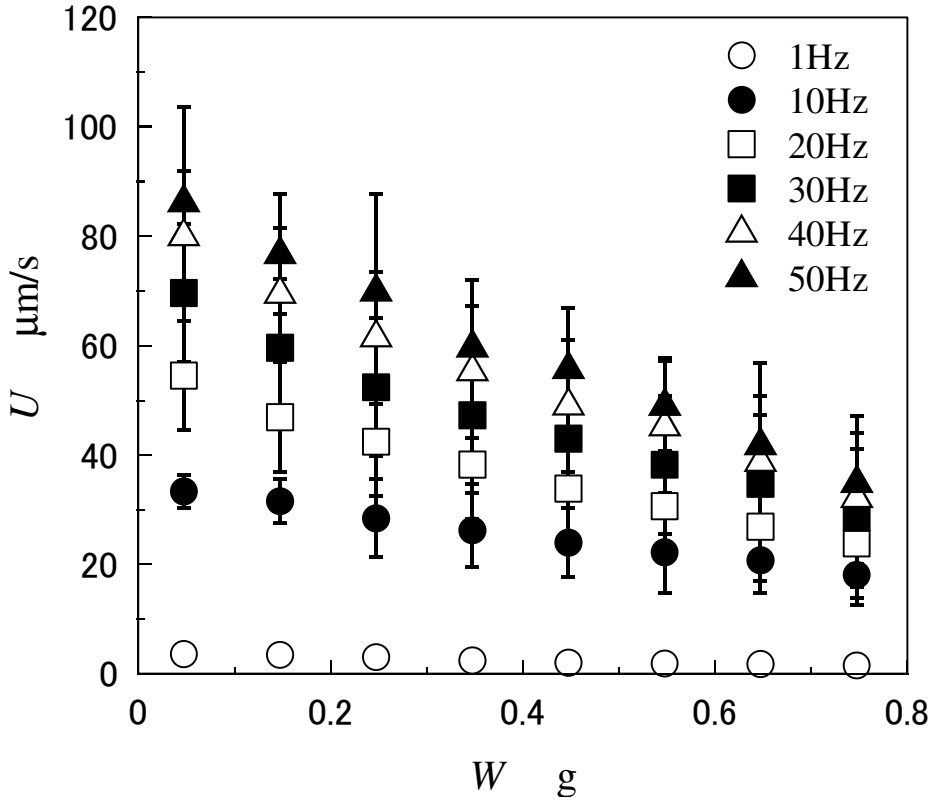

Fig. 3.20 Effect of the mass of the upper plate on the average driving speed of the upper plate

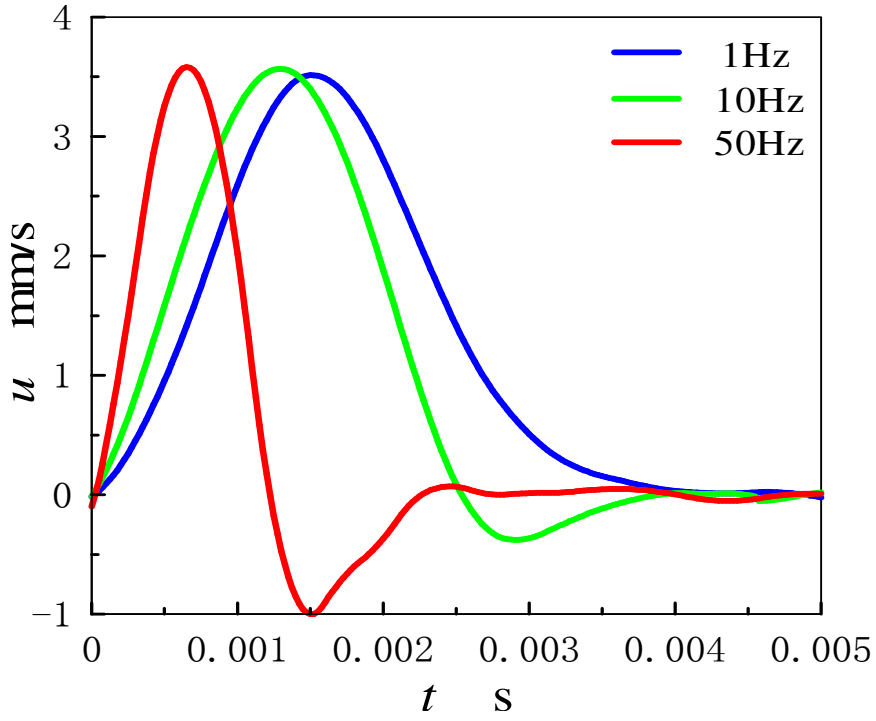

Fig. 3.21 Effect of the frequency of the applied voltage on the instantaneous driving speed of the upper plate

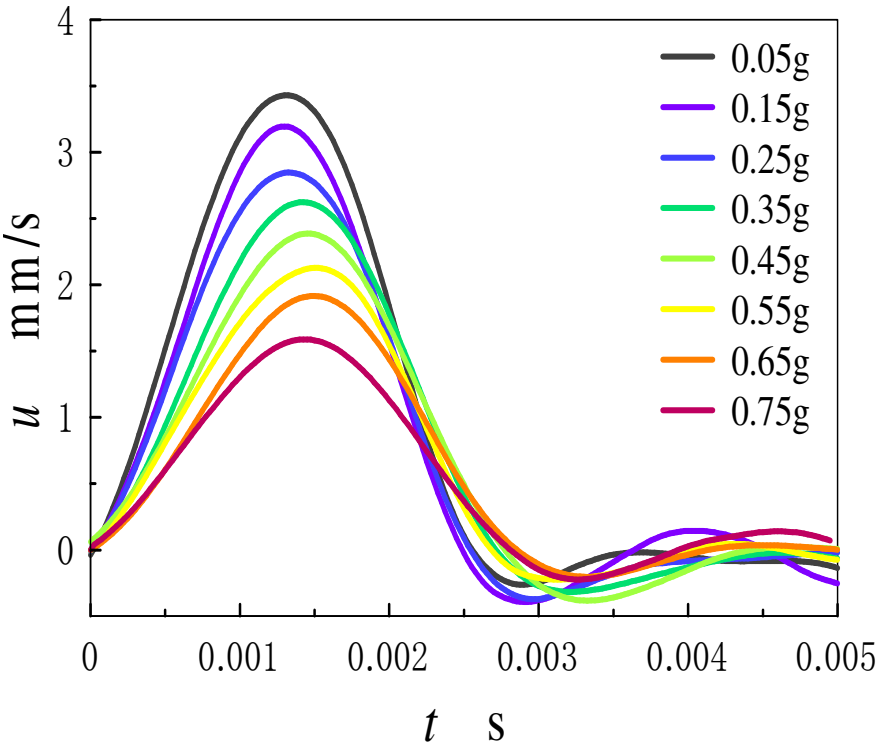

Fig. 3.22 Effect of the mass of the upper plate on the instantaneous driving speed of the upper plate

The averaged driving speed of the upper glass plate increases with increasing the voltage or frequency of the pulsed electric field and decreases with increasing the duty ratio. It is found that the speed can be controlled by these input factors.

3.3.3 Driving Force

Force Analysis

The driving force of the liquid crystalline actuator used in this work is too small to be measured directly. Thus, we have estimated the total force F acting on the upper glass plate by differentiating the time series of the driving speed as:

$$F = m \frac{\Delta u}{\Delta t} \tag{3.1}$$

Here, m is the weight of the upper glass plate, Δu the increment of the driving speed in Δt, and Δt the time between sequential frames of the video (1/4000s).

The resulting force from the Eq. 3.1 must include the driving force generated by the liquid crystalline flow, the friction between the spacer particles and the glass plates, and the surface tension at the edge of the upper glass plate. The surface tension at the edge of the upper glass plate and the friction between the spacer particles and the glass plates are against the movement of the upper glass plate. They are strongly depends on the embodiments of the liquid crystalline actuators. The total force acting on the upper glass plate can be written as:

$$F = m \frac{\Delta u}{\Delta t} = m \frac{du}{dt} = \tau A - \mu mg - \gamma L \tag{3.2}$$

$$F_{LC} = \tau A \tag{3.3}$$

Here, Δu the increment of the driving speed in Δt, and Δt the time span between the sequential frames. A the area of the upper glass plate, μ the friction coefficient, γ

surface tension coefficient, L the length along the upper glass plate edge, and τ the shear force by the backflow.

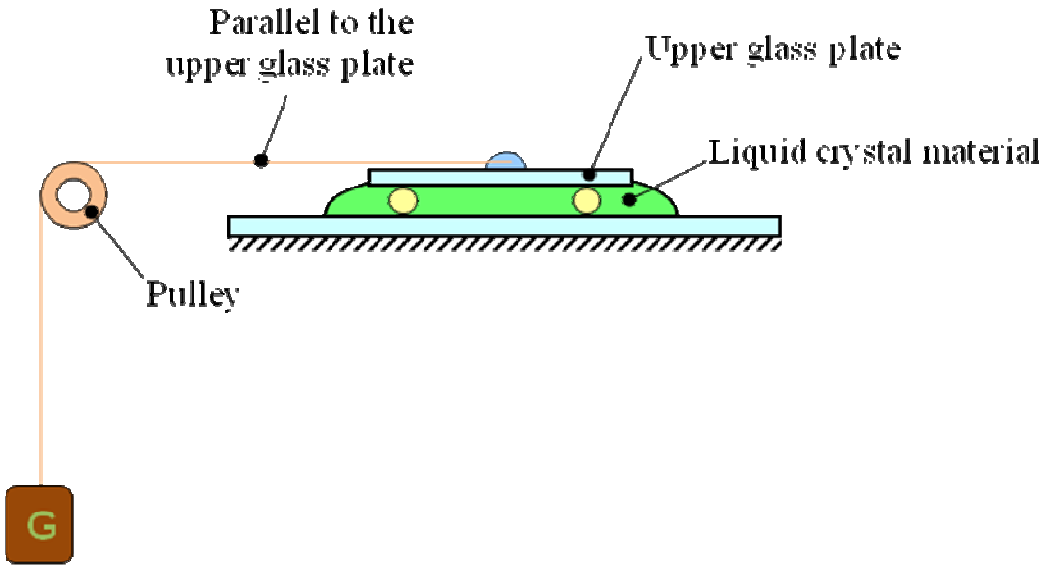

Fig. 3.23 Experimental setup for measuring the resistance forces

In the experiment of resistance forces measurement, the lower plate was secured, and the upper plate surface slides over the lower one, as shown in Fig. 3.23. Without electric fields, the director n was uniformly oriented along the preferred direction. The weight which was bypass through a pulley parallel with the plates supporting the upper surface measured the friction force between the surfaces, which were recorded on chart recorder as a function of time. The weight was suspended by long strings with its shaft connected to the upper plate. A wide range of sliding velocities was carried out with various weights. The sliding is smooth and liquid-like for the nematic phases.

A simple analysis accounts for these experimental observations. We consider several mechanisms that contribute to the total friction factors acting on the interface.

First, in fluid-glass lubrication, the friction coefficient is partly determined by the viscosity of the lubricant. Nematic liquid crystals are relatively good lubricants and additives. When a sufficient voltage is applied, the director of liquid crystal tends to be parallel to the field. This causes a marked increase in viscosity for the backflow across the field, which is called the electro-viscous effect. According to that, by using parallel

orientation surfaces, if the effects of pressure and temperature can be neglected, the necessary voltage, in order to realize the system, we applied the voltage about 10V.

Second, the surface tension coefficient of the glass-5CB interface is constant at a temperature. Surface tension, represented by the symbol τ is defined as the force along a line of unit length, where the force is parallel to the surface but perpendicular to the line. Surface tension is therefore measured in forces per unit length. In this experiment, at temperature 25℃ (5CB has the nematic phase about 23-35℃), the upper plate is square and each side of length is L. The upper plate will be pulled by a force equal to $4\tau L$ (the factor of 4 is because the upper plate has four equal sides).

Third, we considered an idealized case for the liquid crystal cell that assumed the microspheres mixed in the liquid crystal were perfectly smooth and kept their configuration even the load of the upper plate increasing. Suppose the upper plate rested on the particles and that at the region of contact was considered to be plane so that the relation motion between the upper plate and microsphere particles was considered to be rolling friction.

It is accepted that friction between two solid surfaces is due to the opposition of surface asperities on the one hand and surface adhesion on the other. Friction is independent of the contact area (Amontons law). The friction force is measured as the resistance opposed to the movement of a body submitted to both a vertical pressure P and a horizontal force F_s. The friction coefficients between the glass plate surface and microspheres, μ, is defined by the relation: $\mu = F_s / P$.

Finally, the viscosity coefficients generally measured in shear flow for nematic liquid crystal 5CB ordered by electric field is η which for the liquid crystal with its director parallel to the flow direction. In general, the friction force of the liquid crystal cell F_s does not point along v_∞. Shear stress σ is the force that a flowing liquid exerts on a surface, per unit area of that surface, in the direction parallel to the flow. After a steady shearing flow has been imposed on a fluid for a suitable period of time, the shear stress often comes to a steady state, $\sigma(\dot{\gamma})$, which depends on the imposed shear rate $\sigma(\dot{\gamma})$.

In nematic phases, the friction force decreases with increasing sliding velocity. This indicates an increased ordering with increasing shear rate; that is molecules are given less time to relax back to an entangled or disordered configuration, which increases the fluidity. This is consistent with the shear thinning observed in the viscosity measurements.

According the above elaborate, we can get the equation as follow:

$$G-(\gamma_{LC}\upsilon+\mu mg+\gamma L)=0 \tag{3.4}$$

We measured the different sizes of the upper glass plate, which is 10×10mm, 15×15mm and 20×20mm, respectively. According to the equation (3.4), the physical constants μ and γ were measured as $\mu \approx 0.1276$ and $\gamma \approx 33.6\times10^{-3}$N/m, respectively.

Reduce Discrete Error

The discrete displacement was analyzed from the subsequent images. a is the acceleration of the upper plate, which is obtained by differentiating the displacement function twice.

$$v=\lim_{\Delta t\to 0}\frac{\Delta x}{\Delta t} \tag{3.5}$$

$$a=\lim_{\Delta t\to 0}\frac{\Delta v}{\Delta t} \tag{3.6}$$

According to the equations (3.5), (3.6), as Δt dwindles approaching to zero, the instantaneous velocity and instantaneous acceleration approaches a limiting value which is the velocity and acceleration at that instant.

In this work, we use the method of spline to eliminate the effect of the limited frame speed of high-speed camera. A spline is a sufficiently smooth piecewise-polynomial function. In interpolating problems, spline interpolation is often preferred to polynomial interpolation because it yields similar results, even when using low-degree polynomials, while avoiding Runge's phenomenon for higher degrees. On the hand, the splines are popular curves because of the simplicity of their

construction, their ease and accuracy of evaluation, and their capacity to approximate complex shapes through curve fitting and interactive curve design. Cubic spline can produce a curve that appears to be seamless over all the data and the second derivative is continuous. Thus the spline interpolation reduced the discrete problem in some extent.

Fig. 3.24 show the speed and the acceleration of the upper plate differentiated from the position data of Fig. 3.8 after using FFT to reduce noises and using spline to reduce the discrete error. The speed and acceleration reach to their maximum values at the onset of every cycle, and then they decrease. Because as the molecules gradually rotate away from the equilibrium, the elastic torque of the molecule becomes larger to resist the driving force generated by the electric field. When the voltage is turned OFF, the driving force disappears. The speed and acceleration reach to negative maximum values and finally to zero by the elastic torque.

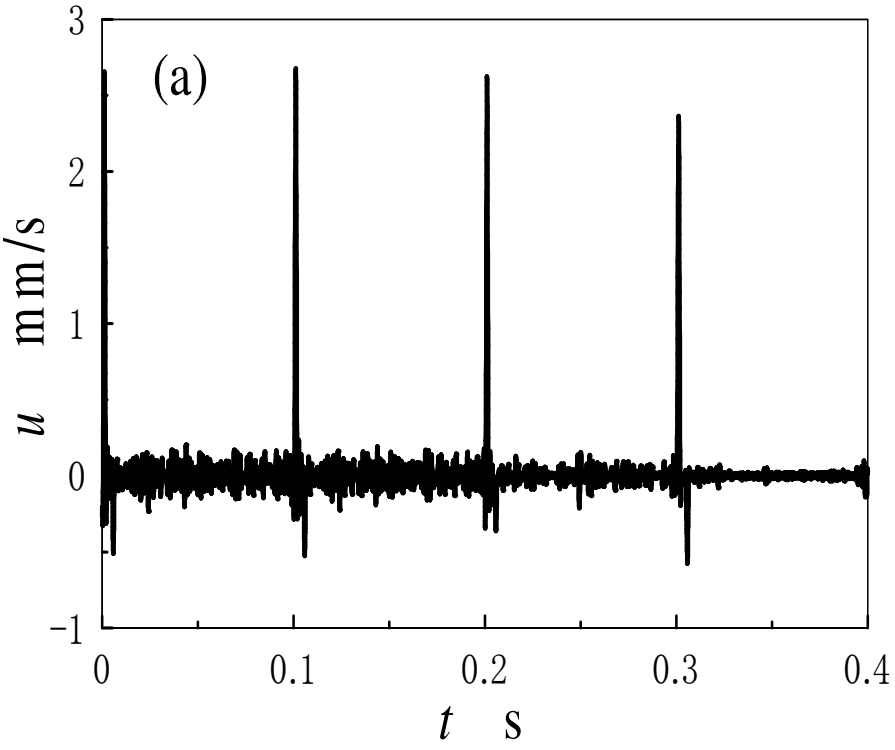

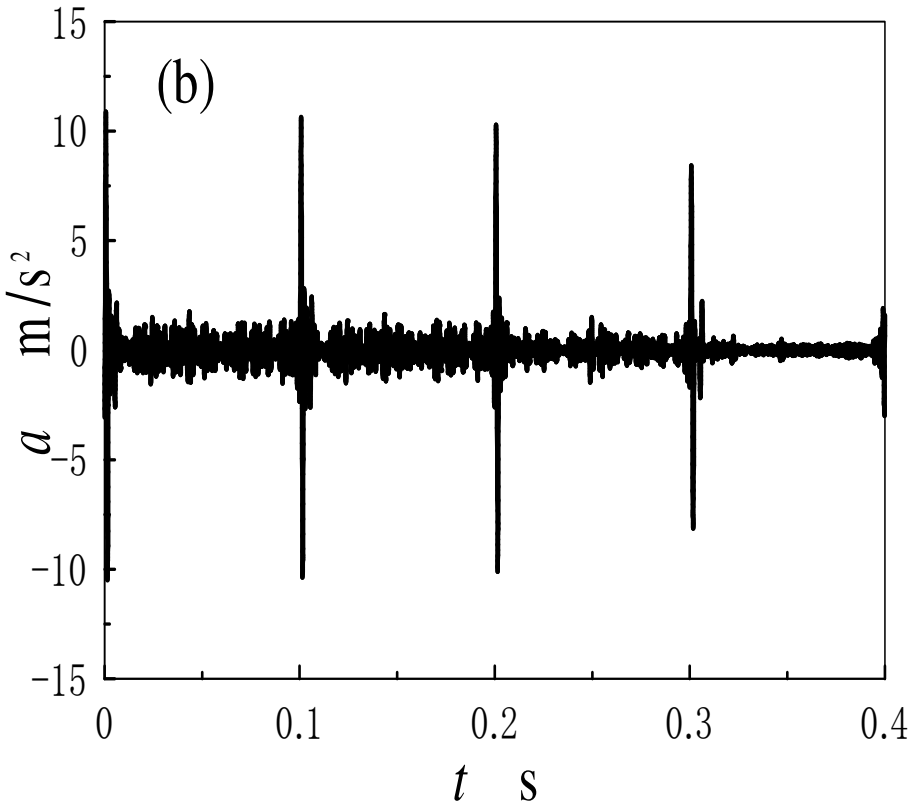

Fig. 3.24 (a) The velocity of the actuator as the function of the time (b) The acceleration of the actuator as the function of the time

The effect of the applied voltage and the frequency

Figure 3.25 shows the effect of the applied voltage on the maximum driving force per unit area generated by the liquid crystalline flow. Although the driving speed drastically increases with the voltage, as shown in the Fig. 3.20, the maximum driving force shows only slight increase with the increase of the applied voltage. The order of the maximum force is of tens N/m^2. As mentioned above, the maximum driving force is composed of three components, i.e., the force F, the friction $\mu_k mg$, and the surface tension τ_s. Among these three components, the friction and surface tension are constant for the certain weight of upper glass plate ($\mu_k mg + \tau_s \approx$ 14N/m^2), and the upper glass plate accelerated when the force generated by the liquid crystalline flow overcome this force. The effective force which costs to drive the upper plate is the F_{LC}-14N/m^2, and this value drastically changes with the voltage. It is also found that the maximum driving force increases with the frequency increase.

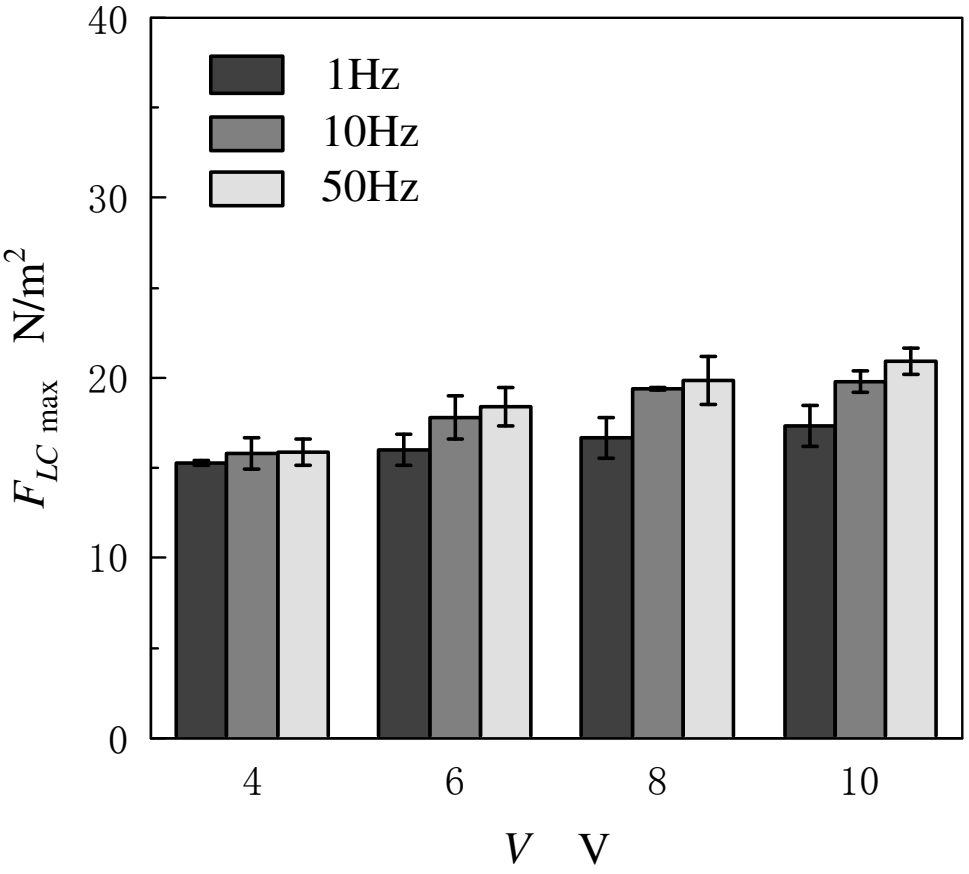

Fig. 3.25 Effect of the applied voltage on the driving force generated by the liquid crystal

The effect of the Duty ratio of the applied voltage

Figure 3.26 shows the effect of the duty ratio on the maximum driving force per unit area of liquid crystalline actuator. It can be seen from the figure that duty ratio has no effect on the maximum driving force, since the force exhibit its maximum value just after the voltage turned ON.

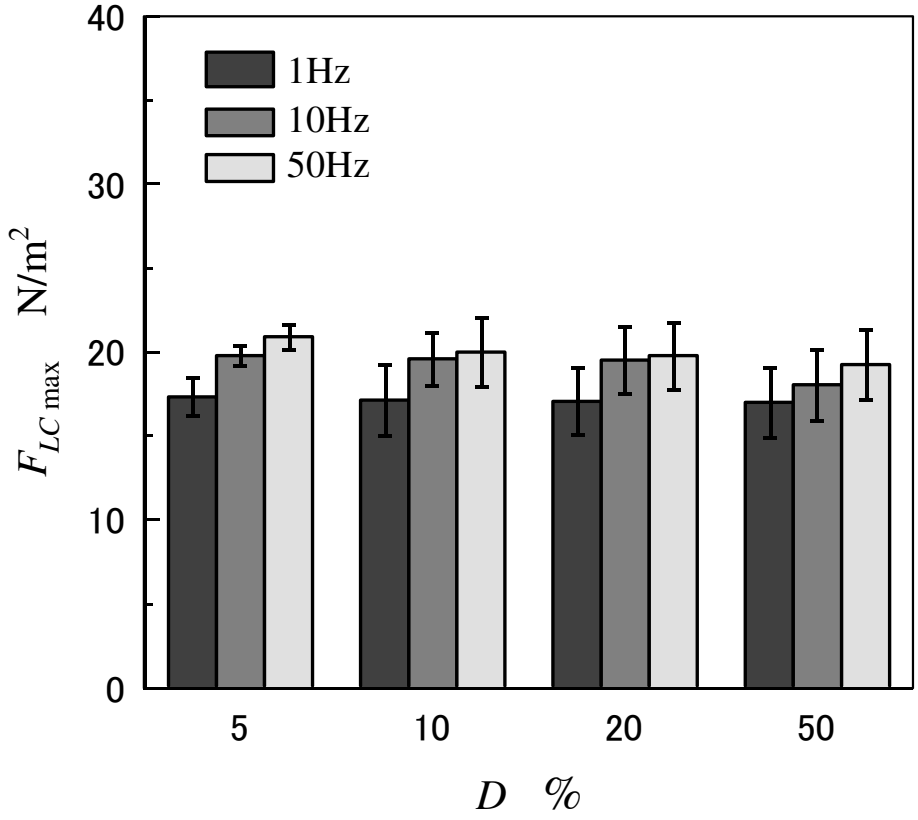

Fig. 3.26 Effect of the Duty ratio on the driving force generated by the liquid crystal

The effect of the mass of the upper plate

The maximum acceleration increases with the frequency as shown in Fig. 3.27. Because the molecules have enough time to rotate until they are parallel to the applied field direction at ON-state period for the low frequency. However, for the higher frequency f = 10Hz or 50Hz, the molecules start rotating back before the molecular orientation reaches the direction parallel to the applied field direction. Thus, the maximum acceleration becomes larger than that for f = 1Hz, 2Hz and 5Hz, shown in the Fig. 3.27. According to Eq. 3.2, the driving force is composed of three components. The driving force $F = ma$, the friction and surface tension are constant for the certain weight of upper glass plate ($m \approx 0.0475$g, $\mu mg + \gamma L \approx 14$N/m2). Thus, the relationship between the maximum driving force F_{LC} max and the loads is shown in Fig. 3.28. It can be seen that the frequency has no obvious effect on the maximum driving force. On the other hand, the driving force generated by the backflow increases

as the loads increasing. To explain this observation we considered an extreme condition that the lower and upper glass plates are fixed (See Fig. 3.29(a)). The S-shape flow can exert a shear force on the bounding plates without dissipation. When the upper plate is set movable (See Fig. 3.29(b)), the effective shear force acting on the movable upper plate will decrease as the function of the speed of upper plate. As there is an inverse relationship between speed of upper plate and the loads (See Fig. 3.20), consequently, the driving force of the actuator increased with the added loads.

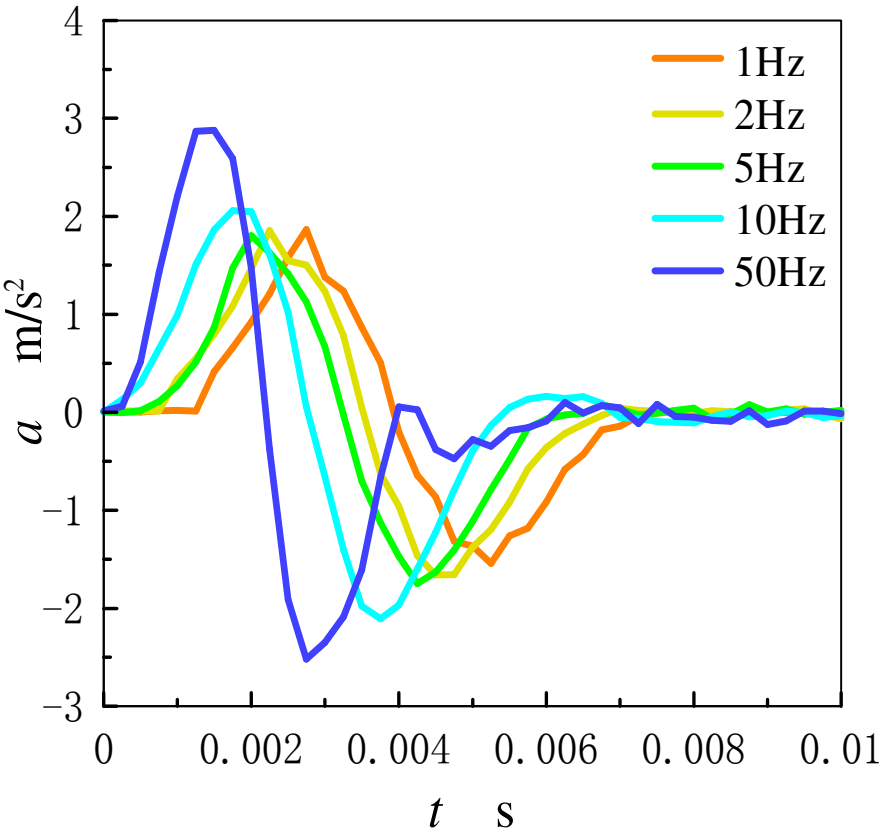

Fig. 3.27 Effect of the mass of the upper plate on the driving force generated by the liquid crystal

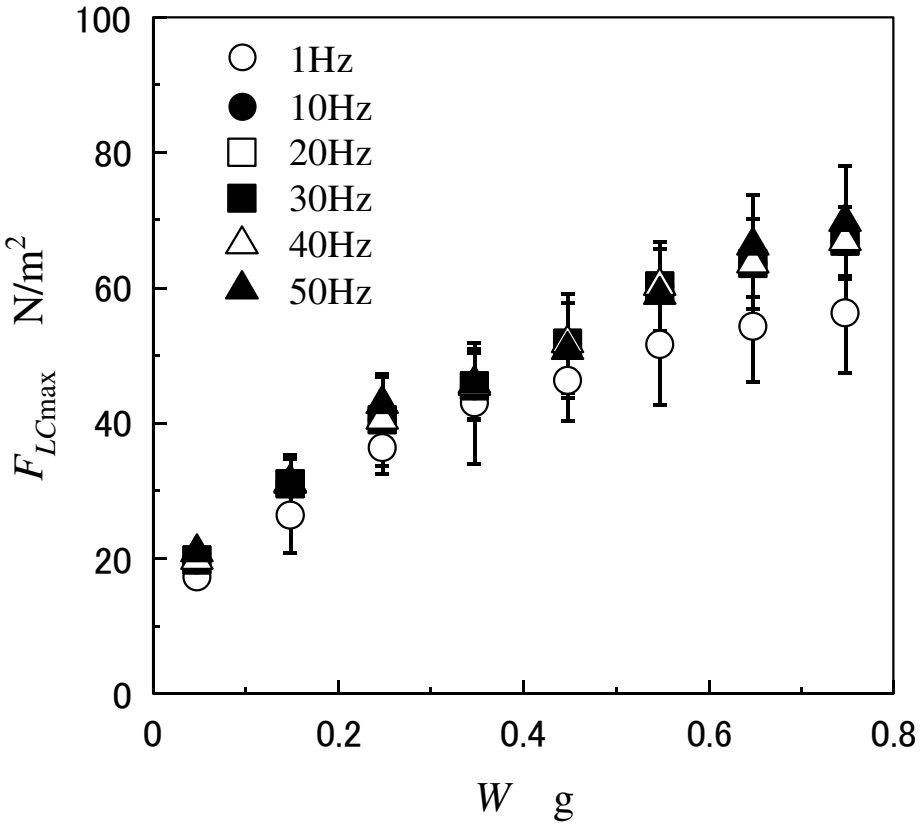

Fig. 3.28 Effect of the mass of the upper plate on the driving force generated by the liquid crystal

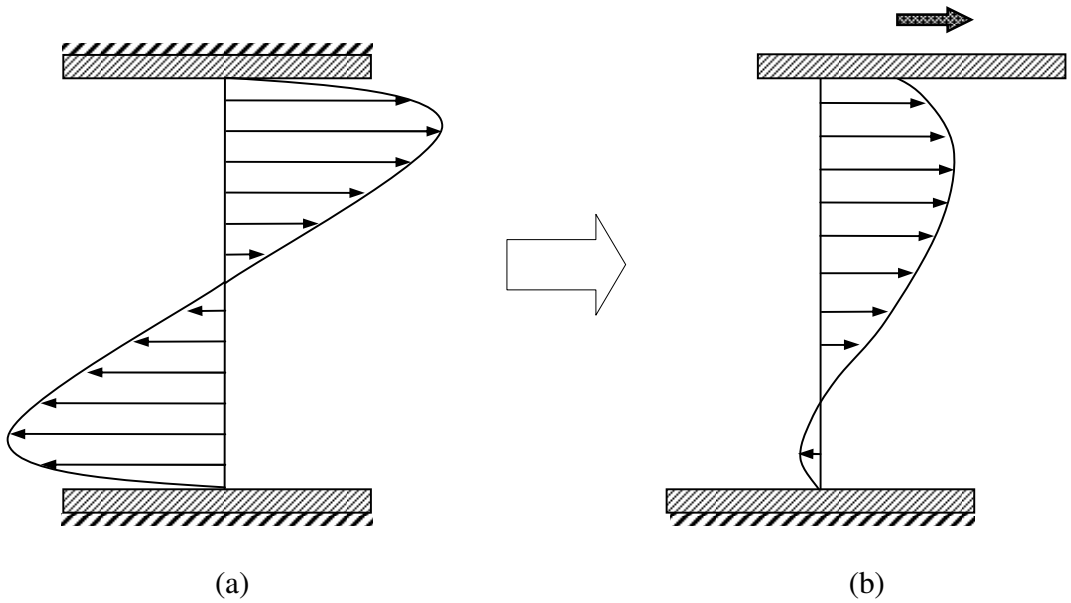

Fig. 3.29 Effect of the mass of the upper plate on the driving force generated by the liquid crystal

3.4 Summary

The maximum driving force generated by the liquid crystalline flow is estimated by differentiating the time series of the driving speed. The force is estimated as tens N/m^2 for V = 10V. This force is comparable to that of other kinds of actuators. The RE type electro-conjugate fluid motors can generate the maximum driving force per unit area about tens of N/m^2 for V = 5KV. The electrostatic actuator can produce a force density of 20N/m^2 for V = 50V. The result suggests that the liquid crystalline micro-actuator can provide a sufficient force at low voltage.

Table 3.2 The driving force of micro actuators

Kind of micro actuator	Driving Voltage	Driving Force	Stroke
Liquid crystalline actuator	10V	70N/m^2	Infinite
Comb type electrostatic actuator	50V	20N/m^2	Infinite
Stacked type piezoelectric actuator (PZT)	KV	5KN/cm^2	Short
RE type electro-conjugate fluid actuator	5KV	10N/m^2	Infinite

Chapter 4

Measurement of Energy Efficiency of Liquid Crystalline Actuators

4.1 Introduction

Actuators can be treated as active transformers that transform one type of energy into another form with a transfer function. Design of the actuator is decided by how to obtain the physical energy required. Four different sources of energy or work are involved in a given actuator: input (P_{in}) and output (P_{out}) powers, power drawn from the power supply (P_s), and internal power consumption or "wasted" power (P_w). The conservation of energy requires:

$$P_{in} + P_s = P_{out} + P_w \tag{4.1}$$

The efficiency, η, in the transduction process in an actuator is defined as the ratio of the output mechanical energy, P_{out}, to the input electrical energy, P_{in}.

$$\eta = \frac{P_{out}}{P_{in}} \times 100\ \% \tag{4.2}$$

Ideally, actuators are lossless devices, and, thus, efficiency in an ideal situation should be close to 100%. In practice, various different dissipative phenomena take

place in the transducer or accompanying components, producing lower efficiency.

The transduction efficiency of all actuator technologies is a dynamic parameter. In general, the efficiency of the actuator is a function of the actuation conditions.

As a capacitor, the input energy of liquid crystalline actuator is very difficult to be measured, because the time for charging is very short and the current is too small to be buried in the noise from the experimental environment.

This chapter provides the results of testing and evaluation of the energy efficiency of liquid crystalline actuator. It describes the setup used for testing the input power of liquid crystalline actuator. Subsequently, the test procedures and experimental results are discussed. Analysis of these results forms the final section of this chapter.

4.2 Experimental

4.2.1 Liquid Crystalline Actuator Cell Preparation

The experimental liquid crystalline cell as shown in Fig. 4.1 was prepared. The liquid crystalline material, 4-n-pentyl-4`-n-cyanobiphenyl (5CB), was placed between two parallel glass plates with 10μm gap, which was achieved by mixing small spherical particles of 10μm diameter. The size of the upper glass plate and the lower glass plate are 10×10mm and 20×20mm respectively. The mass of the upper glass plate is about 0.0475g. The bounding glass plates were coated with an optically transparent ITO layer to apply an electric field onto the liquid crystal, and a thin rubbed polyimide alignment layer to obtain homogeneous molecular orientation field at equilibrium state. An electrode is connected to the upper plate through the steel rod and the water droplet to avoid the contact friction. In order to reduce the effect of resistance of the electric circuit, the steel rod and the electrode clamps are treated of gold plated. By applying a pulsed rectangle electric field between the glass plates, liquid crystalline backflow is induced and the upper plate will be driven by the flow.

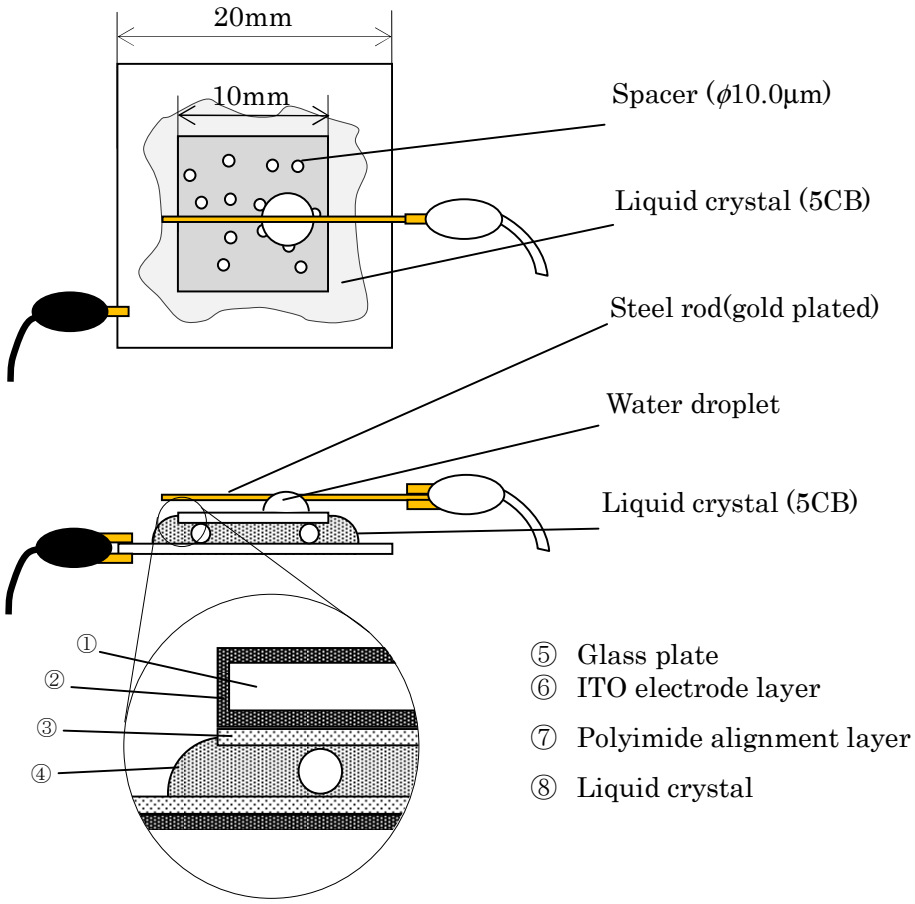

Fig. 4.1 Liquid crystalline actuator cell

4.2.2 Experimental Setup

As a capacitor, the input energy of liquid crystalline actuator is very difficult to be measured, because the time for charging is very short and the current is too small to be buried in the noise from the experimental environment. In this work, we chose the precision power analyzer (N4L PPA5500). The setup is shown in Fig. 4.1 and the specification of PPA5500 is shown in Table 4.1. It can maintain the wide frequency range, exceptional noise rejection, large voltage and current measurement ranges and greater processing power. The PPA is fitted with either 10, 30 or 50Arms internal shunts. In our experiments, the 10Arms shunt was chosen for measuring the power source of liquid crystalline actuator. It can measure 3mApk to 30Apk (10Arms) in 9

ranges and the accuracy of measurement is 0.02% Rdg + 0.04% Rng + (0.004%×KHZ) + 10μA.

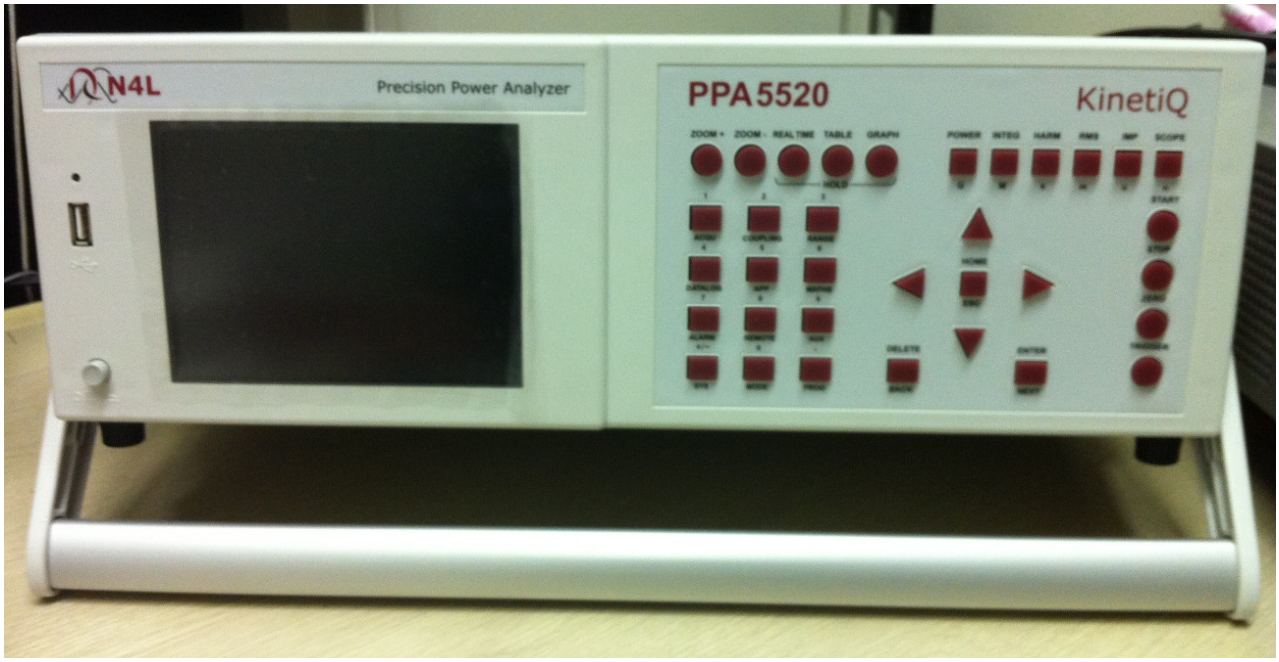

Fig. 4.2 Precision Power Analyzer PPA5500 (N4L)

Table 4.1 Specification of PPA 5500

Measurement	*W*, *V*A, *V*Ars,pf, *V*&*A* – rms, ac, dc, pk, cf and surge Frequency, phase, fundamentals and impedance Harmonic, THD, TIF, THF, TRD and TDD Integrated values Datalog Sum and Neutral values
Frequency Range	DC and 10mHz to 2MHz (10Arms or 30Arms versions) DC and 10mHz to 1MHz (50Arms)
Voltage Input	Ranges – 300mVpk to 3000Vpk (1000Vrms) in 9 ranges 20% over-range ability maintains 300Vpk range with 240 Vrms Accuracy – 0.02% Rdg + 0.04% Rng + (0.004%×kHz) + 1mV External sensor input to 3 Vpk – BNC connector
Current Input	The PPA is fitted with either 10, 30 or 50 Arms internal shunts
	10Arms Shunt (4mm safety type connection terminals) Ranges – 3mApk to 30Apk (10Arms) in 9 ranges Accuracy – 0.02% Rdg + 0.04% Rng + (0.004%×kHz) + 10uA
	30Arms Shunt (4mm safety type connection terminals) Ranges – 30mApk to 300Apk (30Arms) in 9 ranges Accuracy – 0.02% Rdg + 0.04% Rng + (0.004%×kHz) + 100uA
	50Arms Shunt (4mm safety type connection terminals) Ranges – 100mApk to 1000Apk (50Arms) in 9 ranges Accuracy – 0.02% Rdg + 0.04% Rng + (0.004%×kHz) + 100uA
	External sensor input to 3 Vpk – BNC connector
Phase Accuracy	5 millidegrees + (10 millidegrees × kHz) 10 millidegrees + (20 millidegrees × kHz) (50Arms shunt)
Watts Accuracy	[0.03% + 0.03%/pf + (0.01%×kHz)/pf] Rdg + 0.05% VA Rng
Common Mode Rejection	Total Common Mode and Noise effect on current channels
	Applied 250V @ 50Hz – Typical 1mA (150dB) Applied 100V @ 100Hz – Typical 3mA (130dB)

Datalog	Up to 4 user selectable measurement functions (30 with optional PC software) Datalog window : From 10ms with no gap between each log
Sample Rate	Real time no gap 2.2Ms/s on all channels

On the other hand, with low-current measurements, we must take care with interconnects to ensure maximum noise reduction and optimal shielding. Consider the following when making low-current measurements:

- 50/60 Hz line noise pickup is the most common and considerable source of noise. We can reduce the effect of this noise by using proper cabling, including shielded cables and coaxial cables. Digital multimeters (DMMs) integrated into the system we choose handle the residual line noise rejection very well. At 61/2-digit measurement speed, the line noise rejection is typically high enough to virtually eliminate the noise from the signal, giving us confident and accurate readings. The 50/60 Hz line-induced noise can easily saturate the sensitive preamplifier circuitry of any low current ammeter. Once this happens, no amount of filtering can recover measurement accuracy. Therefore, shielded cables are a must.

- Triboelectric effects arise from the movement of a conductor against an insulator. Cables designed to minimize this effect are available. Reducing cable movement with tie-downs or other fixtures also minimizes this effect.

- Electrostatic pickup is another difficult interference effect. Its roots can once again be traced to poor shielding. Anything is charged with some potential, including the human body. People, hands, and so forth moving near the DUT or cabling during a low-current measurement will induce a current determined by the partial derivative.

- Piezoelectric effects are caused by the physical deflection of an insulator. Reducing

the amount of stress on a device helps to minimize this effect.

- Leakage currents are often the result of contaminants around the device of interest. These contaminants provide an additional current path that causes measurement error. Solder flex and fingerprints (oil, salt, and so on) can be sources of contamination. Many contaminants can be cleaned using alcohol or a similar solvent.

4.2.3 Electric Circuit Design

In this experiment, we plan to record the input power, output power and energy efficiency for the conditions with different combination of the weight of the upper glass plate of liquid crystalline actuator and the voltage, frequency, and duty ratio of the input electric field. The impedance and capacitance of the liquid crystalline actuator is affected by changing the parameters including voltage and frequency of the input electric field.

Due to cylindrical symmetry of crystalline structure the number of fundamental components of liquid crystals is reduced to two: $\varepsilon_{\parallel}$ and $\varepsilon_{\perp}$ are dielectric permittivity components along and perpendicular to the director, respectively, while the dielectric anisotropy is $\Delta\varepsilon=\varepsilon_{\parallel}-\varepsilon_{\perp}$. The description of procedures to measure $\varepsilon_{\parallel}$, $\varepsilon_{\perp}$ and $\Delta\varepsilon$ are the prime objective of this presentation. the dielectric permittivity ($\varepsilon_{\parallel}$ and $\varepsilon_{\perp}$ are dielectric permittivity components along and perpendicular to the director) of liquid crystalline molecules can be strongly influenced by these parameters.

Secondly, the impedance of liquid crystal is affected by the frequency of the applied voltage. Electric impedance of nematic liquid crystal (5CB) cells has been measured to detect ion behavior by Hitoshi and Masahiro. The experimental results of frequency properties of impedance is shown in Fig. 4.3. The vertical axis denotes absolute value of impedance, and the horizontal axis, frequency. Open symbols show the data obtained at room temperature and sold symbols those at 23±1℃. Triangles are the data for unbiased cell and circles for the 10V dc biased cell.

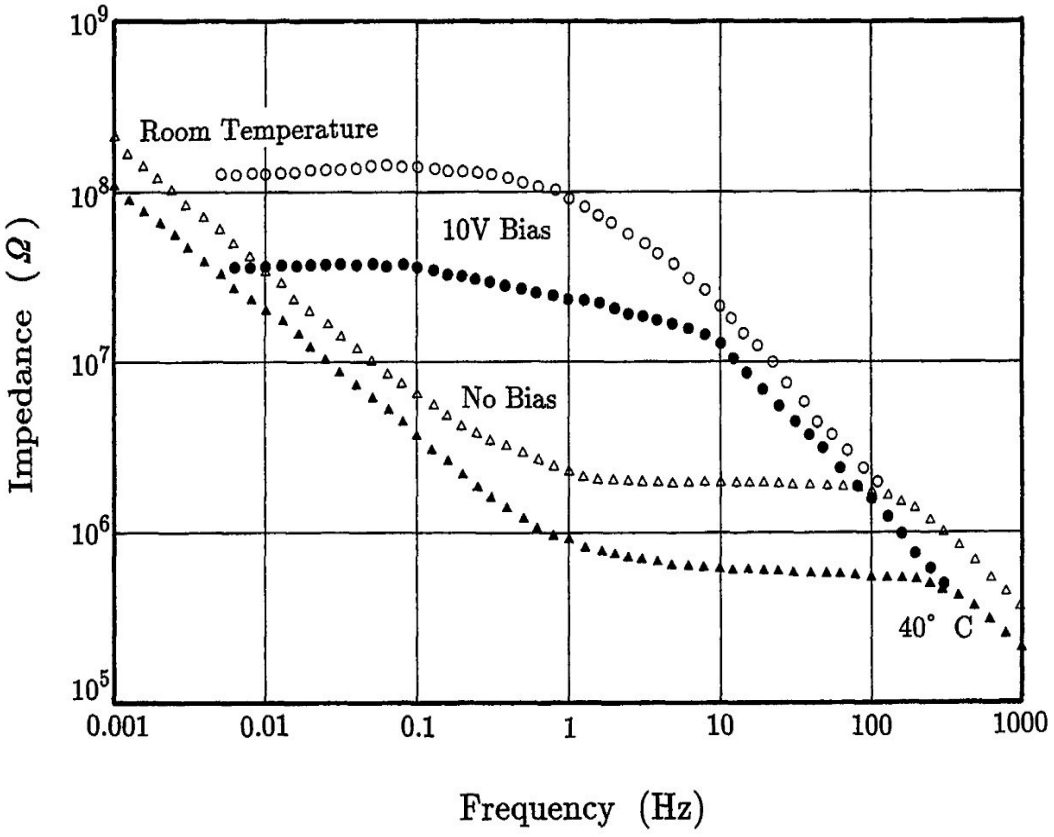

Fig. 4.3 Experimental results of frequency properties of impedance

In this experiment, the precision power analyzer (PPA5500 10Arms) was chosen for measuring the input power of liquid crystalline actuator. This power analyzer should support external shunt resistors or current transformers. Thus, we should selected the external shunt resistors depending on the impedance of the measuring target. The Impedance analyzer (PSM1700 *N4L)* was used to measure the impedance and capacitance of liquid crystalline actuator before measuring the input power, as shown in Fig. 4.4.

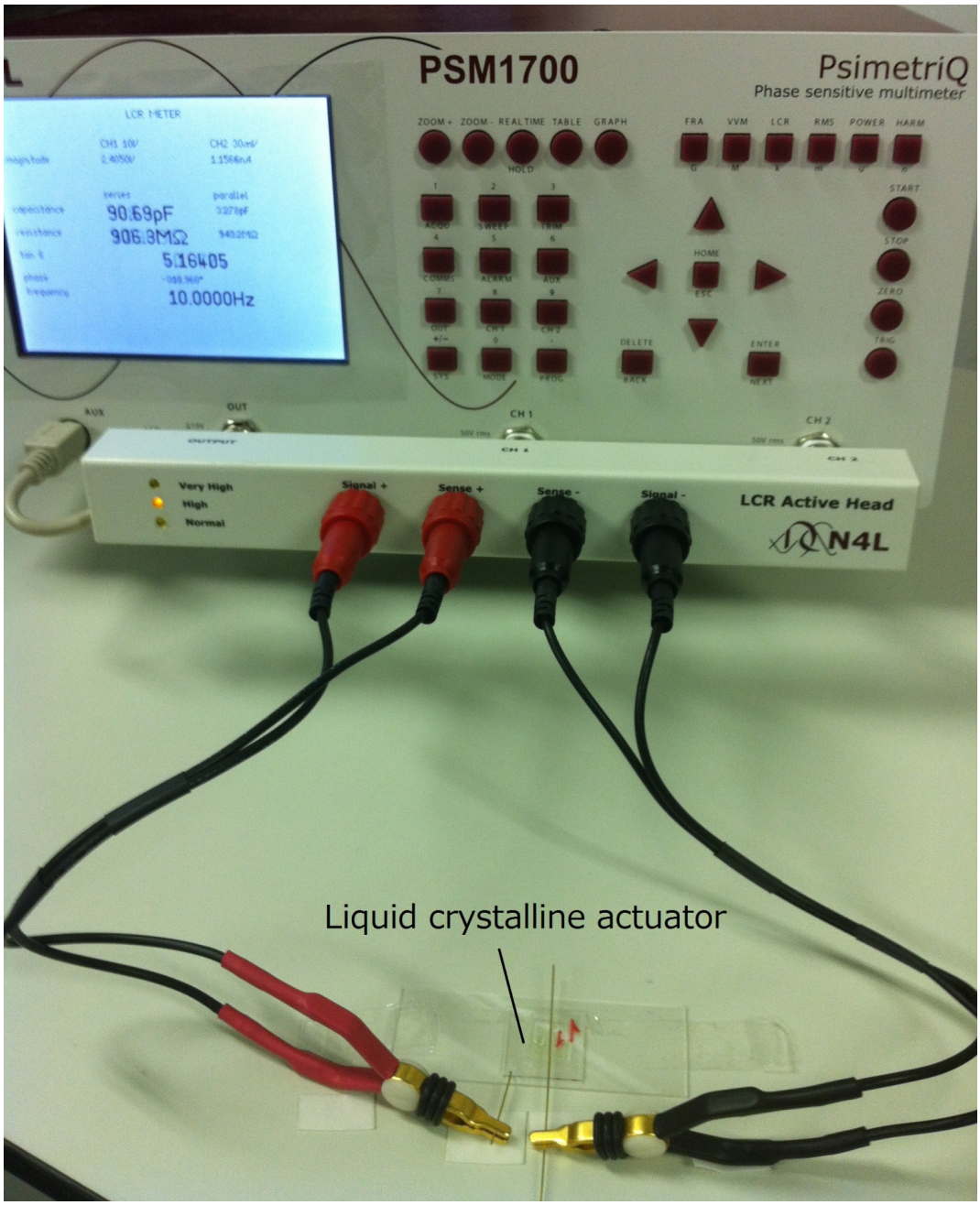

Fig. 4.4 Measurement of Impedance and capacitance of liquid crystalline actuator by Impedance analyzer (PSM1700 *N4L)*

According to the impedance of liquid crystalline actuator we measured, the electric circuit is designed which is shown in Fig. 4.5. The external shunt resistors is about 1%~2% of the impedance of the liquid crystalline actuator cell to protect the instrument and measure precisely.

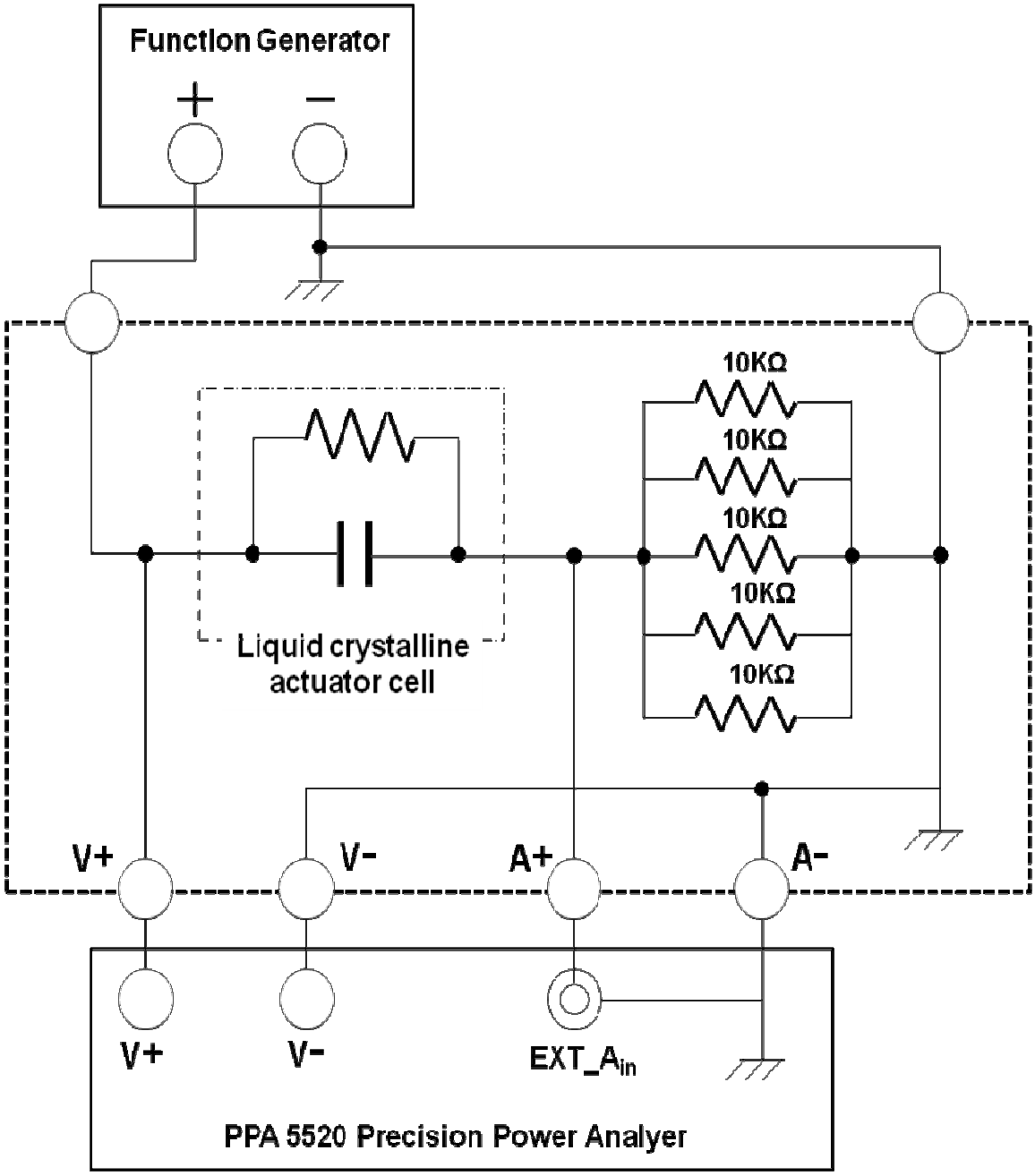

Fig. 4.5 Electric circuit of power measurement of liquid crystalline actuator

4.2.4 Experimental Method

The effective circuit of the filled LC cell contains resistance of the electrodes (R_0), capacitance and resistance of the polyimide layer (C_p and R_p), and capacitance and

resistance of the LC layer (C_{lc} and R_{lc}), respectively.

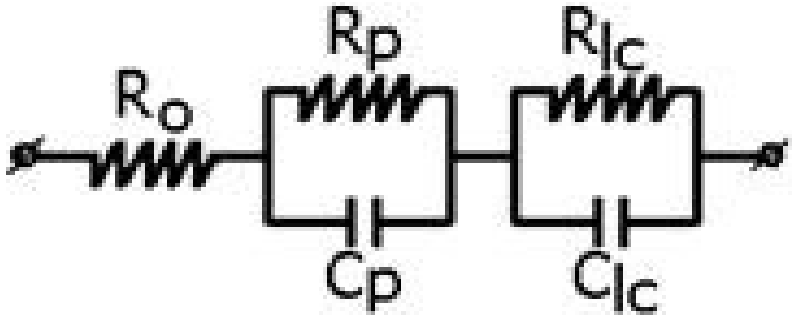

Fig. 4.6 Effective circuit of the filled cell: R_0 is resistance of the electrodes, C_p and R_p are capacitance and resistance of the polyimide layer, and C_{lc} and R_{lc} are capacitance and resistance of the LC layer, respectively.

The impedance of the effective circuit shown in Fig.4.4 is calculated as a sum of impedances:

$$\hat{Z}_f = \hat{Z}_{R_0} + \hat{Z}_{R_pC_p} + \hat{Z}_{R_{lc}C_{lc}} = R_0 + \frac{R_p}{1+i\omega R_p C_p} + \frac{R_{lc}}{1+i\omega R_{lc} C_{lc}} = \ldots = \mathrm{Re}\left[\hat{Z}_f\right] + i \cdot \mathrm{Im}\left[\hat{Z}_f\right] \tag{4.3}$$

where

$$\mathrm{Re}\left[\hat{Z}_f\right] = R_0 + \frac{R_p}{1+\left(\omega R_p C_p\right)^2} + \frac{R_{lc}}{1+\left(\omega R_{lc} C_{lc}\right)^2}$$

and

$$\mathrm{Im}\left[\hat{Z}_f\right] = -\left(\frac{\omega C_p R_p^2}{1+\left(\omega C_p R_p\right)^2} + \frac{\omega C_{lc} R_{lc}^2}{1+\left(\omega C_{lc} R_{lc}\right)^2}\right). \tag{4.4}$$

The impedance and capacitance of the liquid crystalline actuator is affected by changing the parameters including voltage and frequency of the input electric field. In order to remove the effect of the impedance and capacitance on the input power of the liquid crystalline actuator, the power consumed by the impedance and capacitance

should be subtracted from the input power of liquid crystalline actuator we measured by PPA5500. So firstly we measure the impedance and capacitance of the liquid crystalline actuator at an experimental condition. Secondly, we operate the resistances and capacitors which reach the value of the impedance and capacitance we measured at first step. Then we use the exactly same two channel and two electric circuit to measure the input power of liquid crystalline actuator and the resistance and capacitors at the same time and record them. The effect of resistance of the electrodes (R_0), capacitance and resistance of the polyimide layer (C_p and R_p), and capacitance and resistance of the LC layer (C_{lc} and R_{lc}) are removed from the input power of liquid crystalline actuator.

In order to remove the effect of the impedance and capacitance of the liquid crystalline actuator, we record the power consumed by the resistance and capacitor of the liquid crystalline actuator. As shown in Fig. 4.7. We use two same channels to measure the powers consumed by the liquid crystalline actuator and the resistance and capacitor at the same time.

Figure 4.8 is the photocopy of experimental setup of power measurement. We use aluminum foil to cover on the electric circuit showed in Fig. 4.7. the aluminum foil cover is operated to be a faraday cage to shield external electrical fields.

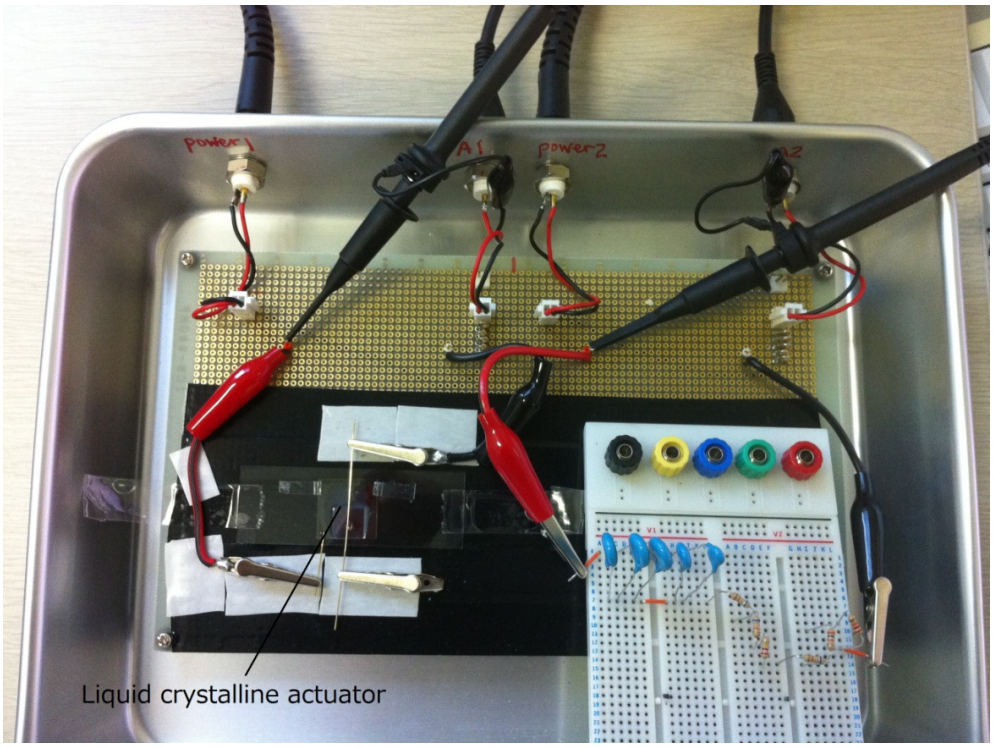

Fig. 4.7 Two same channels for power measurement of liquid crystalline actuator

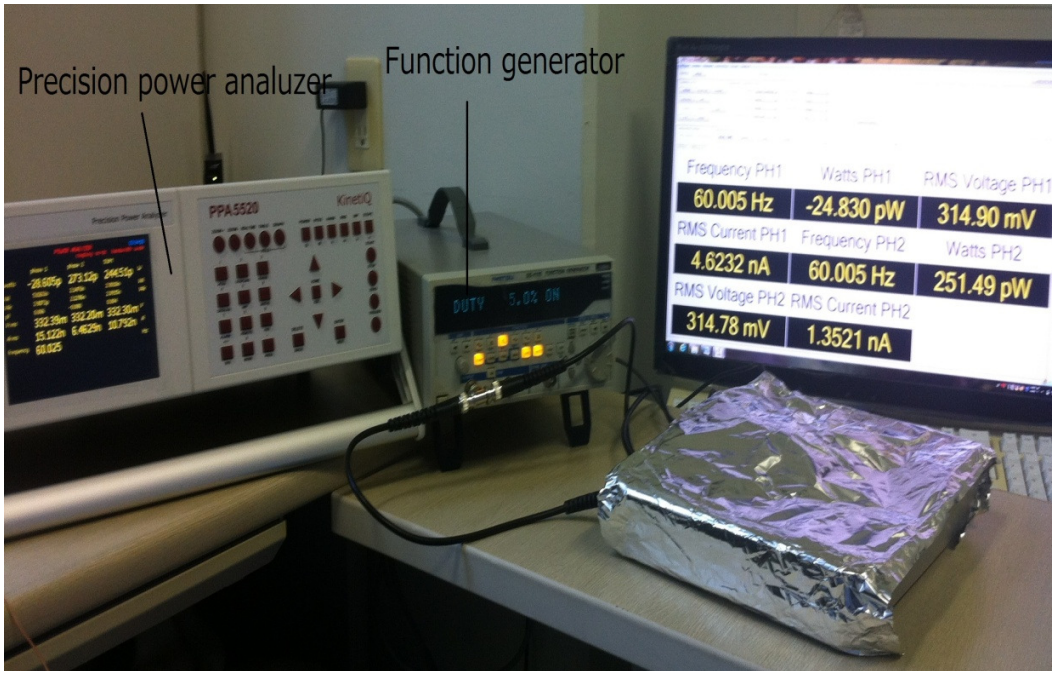

Fig. 4.8 Experimental setup of power measurement of liquid crystalline actuator

4.3 Results and Discussion

4.3.1 Input Power

As the above introduced, we use the precision power analyzer (PPA5500) to measure the input power of liquid crystalline actuator. The input power is calculated from the voltage and current measured directly. The figure 4.9 is the waveform of the voltage and current of liquid crystalline actuator. From this figure, we can easily observe that when the voltage is turned ON, the liquid crystalline actuator starts to charging. The current reach the maximum value. After that the current decreases to zero because the liquid crystalline actuator stop charging. When the voltage is turned OFF, the liquid crystalline actuator turns to discharging.

Figure 4.10 and Figure 4.11 shows the relationship between the frequency of input voltage and input power of liquid crystalline actuator. The experimental condition is set as follows: the frequency f = 10~100Hz, the duty ratio D = 5% of the pulsed voltage. As increasing the frequency of the input voltage, the input power is consumed by the liquid crystalline actuator increased linearly. As we explained before, the liquid crystalline actuator cell is a capacitor which is charging when the voltage is turned ON. So as the frequency of the input voltage increases, the frequency for charging corresponds to increase. Because every time of charging consumes power, the number of times of charging will affect the quantity of the consumed power.

From Figure 4.10, it also can be observed that the liquid crystalline actuator needs more power when the input voltage is set 10V than that is set 5V. We recorded the capacitance and impedance at different conditions, as shown in Fig. 4.12 and Fig. 4.13. The capacitance and impedance of the liquid crystalline actuator increases as the increasing voltage. Thus, the voltage 10V consumes more input power than that the voltage 5V.

And from the Fig. 4.11, we can find that the weight of the upper glass plate affects the input power. Because as the weight of the upper glass plate increase, the liquid crystalline actuator need more power to drive the upper glass plate to move.

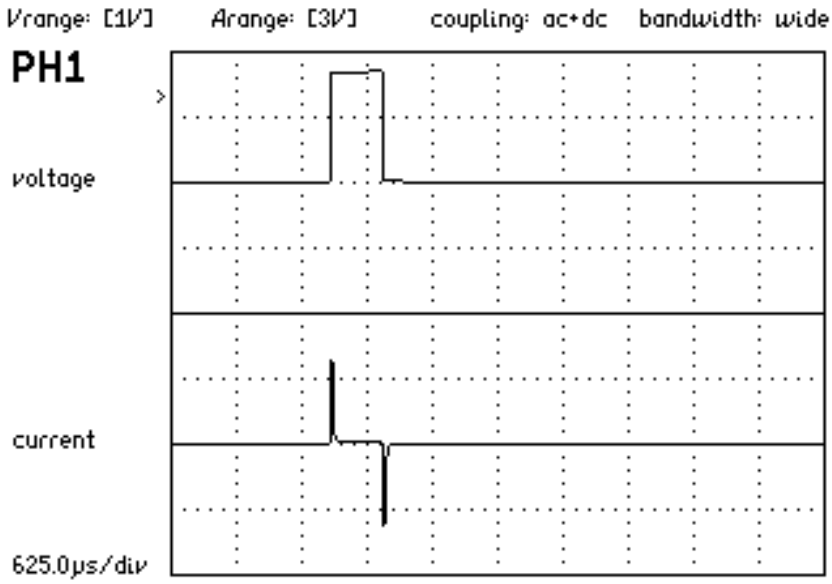

Fig. 4.9 The measured waveform of the voltage and current of liquid crystalline actuator from PPA5500

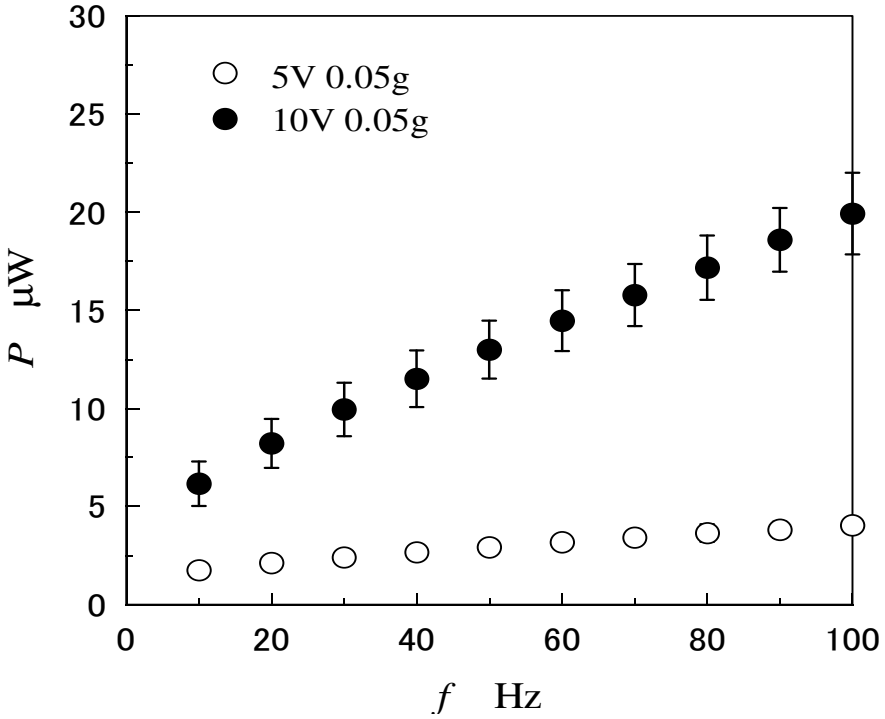

Fig. 4.10 The relationship between the frequency of input voltage and input power of liquid crystalline actuator

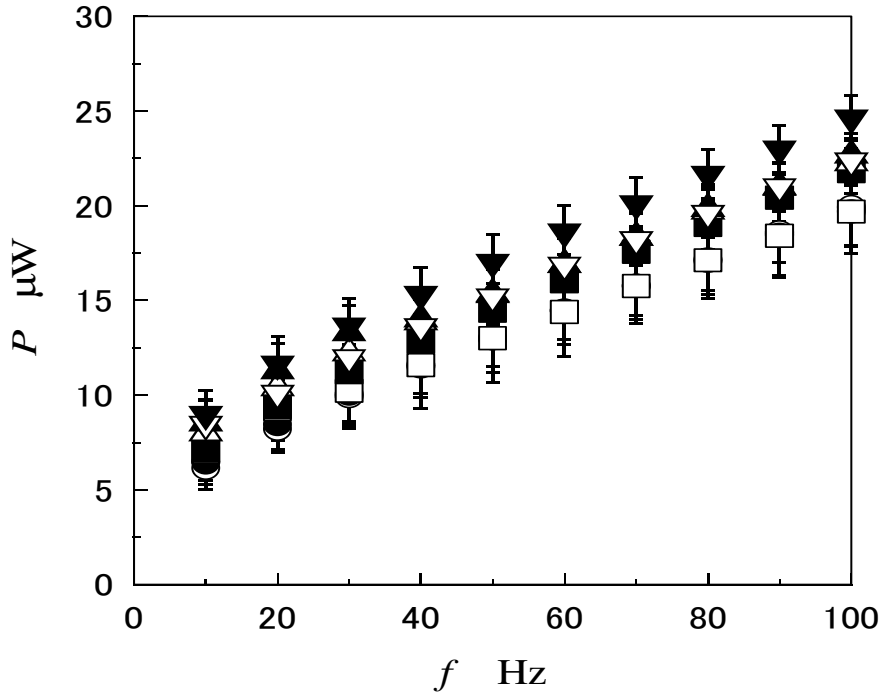

Fig. 4.11 The relationship between the frequency of input voltage and input power of liquid crystalline actuator(○10V 0.05g; ●10V 0.15g; □10V 0.25g; ■10V 0.35g; △10V 0.45g; ▲10V 0.55g; ▽10V 0.65g; ▼10V 0.75g)

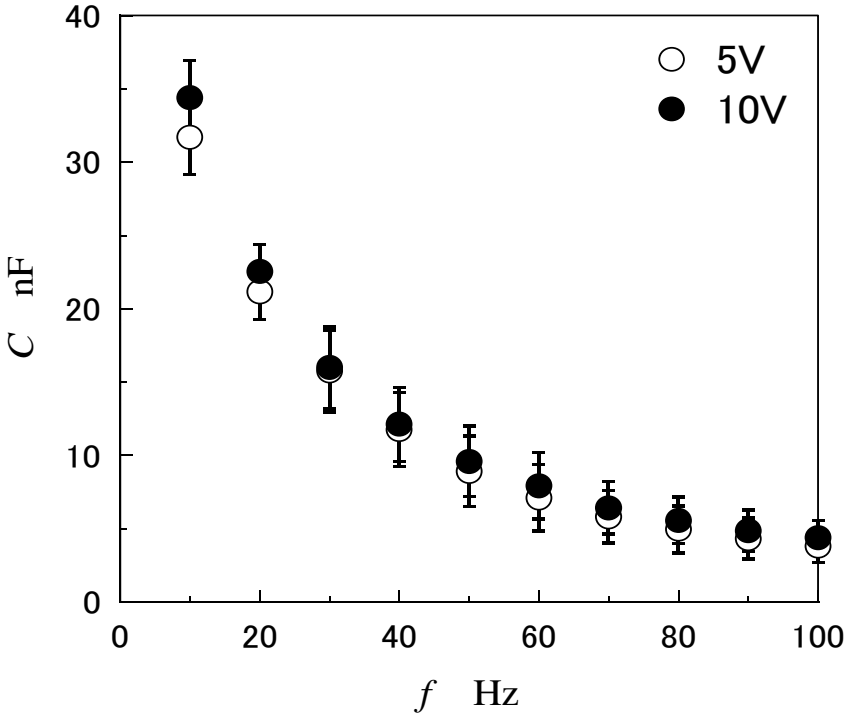

Fig. 4.12 The relationship between the frequency of input voltage and capacitance of liquid crystalline actuator

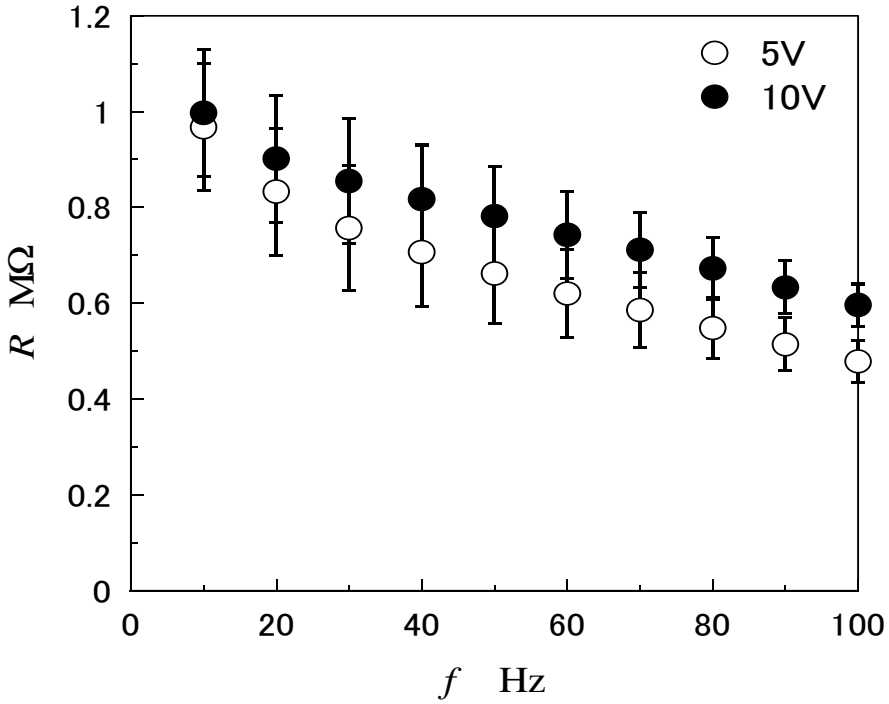

Fig. 4.13 The relationship of the frequency of input voltage and impedance of liquid crystalline actuator

4.3.2 Output Power

Figure 4.14 and Figure 4.15 shows the relationship between the frequency of input voltage and output power of liquid crystalline actuator. The experimental condition is set as follows: the frequency f = 10~100Hz, the duty ratio D = 5% of the pulsed voltage. The output power is the power converted from the electric power by the liquid crystalline actuator. As increasing the frequency of the input voltage, the output power increases because of the average driving speed. The output power can be calculated from the equations as follows:

$$P_{out} = \frac{F_{LC} \cdot S}{t} \tag{4.5}$$

$$F_{LC} = \mu mg + \gamma L \tag{4.6}$$

Here, S the displacement of the upper glass plate, F_{LC} the driving force by the

liquid crystal, μ the friction coefficient, γ surface tension coefficient, and L the length along the upper glass plate edge.

In order to analysis the motion of liquid crystalline actuator, we recorded the movement of the upper glass plate for a relatively long period, as shown in Fig. 4.16. The vertical axis of the figure is the position x along the moving direction of the upper plate. The linear movement of the upper plate is observed. Thus, we can easily get that the upper glass plate is driven by the liquid crystal at a constant speed. So the Equation (4.5) can convert as Equation (4.7)

$$P_{out} = F_{LC} \cdot U \tag{4.7}$$

Here, U is the average speed of the upper glass plate. The average speeds at different conditions are recorded showed in Fig. 4.17 and Fig. 4.18. As the frequency of the applied voltage increases, the average speed increases functionally. Thus, the output power increases as the increasing frequency of the applied voltage as shown in Fig. 4.14 and Fig. 4.15.

From Figure 4.14, it also can be observed that the liquid crystalline actuator generates more power when the input voltage is set 10V than that is set 5V. As shown in Fig. 4.17, the average speed of the applied voltage 10V is times bigger than that of the applied voltage 5V. And from the Fig. 4.15, we can find that the weight of the upper glass plate also affects the input power.

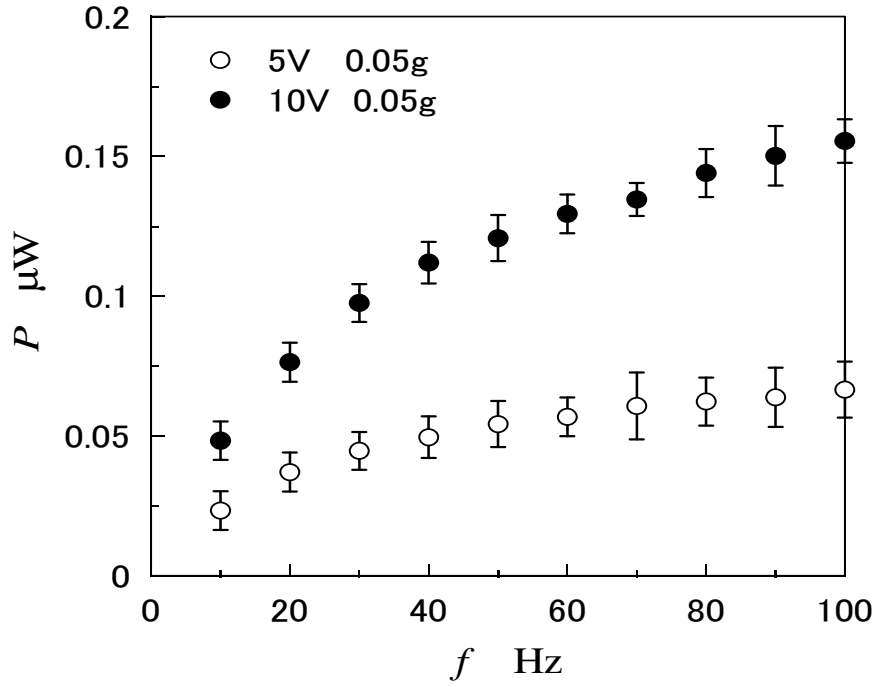

Fig. 4.14 The relationship of the frequency of input voltage and output power of liquid crystalline actuator

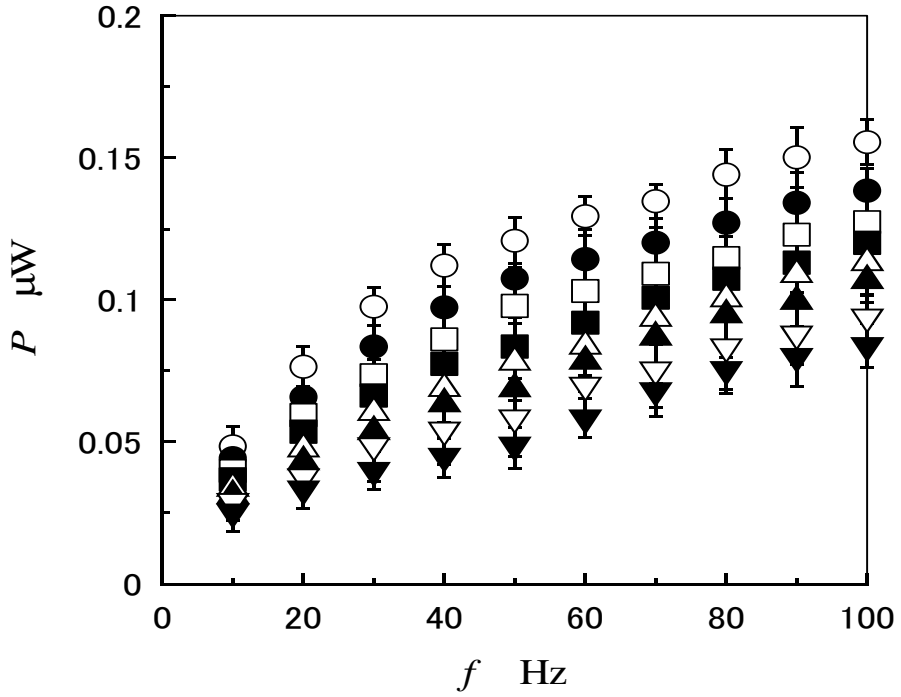

Fig. 4.15 The relationship between the frequency of input voltage and output power of liquid crystalline actuator(○10V 0.05g; ●10V 0.15g; □10V 0.25g; ■10V 0.35g; △10V 0.45g; ▲10V 0.55g; ▽10V 0.65g; ▼10V 0.75g)

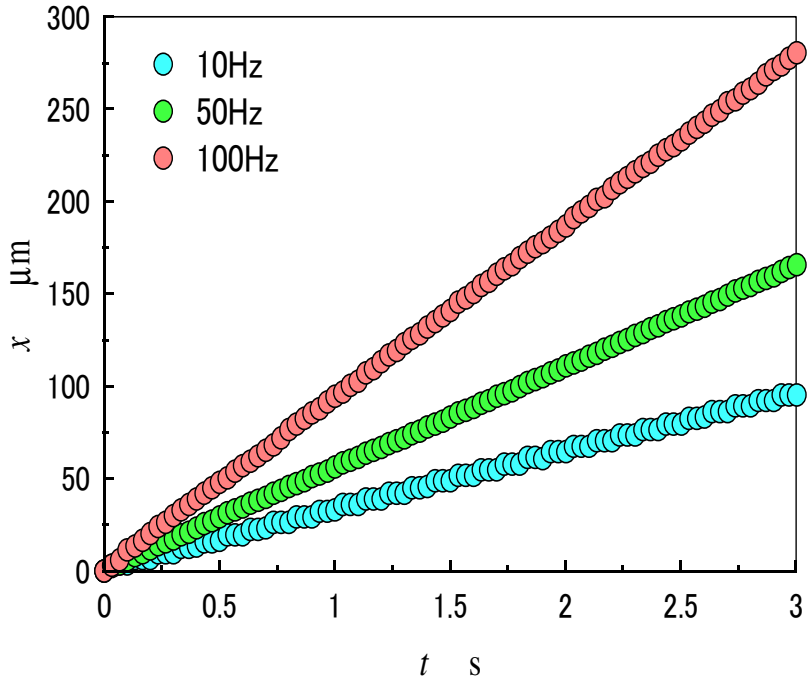

Fig. 4.16 The location of the actuator as the function of the time

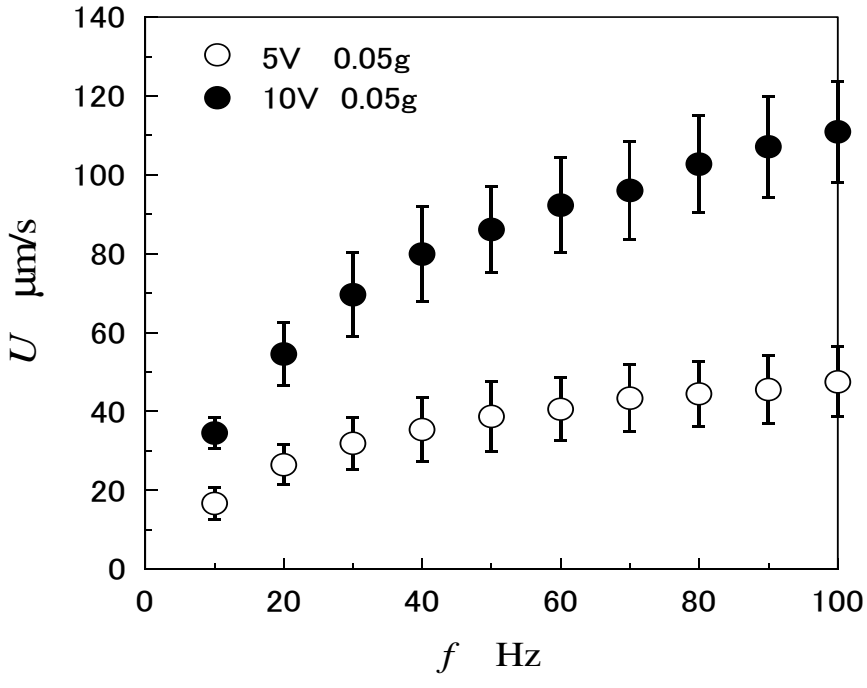

Fig. 4.17 The relationship between the frequency of input voltage and the average speed of liquid crystalline actuator

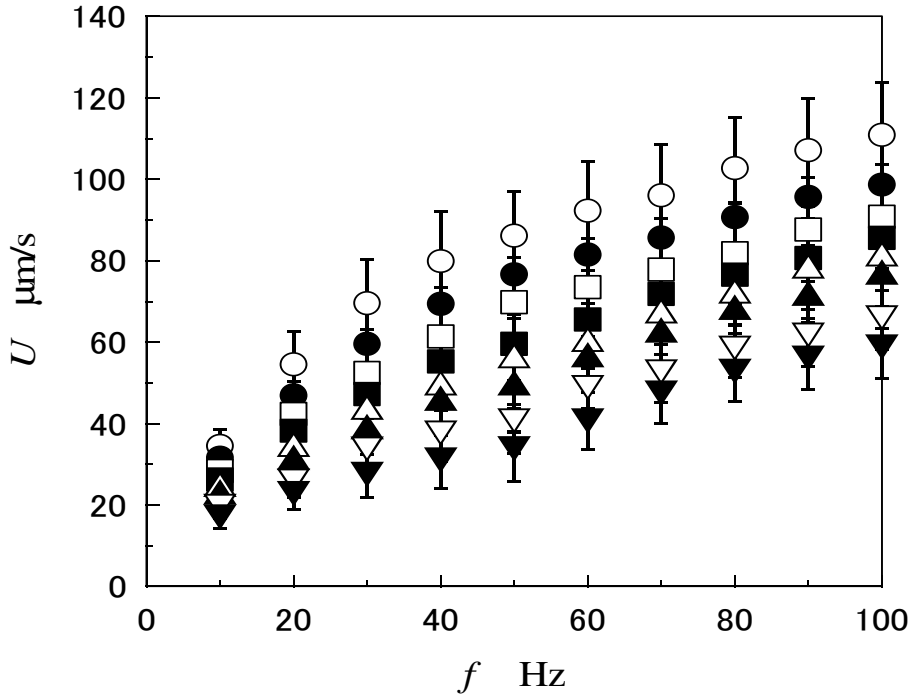

Fig. 4.18 The relationship between the frequency of input voltage and the average speed of liquid crystalline actuator(○10V 0.05g; ●10V 0.15g; □10V 0.25g; ■10V 0.35g; △10V 0.45g; ▲10V 0.55g; ▽10V 0.65g; ▼10V 0.75g)

4.3.3 Energy Efficiency

Figure 4.19 and Figure 4.20 show the relationship between the frequency of input voltage and the energy efficiency of liquid crystalline actuator. This energy efficiency is calculated from the input power consumed from the liquid crystalline actuator. From figure 4.12 and figure 4.13, the capacitance and impedance of the liquid crystalline actuator decreases as the increasing frequency of the input voltage. Thus the capacitance and impedance of the liquid crystalline actuator affect the energy efficiency of liquid crystalline actuator. Because of this reason, we must remove these effects from the calculations. The energy efficiency removed the effects of the capacitance and impedance is showed in Fig. 4.21 and Fig. 4.22.

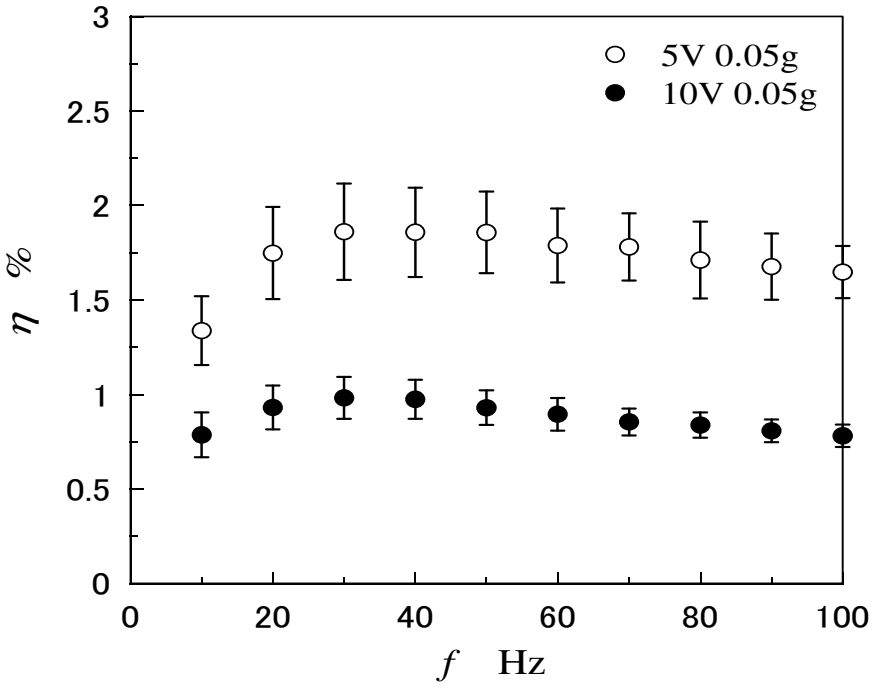

Fig. 4.19 The relationship of the frequency of input voltage and energy efficiency of liquid crystalline actuator

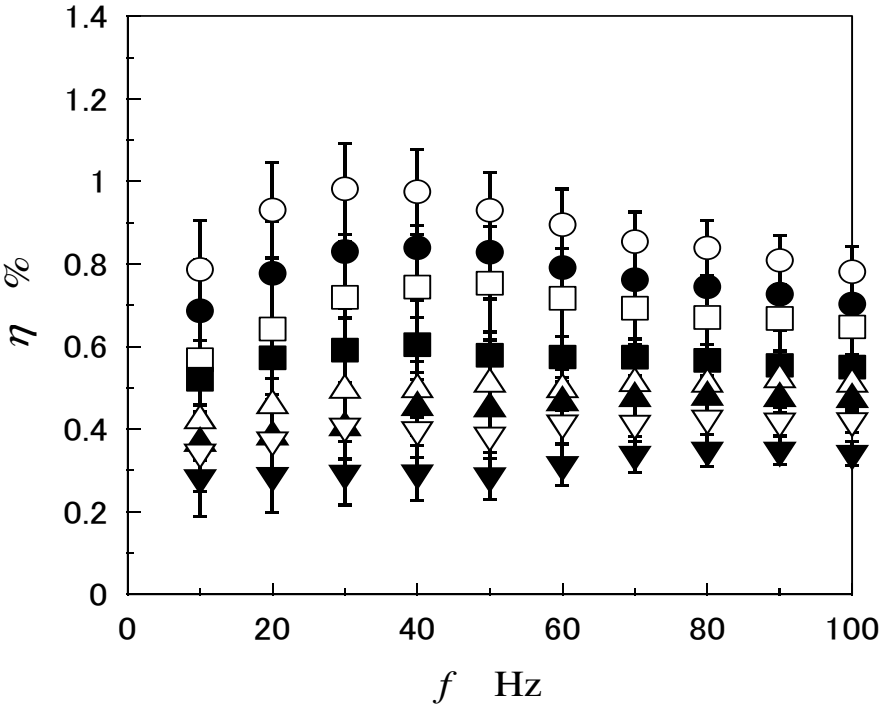

Fig. 4.20 The relationship of the frequency of input voltage and energy efficiency of liquid crystalline actuator （○10V 0.05g; ●10V 0.15g; □10V 0.25g; ■10V 0.35g; △10V 0.45g; ▲10V 0.55g; ▽10V 0.65g; ▼10V 0.75g）

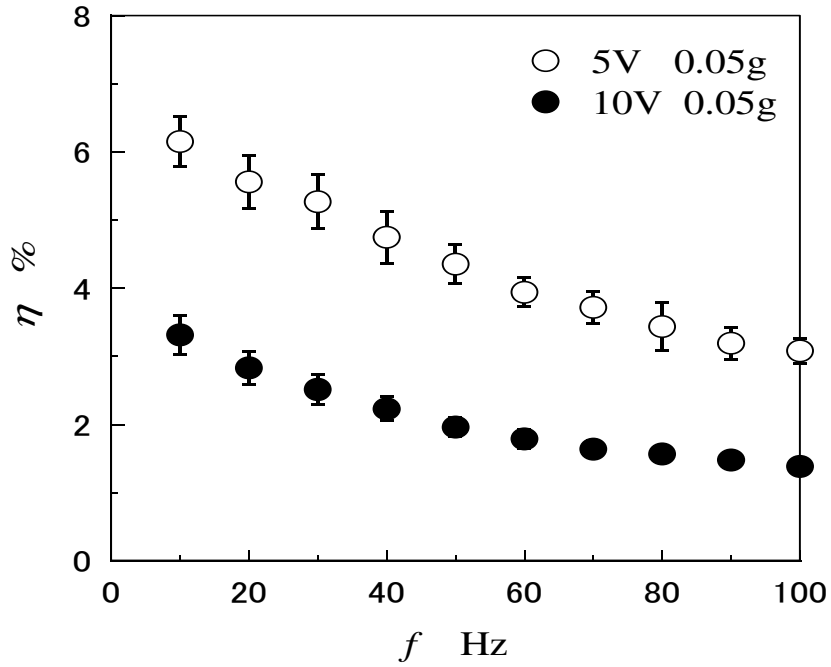

Fig. 4.21 The relationship of the frequency of input voltage and energy efficiency of liquid crystalline actuator (removed the effect of the capacitance and impedance of liquid crystalline actuator)

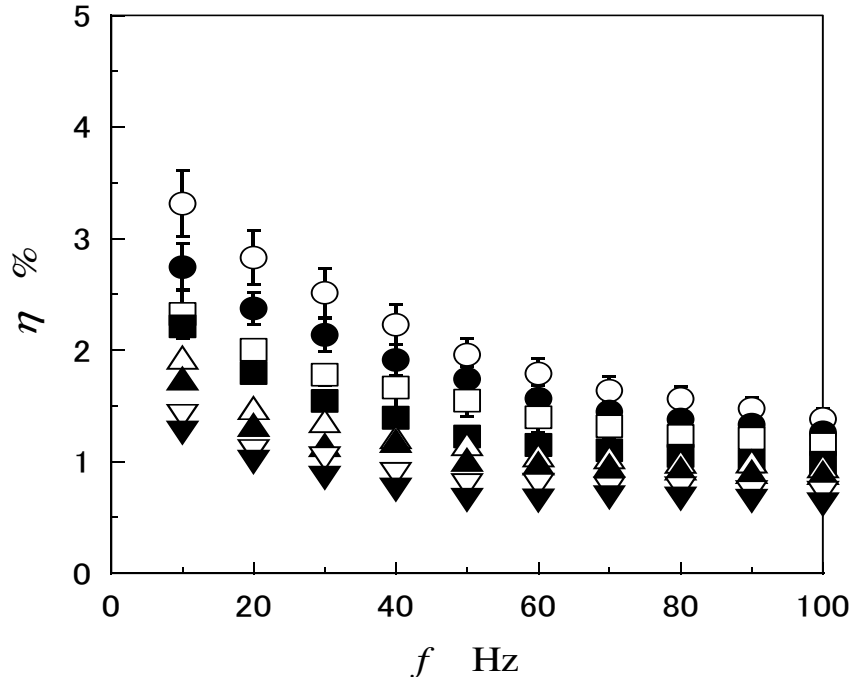

Fig. 4.22 The relationship of the frequency of input voltage and energy efficiency of liquid crystalline actuator (removed the effect of the capacitance and impedance of liquid crystalline actuator) (○10V 0.05g; ●10V 0.15g; □10V 0.25g; ■10V 0.35g; △10V 0.45g; ▲10V 0.55g; ▽10V 0.65g; ▼10V 0.75g)

From Figure 4.21 and Figure 4.22 shows the relationship between the frequency of input voltage and energy efficiency of liquid crystalline actuator, which have been removed the effects of the capacitance and the impedance of the liquid crystalline actuaotor. The experimental condition is set as follows: the frequency f = 10~100Hz, the duty ratio D = 5% of the pulsed voltage. As increasing the frequency of the input voltage, the energy efficiency of liquid crystalline actuator decreases. As we explained before, the liquid crystalline actuator cell is a capacitor which is charging when the voltage is turned ON. So as the frequency of the input voltage increases, the frequency for charging corresponds to increase. Because every time of charging consumes power, the number of times of charging will affect the quantity of the consumed power. Thus the energy efficiency decreases as the increasing frequency.

From Figure 4.21, it also can be observed that the energy efficiency of liquid crystalline actuator when the input voltage is set 5V is larger than that is set 10V.

In order to observe the effect of the weight of the upper glass plate on the energy efficiency of liquid crystalline actuator clearly, we record the relationship between the weight of the upper glass plate and the energy efficiency of liquid crystalline actuator, as shown in Fig. 4.23. As increase the weight of the upper glass plate, the energy efficiency decreases linearly.

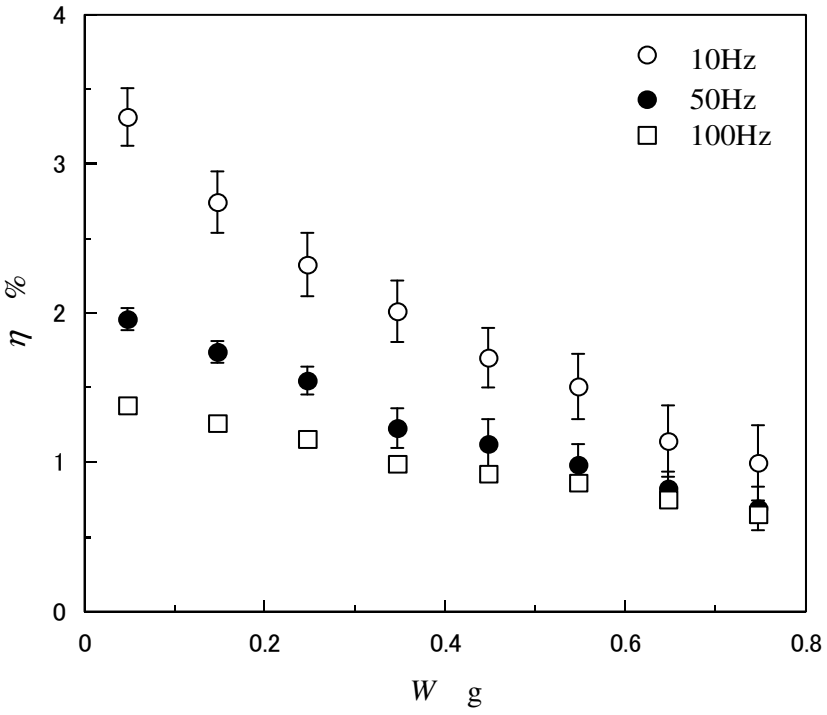

Fig. 4.23 The relationship of the weight of upper glass plate and energy efficiency of liquid crystalline actuator

4.4 Summary

The maximum energy efficiency of the liquid crystalline actuator is about 3.5% at 10V. When the voltage is 5V, the maximum energy efficiency is about 7%. Although the efficiency is relatively low compared with other actuators, the liquid crystalline actuator is useful for the micro-sized machines which cannot be achieved with other actuators.

Chapter 5

General Conclusion and Future Inquires

5.1 Optimization and Enhancement of Liquid Crystalline Actuator

Based on the measurement of driving force and energy efficiency, it is expected to optimize the design of actuator to achieve the best performance in the application. The liquid crystalline material, the experimental temperature, and the experimental preparation process affect the actuator performance. So we set the optimum experimental factor for the prototype of liquid crystalline actuator. On the other hand, the driving force and the energy efficiency are affected by the frequency of the input voltage. We discuss the experimental conditions which the driving and the energy efficiency can reach their maximum value simultaneously.

5.1.1 Improve the Experiment Environment

Experimental Temperature

The liquid crystal 5CB has simple phase transitions. It changes from a solid to a nematic liquid crystal at 22.5℃, and melts to an isotropic liquid at 35℃. On a microscopic level, the rod-like 5CB molecules are locked in place and aligned when the sample is a solid. When the sample becomes a liquid crystal, the molecules are free to translate and can rotate somewhat. So the experiment temperature must be

controlled at 25℃.

Surface Aligning Condition

In a liquid crystal device, polymer layer play an important role in molecular alignment and charge injection. It is known that the dielectric anisotropy of nematic liquid crystals plays an important role in the application of the electrical effect to display devices. Thus, we concludes that the consumption of electric power increases and ionic impurities, which might cause the misalignment of liquid crystal molecules during the operation, shortens the life of the liquid crystalline actuator. Consequently, the behaviour of ionic impurities in the liquid crystalline materials and the mechanism of charge generation on the electrodes is of great concern.

Pretilt Angle

As a result of the surface rubbing, a small tilt angle exists for the liquid crystal director. The pretilt angle is very important when an electric field is applied to the liquid crystalline cell to reorient the liquid crystal director. Having no polarity, the rod-like liquid crystal molecules can turn in two ways following the application of an electric field, if the electric field is initially perpendicular to the molecular axis.

A small pretilt angle not only ensures a single domain upon switching, but also speeds up the switching process.

ITO layers

Because of its transparency, high conductivity, good etch ability, hardness and good adherence on glass, indium tin oxide (ITO) is used as the electrode material in my work. Unfortunately, ITO electrodes show relatively high resistance for electric current, because of that this material is not the best choice for the dielectric measurements especially at the high frequencies. Gold, silver, and aluminum are more suitable materials for the dielectric studies. Electrodes should be etched by using standard photolithography technique to get well defined form and size of the capacitor. Not that very thin metals layers with thickness around or less than 100Å usually show an island structure and poor conductivity.

5.1.2 Optimal the Experimental Conditions

From the results proposed in Chapter 3 and Chapter 4, we know that the driving force and the energy efficiency are affected by the frequency of the input voltage. We combine Fig. 3.29 and Fig. 4.22 to Fig. 5.1. Figure 5.1 shows the effect of the frequency of the input voltage on the maximum driving force and the energy efficiency of the liquid crystalline actuator. Because of the high-speed camera, the driving force just can be measured under the frequency from 1Hz~50Hz. Compared these two performance, when the frequency is 30Hz, the maximum driving force and the energy efficiency reach the relatively maximum value simultaneously.

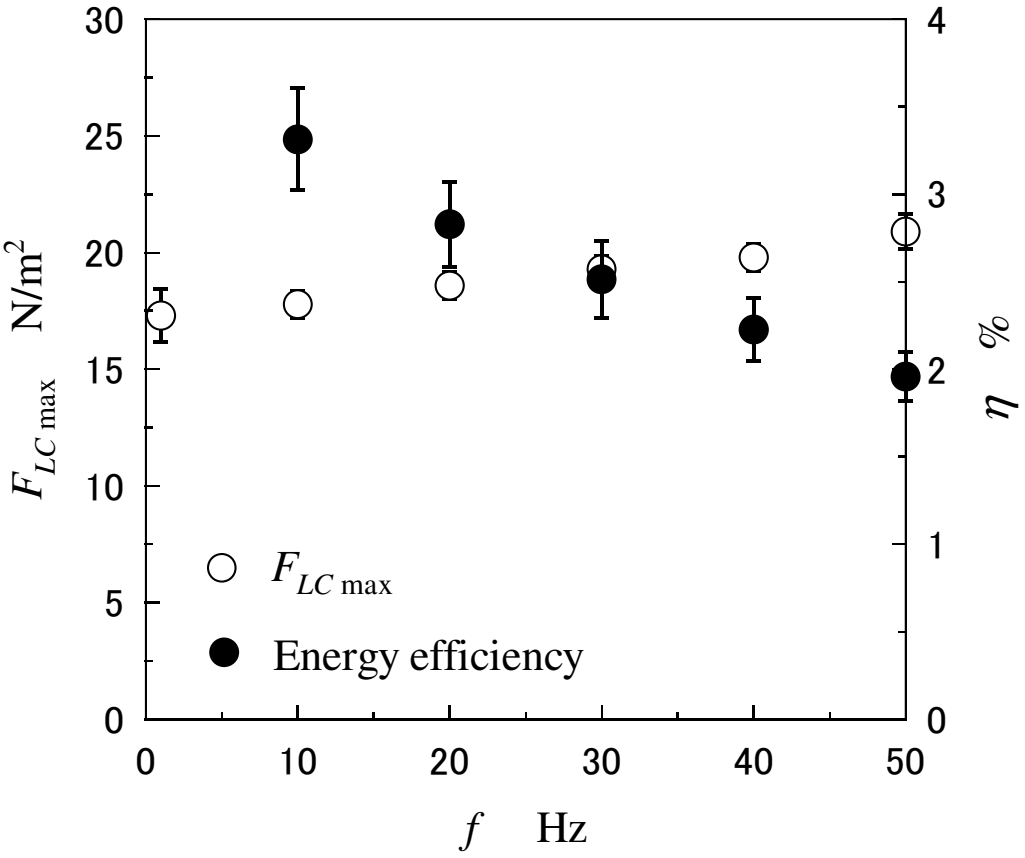

Fig. 5.1 Effect of the frequency of the input voltage on the maximum driving force and the energy efficiency of liquid crystalline actuator

5.2 General Conclusion

We have performed the experiments on the driving performances, such as the motion trajectory, driving speed, driving force, energy efficiency of the liquid crystalline actuators and we have successfully measured them. The obtained conclusions are as follows.

The upper glass plate of the liquid crystalline cell shows the step-like periodic movements when the pulsed electric field is applied. A large forward movement and a small backward movement of the upper glass plate of the liquid crystal cell are observed corresponding to the turn ON and OFF of the electric field.

The averaged driving speed of the upper glass plate increases with increasing the voltage or frequency of the pulsed electric field and decreases with increasing the duty ratio. It is found that the speed can be controlled by these input factors.

The driving force is obtained through image analysis. The maximum driving force generated by the liquid crystalline flow is estimated by differentiating the time series of the driving speed. From the results it is found that the maximum driving force per unit area is 70N/m^2 for V = 10V. This force is comparable to that of other kinds of actuators. The RE type electro-conjugate fluid motors can generate the maximum driving force per unit area about tens of N/m^2 for V = 5KV. The electrostatic actuator can produce a force density of 20N/m^2 for V = 50V. The result suggests that the liquid crystalline micro-actuator can provide a sufficient force at low voltage.

The energy efficiency of the liquid crystalline actuator becomes maximum at f = 100Hz. The maximum energy efficiency of the liquid crystalline actuator is about 3.5% at 10V. When the voltage is 5V, the maximum energy efficiency is about 7%. Although the efficiency is relatively low compared with other actuators, the liquid crystalline actuator is useful for the micro-sized machines which cannot be achieved with other actuators.

All of the information of the performances, the driving speed, the driving force, and the energy efficiency, of the liquid crystalline actuator is explored.

5.3 Future Inquires

This dissertation focuses on the measurement of the driving force and the energy efficiency of Liquid crystalline Actuators. However, there are several future inquires that can be pursued to extend current work.

In the dissertation, the driving force is only measured underthe frequency from 1Hz~50Hz due to the technical limitation of high-speed camera. Towards a unified dataset, which enable user to predict the driving force based on the voltage and frequency of input electrical field, the data in the higher frequency than 50Hz is also needed. If we improve the frame rate of high-speed camera and the sensor of high-speed camera isn't affected by the light source, the motion of liquid crystalline actuator at high frequency can be captured by the high-speed camera. Thus, the driving force of liquid crystalline actuator at the frequency higher than 50Hz can also be analyzed.

The results presented in chapter 4 demonstrated that the maximum energy efficiencies of the liquid crystalline actuator are about 3.5% at 10V, and 7% at 5V, respectively. This efficiency is relatively low compared with other actuators. We expected to optimize the design of actuator and enhance the energy efficiency by changing the experimental temperature, surface aligning condition, and pretilt angle, as discussed in the Chapter 5. Further investigation of optimization techniques would certainly uncover the optimal experimental conditions to achieve the desirable dynamic performance and the energy efficiency.

Finally, Current crystal crystalline actuator in the dissertation is a simplified prototype in comparison with a realistic system. It was utilized in this dissertation to demonstrate the relationship between the important dynamic properties (e.g., driving force, energy efficiency) and the input parameters (e.g., the) in the ideal experimental environment. Although this will provide an important reference for a realistic application, the situation is more complex in the real world. It is necessary to confirm the current results in the realistic situations, especially in the environments with the rapid changes in temperature, and human body for biomedical application.

Publication List

Journals:

[1] Measurement of Driving Force of Liquid Crystalline Actuators, Applied Physics Letters. (to be submitted)

[2] Evaluation of the Driving performance of Liquid Crystalline Actuators 液晶駆動性アクチュエータ性能の評価, JSME. (to be submitted)

[3] Measurement of Energy Efficiency of Liquid Crystalline Actuators, Applied Physics Letters. (to be submitted)

Conferences:

[1] Measurement of Driving Force of Liquid Crystalline Actuators, 5th Pacific Rim Conference on Rheology, 5 Aug. 2010, Hokkaido

[2] Driving Performance of Liquid Crystalline Actuators , Proceedings of ASME-JSME-KSME Joint Fluids Engineering Conference 2011, July 24-29, 2011, Hamamatsu.

[3] Evaluation of the Driving performance of liquid crystalline actuators, Fluids Engineering Division・The Japan Society of Mechanical Engineers 日本機械学会・流体工学部門・複雑流体研究会, 2011.

Acknowledgment

First, I would like to thank my advisor Professor Tsuji Tomohiro and Chono Shegeomi, for their kind support in my three years doctoral study. They give me the opportunity to study at KUT and guided me to the new field of liquid crystal. Professor Tsuji Tomohiro not only teach me by words and but also influence me by deed, he showed me different ways to approach a research problem and how to use the elegant way to express the idea. I am impressed by his intelligence and enthusiasm to work; I also like his humor and decency in daily life.

Next, I'd like to thank members of the Chono and Tsuji's Lab and my friends at KUT.

I have received support in the form of scholarships, facilities or travel grant from Grant-in-aid for scientific researches, the Special subsidies in subsidies for ordinary expenses of private schools from the Promotion and Mutual Aid Corporation for Private Schools of JAPAN, and Kochi University of Technology. This research would have been impossible without that generous support.

Meanwhile, I would like to thank my parents, your concerns and loves helped me to face and conquer the difficulties during my study and life in Japan.

References

Abe, P., and Yokota, S., 2003. “A Micro Actuator using ECF-Jet with Needle-type Electrode”, Proc. FLUCOME`03, CD-ROM.

A. D. Rey and M. M. Denn, J. Non-Newtonian Fluid Mech. 27, 375 (1988).

A. D. Rey and M. M. Denn, Annu. Rev. Fluid Mech. 34, 233 (2002). [ISI]

Ahn, C. H.; Kim, Y. J. and Allen, M. J. (1993), A planar variable reluctance magnetic micromotor with fully integrated stator and coils, Journal of Microelectromechanical Systems 2: 165-173.

A. Sasaki and S. Naemura, Eds., Liquid Crystal Displays. Tokyo, Japan: Kogyochosakai, 1993.

Berreman, D. W., 1975. “Liquid-Crystal Twist Cell Dynamics with Backflow”, J. Appl. Phys., 46, pp.3746-3751.

Boulet, B. and Hayward, V. (1993). Characterization, modeling and identi_cation of a high performance hydraulic actuator for robotics. Technical Report TR-CIM-93-9, McGill Centre for Intelligent Machines.

Brochard, F., 1973. “Backflow Effects in Nematic Liquid Crystalline”, Mol. Cryst. Liq. Cryst. 23 , pp.51-58.

Bustillo, J. M., Howe, R. T., and Muller, R. S., 1998. “Surface micromachining for microelectromechanical systems”, Proceedings of the IEEE, 86, pp. 1552-1574.

Cenk, A., Andrei, M. S., 2008. “MEMS Vibratory Gyroscopes: Structural Approaches to

Improve Robustness", Springer, 2nd ed., pp. 111-121.

Cho, H. J. and Ahn, C. H. (2002), A bidirectional magnetic microactuator using electroplated permanent magnet arrays, Journal of Microelectromechanical Systems 11: 78-84.

Chono, S., and Tsuji, T., 2006. "Development of Micro-Actuators Driven by Liquid Crystals (1st Report, Generation of Flow and Its Mechism)", Transactions of the Japan Society of Mechanical Engineers, Series B, 172 (715), pp.96-101.

Chono, S., Tsuji, T., and M. M. Denn, J. Non-Newtonian Fluid Mech. 79, 515 (1998).

Colgate, J. E. and Brown, J. M. (1994). Factors a_ecting the z-width of a haptic display. In Proc. IEEE International Conference on Robotics and Automation, pages 3205{3210.

Dargahi, J.; Parameswaran, M. and Payandeh, S. (2000), A micromachined piezoelectric tactile sensor for an endoscopic grasper - theory, fabrication and experiments, Journal of Microelectromechanical Systems 9: 329-335.

Dario, P., valleggi, P., Carrozza, M. C. , Montesi, M. C. and Cocco, M., 1992. "Microactuators for microrobots: a critical survey", 3rd Eur. Workshop Micromaching and Micromechanics MME `92, pp. 141-173.

DeVoe, D. L. (2001), Piezoelectric thin film micromechanical beam resonators, Sensors and Actuators A 88: 263-272.

"Domains in liquid crystals," J. Phys. Chem., vol. 39, pp. 382–388, July 1963.

Dufour, I. and Sarraute, E. (1999), Analytical modelling of beam behaviour under differentactuations: profile and stress expressions, Modelling and Simulation of Microsystems 1: 57-64.

Edwin, O., van A. den B., "Lab-on-a-Chip: Miniaturized systems for bio-chemical

analysis and synthesis", Elsevier Science, 2nd ed., pp. 402-410.

E. F. Carr, "Influence of electric fields on the molecular alignment in the liquid crystal p-(anisalamino)-phenylacetate," Mol. Cryst. Liq. Cryst., vol. 7, pp. 253–268, 1969.

Egawa, S., et al., 1990. "Multi-layered electrostatic film actuator", Proc. IEEE Micro Electro Mech. Syst., pp. 166-171.

Elvin, N. G.; Elvin, A. A. and Spector, M. (2001), A self-powered mechanical strain energy sensor, Smart Materials and Structures 10: 293-299.

Fan, L.; Tai, Y. and Muller, R. S. (1989), IC-processed electrostatic micromotors, Sensors and Actuators 20: 41-47.

Feynman R.,1960. Plenty of Room at the Bottom: An Invitation to Enter a New Field of Physics *Engineering and Science* 22 22-36.

Frank, F. C., 'Liquid crystals. On the theory of liquid crystals', Discuss Faraday, 25, 19 (1958).

Fukuda, T. et al., 1990. "Micro electrostatic actuator with three degrees of freedom", Proc. IEEE Micro Electro Mechanical systems, pp.153-158,105-110.

Fukuda, T. et al., 1992. "New actuators for high-precision micro systems, in Precision", Sensors, Actuators and System, Kluwer Academic Publishers, pp. 1-37.

Fukuda, T. et al., 1992. "Design and experiments of micro mobile robot using electromagnetic actuator", proc. Third IEEE Int. symp. Micro Machine, Human Sei. (MHS'92), pp. 77-81.

Fujita, H. (1998), Microactuators and micromachines, Proceedings of the IEEE 86: 1721-1732.

"George Heilmeier. The liquid crystal display," Wall Street J., May 24, 1993.

G. H. Heilmeier, "Liquid crystal displays: An experiment in interdisciplinary research

that worked," IEEE Trans. Electron Devices, vol. ED-23, July 1976.

G. H. Heilmeier and L. A. Zanoni, "Guest-host interactions in nematic liquid crystals. A new electro-optic effect," Appl. Phys. Lett., vol. 13, no. 3, pp. 91–92, 1968.

G. H. Heilmeier, L. A. Zanoni, and L. A. Barton, "Dynamic scattering: A new electrooptic effect in certain classes of nematic liquid crystals," Proc. IEEE, vol. 56, pp. 1162–1171, July 1968.

Gorbet, R.B. and Russell, R.A., 1995. "A Novel Differential Shape Memory Alloy Actuator for Position Control", Robotica, vol. 13, Cambridge University Press, Cambridge, UK, pp. 423-430.

Gordon E. Moore, Life fellow., 1965. "Cramming more components onto integrated circuits", Electronics, 38(8).

Grade, J. D.; Jerman, H. and Kenny, T. W. (2003), Design of large deflection electrostatic actuators, Journal of Microelectromechanical Systems 12: 335-343.

Grant, D. and Hayward, V. (1995). Design of shape memory alloy actuator with high strain and variable structure control. In Proc. IEEE International Conference on Robotics and Automation.

Gray, J. O., Caldwell, D. G., 1996. "Advanced robotics & intelligent machines", Institution of Electrical Engineers.

Guckel, H. (1998), Progress in magnetic microactuators, Microsystem Technologies 5: 59-61. 192

Guckel, H.; Christenson, T. R., et al. (1993), A first functional current excited planar rotational magnetic micromotor, MEMS'93 Proceeding of IEEE Micro Electro Mechanical Systems, Ford Lauderdal, USA.

Guyon, E., Meyer, R. B., and Salán, J., 1979. "Domain Structure in the Nematic

Freedericksz Transition", Mol. Cryst. Liq. Cryst. 54(261)

Hayward, V. (1995). Toward a seven axis haptic device. In IROS.

Hayward, V. and Astley, O. R. (1995). Performance measures for haptic interfaces. In Proceedings of the 7th International Symposium on Robotics Research, Munich, Germany. Springer-Verlag.

Henri, P. D. and Hollerbach, J. M. (1994). An analytical and experimental investigation of a jet pipe controlled electro-pneumatic actuator. In Proc. IEEE International Conference on Robotics and Automation, pages 300{306.

Hatamura, Y., et al., 1990. "Direct coupling system between nanometer world and human world", Proc. IEEE Micro Electro Mech. Syst. (MEMS'BO), pp. 203-208.

Higuchi, T., et al., 1990. "Precise positioning mechanism utilizing rapid deformations of piezoelectric elements", Proc. IEEE Micro Electro Mech. Syst. (MEMS'90), pp. 222-226.

Hirano, T. and Fan, L. S. (1998), High-bandwidth high-accuracy rotary microactuators for magnetic hard disk drive tracking servos, IEEE/ASME Transactions on Mechatronics 3, 156-164.

Hisanaga, M., et al., 1991. "Fabrication of a 4.8 millimeter long microcar", Proc. Second Int. Symp. Micro Machine, Human Sei. (MHS'9I), pp. 43-46.

Ikuta, K., et al., 1994, "Biomedical micro robots driven by miniature cybernetic actuator", Proc. IEEE Micro Electro Mech. Syst. (MEMS'94), pp. 263-268.

Ishihara, H., et al., 1994. "Approach to autonomous micro robot (micro line trace robot with reflex algorithm)", proc, IEEE,sEl~E~ symp, Emerging Technol., Factory Automat. (ETFA'94), pp. 78-83.

J. E. Goldmacher and J. A. Castellano, "Electro-optical compositions and devices," U.S.

Patent 3 540 796, filed Mar. 31, 1967, issued Nov. 17, 1970.

Jenkins, D. F. L.; Cunnungham, M. J., *et al.* (1997), The use of sputtered ZnO piezoelectric thin films as broad-band microactuators, *Sensors and Actuators* **A 63**: 135-139.

John M. Hollerbach, I. W. H. and Ballantyne, J. (1991). A comparative analysis of actuator technologies for robotics. In Khatib, O., Craig, J., and Lozano-P_erez, T., editors, Robotics Review 2. MIT Press.

Judy, J. W. (2001), Microelectromechanical systems (MEMS): fabrication, design and applications, Smart Materials and Structures 10: 1115–1134.

Judy, J. W. and Myung, N. (2002), Magnetic materials for MEMS, MRS Workshop on MEMS Materials, San Francisco, California, April 5-6, 23-26.

Kilby J S.,1964. Miniaturized Electronic Circuits US Patent # 3,138,743

K. Koyama, Development of Electro-Rheological (ER) Fluids (CMC, Tokyo, 1999) [in Japanese].

Kueppers, H. and Leuerer, T. (2002), PZT thin films for piezoelectric microactuator applications, Sensors and Actuators A 97-98: 680-684.

Lagorce, L. K.; Brand, O. and Allen, M. G. (1999), Magnetic microactuators based on polymer magnets, Journal of Microelectromechanical Systems 8: 2-9.

Lau, S. T.; Kwok, K. W.; Chan, H. L. W. and Choy, C. L. (2001), Piezoelectric composite hydrophone array, Sensors and Actuators A 3145: 1-7.

Lee, S. S.; Ried, R. P. and White, R. M. (1996), Piezoelectric cantilever microphone and microspeaker, Journal of Microelectromechanical Systems 5: 238-242.

Li, L. X. and Shen, Y. P. (2001), The optimal design of piezoelectric acoustic control, Smart Materials and Structures 10: 421-426.

Liu, C., Chono, S., and Tsuji, T., 2006. “Development of Micro-Actuators Driven by Liquid Crystals (2nd Report, Effect of Various Parameters)”, Transactions of the Japan Society of Mechanical Engineers, Series B, 172 (721), pp.2235-2241.

Liu, C.; Tsao, T., et al. (1995), A micromachined permalloy magnetic actuator array for micro-robotics assembly systems, Transducers ’95, 8th International Conference on Solid-State Sensors and Actuators, Stockholm, Sweden.

Madou J. M. (2001), Fundamentals of Microfabrication, CRC Press, New York.

Mosley, M., and Mavroidis, C., 2000. “Design and Dynamics of A Shape Memory Alloy Wire Bundle Actuator,” Proc. of the 2000 ASME Mechanisms and Robotics Conference, Baltimore MD.

Nakamura, Y., Nakamura, S., Buchaillot, L., Fujita, H., 1997. “A Three-Dimentional Shape Memory Alloy Loop Actuator”, Proc. IEEE the Tenth Annual International Workshop on Micro Electro Mechanical Systems, pp. 262-266.

O. Lehmann, 1889. "Über fliessende Krystalle". Zeitschrift für Physikalische Chemie 4: 462–72.

Oo T N, Iwata T., Kimura, M., and Akahane, T., 2005. “Surface alignment of liquid crystal multilayers evaporated on photoaligned polyimide film observed by surface profiler”, Science and Technology of Advanced Materials, 6 (2) 149-157.

Pister, K. S. J., et al., 1990. “A planar air levitated electrostatic actuator system”, Proc. IEEE Micro Electro Mech. Syst. (MEMS’90), pp. 67-67.

“RCA announces breakthrough in liquid crystal field; demonstrates thin-screen displays of print, pictures, moving images,” presented at the RCA Press Conf., New York, May 28, 1968.

Reinitzer, F. 1888. "Beiträge zur Kenntniss des Cholesterins". Monatshefte für Chemie

(Wien) 9 (1): 421–441.

Robertson, C. (1979), Bimorph drivers-an electric solution, Pennwalt (Europe) 79: 1-8.

Roberts, D. C. and Li, H. (2003), A piezoelectric microvalve for compact highfrequency, high-differential pressure hydraulic micropumping systems, Journal of Microelectromechanical Systems 12: 81-92.

Rosenberg, L. B. and Adelstein, B. D. (1993). Perceptual decomposition of virtual haptic surfaces. In Proceedings IEEE Symposium on Research Frontiers in Virtual Reality.

Ruprecht, R.; Kalb, H.; Kowanz, B. and Bacher, W. (1996), Molding of LIGA microstructures from fluorinated polymers, Microsystem Technologies 2: 182-185.

R. Williams, "Electro-Optical Elements Utilizing an Organic Nematic Compound," U.S. Patent 3 322 485, filed Nov. 9, 1962, issued May 30, 1967.

Sato T., 1996. Micro/Nano Manipulation World *Proceedings of the InternationalConference on Intelligent Robotics and Systems* 834 – 841

Schellin, R. and Hess G. (1992), A silicon subminiature microphone based on piezoresistive polysilicon strain gauges, Sensors and Actuators A 32: 555-559.

Sitti M.,2001. Survey of Nanomanipulation Systems *Proc. of the IEEENanotechnology Conference, Maui, USA* 75 – 80

Takanori, M., Tsuji, T., and Chono, S., 2009. "Development of Micro-Actuators Driven by Liquid Crystals (3rd Report, Visualization of Velocity Profiles between Parallel Plates)", Transactions of the Japan Society of Mechanical Engineers, Series B, l75 (753), pp.953-958.

Tang, W. C.; Nguyen, T. C. H. and Howe, R. T. (1992), Laterally driven polysilicon resonant microstructures, Sensors & Actuators A 20: 25-32.

Todals, M.; Osaka, S., et al. (1979), A new electromotional device, RCA Engineer 25: 24-27.

Wagner, B. and Benecke, W. (1990), Magnetically driven microactuator: design considerations, Microsystems Technologies 838-843.

W. Helfrich, "Conduction-induced alignment of nematic liquid crystals: Basic model

Williamson, M. (1995). Series elastic actuators. Master's thesis, MIT, Department of Electrical Engineering and Computer Science.

Yang. D.K., and Wu. S.T. 2006. Fundamentals of liquid crystal Devices, Wiley, P. 2.

YE, W., Mukherjee, S., MacDonald, N., "Optimal Shape Design of an Electrostatic Comb Drive in Micro-Electro-Mechanical Systems," NSF research report under grant ECS-9321508.

Yokota, S., Hirata, Y., Kondoh, Y., Suzumori, K., Sadamoto, A., Otubo, Y., and Edamura, K., 2001. The Journal of Robotics and Mechatronics, 13(2), pp.140.

Yokota, S., Kondoh, Y., Sadamoto, A. Otsubo, Y. and Edamura, K. 2001. "A Micro Motor Using Electro-conjugate Fluids (ECF) (Proposition of Stator Electrode-type (SE-type) Micro ECF Motors)", Int. J. JSME Ser. C, 44(3), pp. 756-762.

Yoseph, B. C. and Chang, Z. (2000), Piezoelectrically actuated miniature peristaltic pump, Proceeding of SPIE's 7th Annual International Symposium on Smart Structures and Materials, Newport, March 1-5.

Yoshida, K., and Yokota, S., 1993. "Study on High-Power Micro Actuator Using Fuide Power", Proc. of 6th FLOMEKO, Seoul, pp.122-130.

Zurn, S.; Hsieh, M., et al. (2001), Fabrication and structural characterization of a resonant frequency PZT microcantilevers, Smart Materials and Structures 10: 252- 263.